Max-Planck-Institut
für Polymerforschung

Max Planck Institute
for Polymer Research

Achieving a stealth effect of nanocarriers through controlled protein adsorption

Dissertation

Zur Erlangung des Grades
„Doktor der Naturwissenschaften“ (Dr. rer. nat.)
im Promotionsfach Chemie

am Fachbereich 09 - Chemie, Pharmazie und Geowissenschaften
der Johannes Gutenberg-Universität in Mainz

JOHANNES GUTENBERG
UNIVERSITÄT MAINZ

vorgelegt von

Julius Müller

geb. in Buchen (Odenwald)

Mainz, 2018

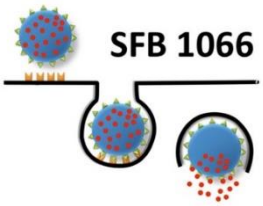

Dekan: [redacted]
1. Gutachter: [redacted]
2. Gutachter: [redacted]

Tag der mündlichen Prüfung: 27.04.18

Abstract

Drug delivery by nanocarriers has evolved into a momentous field of interdisciplinary research. A crucial aspect for the success of any form of future nanotherapeutic is the protein corona, which forms around the surface of a nanocarrier immediately once it enters a bodily fluid like blood plasma. Certain apolipoproteins in this corona are responsible for the 'stealth effect', *i.e.* the non-uptake of a nanocarrier by phagocytes and a resulting long blood circulation time. The aim of controlled biological behavior through a defined 'stealth' protein corona was approached from different sides in this work.

Firstly, with the physical adsorption of poly(phosphoester) surfactants a new approach to the stealth effect of polystyrene nanoparticles was introduced to facilitate and generalize the stealth functionalization strategy. A similar composition of the protein corona as for nanocarriers with poly(ethylene glycol) chains grafted to their surface could be observed. Cellular uptake experiments confirmed a stealth effect for the surfactant-coated nanoparticles.

Afterwards, the role of lipids for the formation of a stealth corona and the consequences for cellular uptake were investigated. Lipoprotein adsorption to nanoparticles was analyzed with various methods and new insights into the mechanism of the interaction with nanoparticles could be gained. Evidence for the disintegration of lipoprotein complexes upon adsorption was found. Moreover, denaturation of important stealth corona proteins by surfactants was analyzed with complementary methods. In this context, the effect of additional cetyltrimethylammonium chloride on the composition of the protein corona was studied and a clear shift could be observed. Two selected apolipoproteins were screened for their sensitivity to surfactant denaturation and significant differences were found. Further, a possible influence of heat inactivation on the folding state and adsorption behavior of proteins was investigated. Finally, the commonly used stealth polymer poly(ethylene glycol) has been tested for possible interaction with proteins.

In conclusion, new findings on the complex interactions of nanoparticle formulations with single proteins and blood plasma could be gained and the potential influence of surfactants could be illuminated. The results gained in this work provide valuable knowledge for future research on this subject.

Zusammenfassung

Die Wirkstoffverabreichung durch Nanoträger hat sich zu einem wichtigen Feld interdisziplinärerer Forschung entwickelt. Ein entscheidender Aspekt für den Erfolg von jeglicher Form eines Nanotherapeutikums ist die Proteincorona, die sich um die Oberfläche eines Nanoträgers bildet, sobald dieser in eine Körperflüssigkeit wie Blutplasma eintritt. Bestimmte Apolipoproteine in dieser Corona sind für den ‚Stealth Effekt' verantwortlich, dieser bezeichnet die verhinderte Aufnahme eines Nanoträgers durch Phagozyten und eine resultierende lange Zirkulationszeit im Blut. Dem Ziel eines kontrollierten biologischen Verhaltens durch eine definierte ‚Stealth' Proteincrona wurde sich in dieser Arbeit von verschiedenen Seiten genähert.

Zunächst wurde mit der physikalischen Adsorption von Polyphosphoester-Tensiden ein neuer Ansatz für den Stealth-Effekt von Polystyrol-Nanopartikeln vorgestellt, um die Strategie der Stealth-Funktionalisierung zu vereinfachen und zu verallgemeinern. Eine ähnliche Zusammensetzung der Proteincorona wie für Nanoträger mit auf der Oberfläche aufgepfropften Polyethylenglycol-Ketten konnte beobachtet werden. Zellaufnahmeversuche bestätigten einen Stealth-Effekt für Tensid-beladene Nanopartikel.

Anschließend wurde die Rolle von Lipiden für die Ausbildung einer Stealth-Corona und die Konsequenzen für die Zellaufnahme untersucht. Die Adsorption von Lipoproteinen an Nanopartikel wurde mit vielfältigen Methoden analysiert und neue Erkenntnisse über den Mechanismus der Wechselwirkung mit Nanopartikeln konnten gewonnen werden. Anhaltspunkte für den Zerfall von Lipoprotein-Komplexen bei der Adsorption wurden festgestellt. Zudem wurde die Denaturierung wichtiger Stealth-Corona-Proteine durch Tenside mit einander ergänzenden Methoden analysiert. In diesem Zusammenhang wurde der Effekt von zusätzlichem Cetyltrimethylammoniumchlorid auf die Zusammensetzung der Protein-Corona studiert und eine klare Verschiebung konnte beobachtet werden. Zwei ausgewählte Apolipoproteine wurden hinsichtlich ihrer Sensitivität gegenüber Tensid-Denaturierung überprüft und signifikante Unterschiede wurden festgestellt. Weiterhin wurde ein möglicher Einfluss von Hitzeinaktivierung auf den Faltungszustand und das Adsorptionsverhalten von Proteinen untersucht. Abschließend wurde das üblicherweise genutzte Stealth-Polymer Polyethylenglycol auf mögliche Wechselwirkung mit Proteinen getestet.

Schließlich konnten neue Erkenntnisse über die komplexen Wechselwirkungen von Nanopartikel-Formulierungen mit einzelnen Proteinen und Blutplasma gewonnen werden und der potentielle Einfluss von Tensiden konnte beleuchtet werden. Die in dieser Arbeit gewonnen Ergebnisse liefern wertvolles Wissen für zukünftige Forschung an diesem Thema.

Table of Contents

1 Introduction

The intentional future use of nanomaterials as drug carriers requires precise control of their biological fate after administration. A long blood circulation time of the nanomaterials is crucial for a targeted delivery with high efficiency. A key parameter for the circulation time is the so-called protein 'corona', which forms around a nanoparticle (NP) in biological fluids like human blood plasma and consists of physically adsorbed proteins.[1-3] As previously investigated by several groups, altering the pattern of the protein corona, in other words controlling the types of proteins adsorbed to a NP, can have a crucial effect on its biological fate.[4-14] More specifically, the presence of certain proteins defined as opsonins in the protein corona marks the NP to be taken up by phagocyte cells and thus be removed from the blood stream.[4, 13, 15] Recently, it was shown that this phagocytosis can be reduced by the enrichment of specific 'stealth' proteins on the NP surface rather than only suppressing unspecific protein adsorption.[13, 16-18] The reduction of unspecific cellular uptake of NPs is referred to as the 'stealth effect'.

The major subject of this work is to control the protein corona in a way to achieve a stealth effect. Several factors influencing protein adsorption, which may have a potential impact on the protein corona, are analyzed. Further, a new approach for NP surface modification towards stealth behavior is pursued.

Currently, the covalent attachment of poly(ethylene glycol) (PEG) chains to the surface of a nanoparticle (NP) − the so-called PEGylation – still represents the standard procedure to obtain a stealth effect for NPs.[9] PEGylation induces a selective protein enrichment of namely clusterin (CLU) and apolipoprotein A1 (Apo-A1) in the protein corona of NPs.[5, 19-20] Due to their different protein corona composition, the PEGylated NPs exhibit a significantly decreased unspecific cellular uptake. Additionally, another polymer class – namely poly(phosphoester)s (PPEs) – was found to induce a similar stealth effect while providing the advantage of being biodegradable.[13]

The chains of each type of stealth polymer are normally linked to the NP surface *via* the formation of covalent bonds after synthesis. However, this covalent attachment requires a high synthetic effort and the process is difficult to control. Therefore, a non-covalent coating of NPs with functional polymeric surfactants is proposed in this work. Surfactants are widely used for the synthesis and stabilization of colloids in solution and thus are present anyway on the surface of most NP samples.[21-23] The application of polymeric surfactants only requires physical adsorption, so it is possible to omit the step of attaching the polymer chains covalently to the surface of the NP (as for PEGylation). With this technique, a surface functionalization similar to PEGylation is possible, while the preparative effort will be significantly reduced.

In order to characterize the adsorption of polymeric surfactants to NPs, isothermal titration calorimetry (ITC) can be applied. ITC is a method, which allows to directly probe adsorption processes through the heat of adsorption and to determine adsorption parameters such as binding affinity, binding enthalpy and stoichiometry. It is therefore particularly suitable to study the adsorption of proteins to NPs, *i.e.* the formation of the protein corona.[10, 24]

Beyond protein adsorption, ITC is further used in this work to probe the adsorption of various surfactants and of lipoprotein complexes to NPs. The adsorption of lipids contained in lipoproteins and the consequent formation of a 'biomolecule corona' is an aspect of the biological behavior of nanocarriers that should not be neglected.

Due to their amphiphilic nature, lipids are predestined to show considerable interaction with the surface of a nanocarrier. Lipids are typically transported in the body by lipoproteins, which are complexes of apolipoproteins, phospholipids, triglycerides, and cholesterol with a size of 7.5 to 80 nm depending on the lipoprotein type.[25-26]

As in recent years an enrichment of apolipoproteins in the protein corona of nanomaterials was found in various different studies, the question came up whether a common driving force for their interaction is present.[27-30] It was therefore speculated that interactions with the lipoproteins as a whole can take place. Protein-mediated interaction of intact lipoproteins with copolymer nanocarriers has first been reported by Hellstrand *et al.*[31] The role of low-density lipoproteins (LDL) and their interactions with specific receptors has recently been investigated in detail by Lara *et al.*[32] Examining the interaction of high-density lipoprotein (HDL) with silica NPs, intact lipoprotein complexes were found in the biomolecule corona.[33] A disintegration of the lipoproteins or the interaction of the single components was not observed.[32-34] Further, lipids are also contained in pulmonary surfactant, which – in contact with NPs – forms a different biomolecule corona than plasma.[34]

Apolipoproteins represent the functional units of lipoproteins and are typically integrated in the shell of lipoproteins with hydrophilic domains facing the outside. By their density, lipoproteins are categorized into three main types among others: high-density lipoproteins (HDL), low-density lipoproteins (LDL) and very low-density lipoproteins (VLDL).[35] The concentration of these different lipoproteins in human blood fluctuates depending on food intake, physical constitution and other factors.

The adsorption of lipoproteins, apolipoproteins and other biomolecules on nanocarriers depends on several parameters such as the nanocarrier material, surface functionalization, protein source, and colloidal stabilization agents, the surfactants.[36] Colloidal systems, which are polymerized for increased stability and are not only based on the self-assembly of amphiphilic molecules, require some sort of surfactant to ensure colloidal stability and avoid inter-particle aggregation.[9, 21, 23] It has been shown in

a previous work that already minimal amounts of surfactant can significantly alter the adsorption behavior of proteins.[36] Moreover, the type and amount of surfactant on nanocarriers significantly determines protein binding affinity and adsorption stoichiometry as well as cellular uptake.[36] Therefore, also the overall composition of the protein corona and thus the presence of stealth proteins is likely to vary upon change of the surfactant concentration. An influence on cell uptake by the positive charge on the surface of NPs, which were stabilized with a cationic surfactant, was reported in literature. More specifically, NPs stabilized with cetyltrimethylammonium chloride (CTMA-Cl) showed high uptake by HeLa cells irrespective of the polymer type.[37]

It is long known that sufficient levels of ionic surfactants, such as sodium dodecyl sulfate (SDS), denature certain proteins.[38-41] For SDS concentrations above 1 mM, complete denaturation was reported for ovalbumin.[39] In SDS polyacrylamide gel electrophoresis (SDS-PAGE), the process of surfactant denaturation is exploited to unfold and linearize the protein chains, allowing a separation of the proteins by chain length (proportional to mass) on the gel.[42]

Typically, binding of the surfactants' ionic head groups to charged regions of the protein through electrostatic interaction occurs.[43-45] Also, there is an additional type of surfactant binding with lower affinity, namely of their hydrophobic tails with hydrophobic pockets of the protein as reported by Nielsen *et al*.[46] In contrast, for some proteins, the native state may also be stabilized by surfactant binding and the free energy of denaturation increases.[47]

In this work, the challenge of controlled protein adsorption for a stealth effect of nanocarriers is approached from different sides. The surfactants present in most NP dispersions for colloidal stabilization have not yet been studied sufficiently regarding their influence on proteins. Possible alterations of the protein corona through surfactants and the consequences for the stealth effect are therefore subject of further investigation in this work. The effect of commercially available surfactant on protein denaturation and on the composition of the protein corona is studied. Furthermore, the physical adsorption of stealth polymers is rather unexplored territory, as the vast majority of publications on stealth nanocarriers refers to the covalent attachment of polymers. Coating of NPs with tailored PPE-surfactants as an alternative to PEGylation is therefore examined. Moreover, analysis of the biomolecule corona, which includes adsorption of other blood constituents such as lipids has only been covered to a low extent compared to the numerous publications on the protein corona in recent years. Still, it remains an open question whether the lipoprotein-nanomaterial interactions are mediated by the proteins or the lipid components. In addition, the influence of the adsorption of lipoproteins on the biological response is not yet reported. Further, the impact of heat inactivation on the folding state of certain proteins and on their adsorption behavior to NPs is investigated. Finally, the interaction of proteins and PEG, still the most common stealth polymer, is probed. A general aim

is to clarify how the specific protein pattern of stealth nanocarriers is preserved even under changing conditions and how a stealth corona can be created on new nanocarrier systems.

2 Theoretical Background

2.1 Blood plasma and proteins

2.1.1 Blood preparations, proteins and other constituents

The probably most essential fluid in the human body, which ensures to keep up its vital functions, is blood. It is a complex mixture consisting of salts, lipids and more than 3000 different proteins.[48] In medical science, different preparations of human blood are distinguished: Blood plasma is centrifuged whole blood, which does not contain blood cells (erythrocytes, leukocytes, thrombocytes). As coagulation factors are still present in plasma (in contrast to blood serum), additives are necessary to avoid coagulation. For this purpose, citrate, ethylenediaminetetraacetic acid (EDTA) or heparin is added to prevent clotting of the plasma. In this thesis, human citrate plasma was used for all experiments.

When clotted blood is centrifuged, blood serum is obtained, which therefore can be described as plasma without coagulation factors.

The entirety of all proteins present in the blood, the proteome, is subdivided into several types of proteins: glycoproteins, chromoproteins, phosphoproteins and lipoproteins (among others). In this work, specific apolipoproteins were studied in detail as they were reported previously to have a crucial effect on the biological fate of a nanocarrier.[13] Apolipoproteins do rarely occur freely as single proteins in blood, but rather as complexes together with lipids. These complexes are called lipoproteins (or chylomicrons).

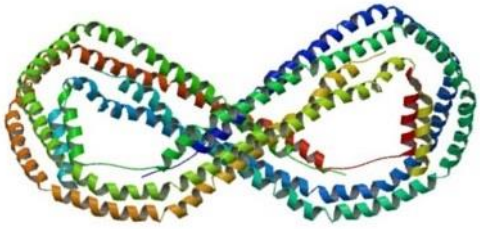

Figure 2.1.1 Structure of Apo-A1 from the protein data base (PDB).[49]

Apolipoprotein A1 (Apo-A1), has a mass of 28 kDa and occurs in high-density lipoprotein and chylomicrons. Its mean level in plasma is 1.4 g L^{-1}, the structure is shown in Figure 2.1.1.[50]

Another important apolipoprotein is clusterin (CLU), also known as apolipoprotein J, which occurs as a heterodimer with a mass of 75 kDa. Despite its low abundance in plasma (0.05 – 0.37 g L^{-1})[51], it has been detected in the protein corona of certain nanocarriers in disproportionately high amounts. For CLU, no crystal structure is available as this protein contains many unfolded regions, so no suitable crystal for X-ray crystallography could be obtained to date.[52-53] However, an α- and β-chain can be distinguished, so that the approximate structure of the heterodimer is known and depicted in Figure 2.1.2.

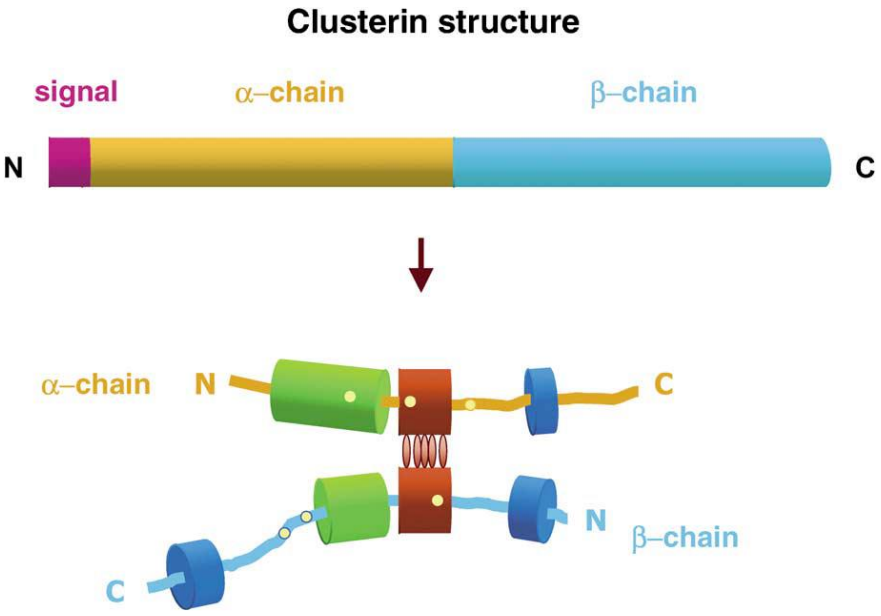

Figure 2.1.2 Schematic depiction of CLU structure.[54] With permission from Elsevier Science Ltd.

2.1.2 Lipoprotein complexes

Lipoproteins form complexes consisting of phospholipids, triglycerides, cholesterol, cholesterol esters, and apolipoproteins. They mainly serve as transport vehicles for lipids.[55] The constituents of lipoproteins are confined in a micelle-like shell of phospholipids, as depicted in Figure 2.1.3. The ionic head groups of the phospholipids are facing to the outside, their hydrophobic tails (alkyl chains) reach into the core of the lipoprotein. The core contains rather hydrophobic lipids, mainly cholesterol esters and triglycerides. Apolipoproteins are integrated in the lipoprotein shell, presenting functional moieties on the surface.[56-57] Besides their role as a structural unit of the shell, the functional moieties of the apolipoproteins are recognized by certain receptors in the body. The apolipoproteins thus guide the lipoprotein to its metabolic destination.

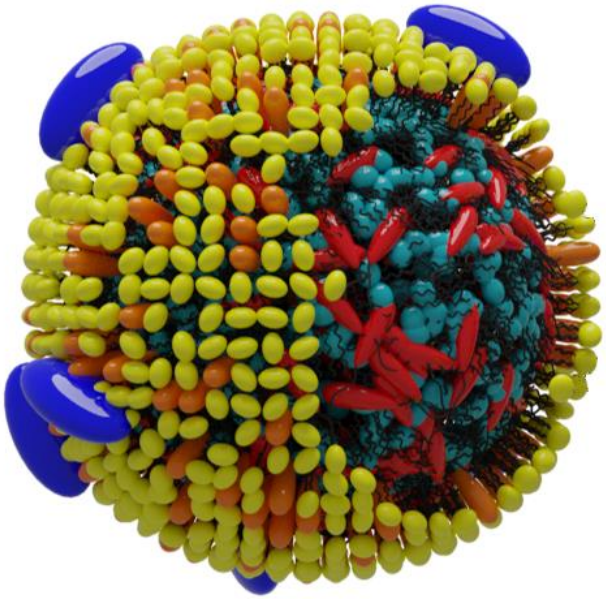

Figure 2.1.3 Structure of lipoproteins (schematic artwork). Blue: apolipoproteins; yellow: phospholipids (head group); red: cholesterol esters; orange: cholesterol; turquoise: triglycerides. Artwork copyright by [redacted].

Three main types of lipoproteins are distinguished by their density: high-density lipoprotein (HDL), low-density lipoprotein (LDL) and very-low-density lipoprotein (VLDL). They differ not only in density, but also in size: HDL forms the smallest and VLDL the largest complexes. Their hydrodynamic diameters range from 7.5 nm for HDL to up to 80 nm for VLDL.[25-26] In Figure 4.2.1 (Results and Discussion), detailed specifications of the respective lipoprotein types are given.

Different apolipoproteins occur in certain types of lipoproteins: apolipoprotein A1 (Apo-A1) in HDL, apolipoprotein B100 (Apo-B100) in LDL and VLDL, and apolipoprotein E (Apo-E) in VLDL. Apo-A1 and Apo-E further occur in chylomicrons, which are large lipoprotein-like particulates (500 – 1000 nm diameter), also referred to as ultra-low-density lipoprotein (ULDL).

2.2 Colloidal systems as nanocarriers for drug delivery

2.2.1 From nanoparticles to hollow nanocapsules with multiple functionality

In the past decades, nanotechnology has been an emerging scientific topic and is now an established field with some early applications.

The idea of drug delivery *via* nanocarriers implies the encapsulation of a drug inside a nanoscaled confinement (*e.g.* nanocapsule, liposome). This enables the targeted delivery of a drug to a certain cell type, for example malign cells like cancer cells. Following this approach, the dosage of the respective drug could be drastically reduced compared to conventional administration, which would result in a decrease of undesired side effects. Different forms of nanocarriers are being investigated for drug delivery, a few of which are depicted in Figure 2.2.1.

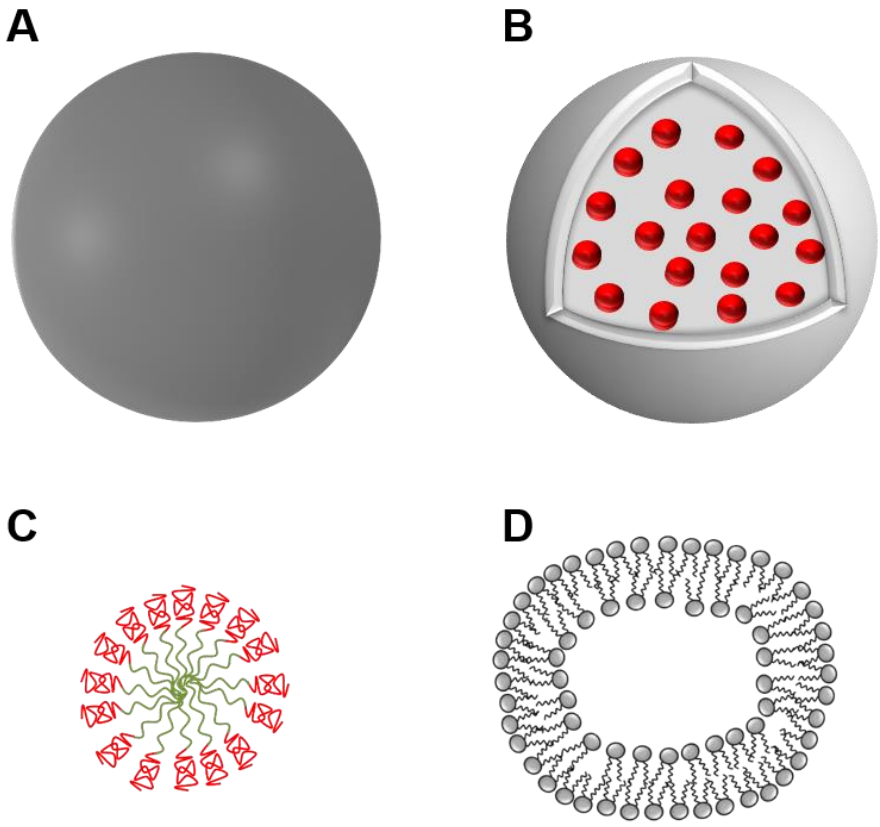

Figure 2.2.1 Different forms of nanocarriers: (A) solid nanoparticle (organic or inorganic), (B) polymeric nanocapsule with payload, (C) polymeric micelle, (D) liposome/polymersome.

Nanoparticles are solid spheres, which are made out of different materials (metals, polymers). Metallic nanoparticles are for example considered as contrasting agents for medical imaging methods.

Moreover, polymeric nanoparticles can serve as a simplified model systems for nanocapsules, as their synthesis bears a higher degree of reproducibility. Nanocapsules are hollow spheres usually made of polymeric material. Their inner cavity can be filled with a payload, *e.g.* with an active pharmaceutical ingredient. Micelles used for drug delivery are usually composed of amphiphilic polymers or oligomers, sometimes with a cross-linked core. Liposomes and polymersomes are consisting of a lipid respectively of a polymer double layer and usually contain a hydrophilic inner core.

Nanoparticles (NPs) made of a variety of materials, ranging from noble metals (gold, silver) to biopolymers (polysaccharides, polylactic acid), can today be synthesized following standard protocols. Polymeric NPs are for example available through the polymerization of styrene, which yields polystyrene nanoparticles (PS-NPs). A common approach for this kind of synthesis is the miniemulsion polymerization.[21, 58] In order to generate droplets and prepare the miniemulsion, ultrasonication or microfluidics can be applied. PS-NPs are suitable model systems for nanocarriers due to their well-established and reproducible synthesis, controllable size and narrow size-distribution. Moreover, it is possible to functionalize the surface of NPs, with covalently bound carboxy (-COOH) or amino groups ($-NH_2$) as the most common types of functionalization. Another meaningful surface modification is the covalent attachment of poly(ethylene glycol) chains (PEGylation) as a way to control protein adsorption.

However, a drawback of PS-NPs is their lack of biocompatibility and biodegradability. This is overcome by the use of biocompatible polymers such as polylactic acid (PLA), dextran or hydroxylethyl starch (HES). Biodegradable hydroxylethyl starch nanocapsules (HES-NCs) can be obtained by inverse miniemulsion polymerization.[59] It is further possible to load HES-NCs with a hydrophilic cargo, providing the possibility for a future use as drug delivery system.

Targeting of certain cell types by nanocarriers can be achieved by the linkage of a specific targeting group to the nanocarrier, which is recognized by a certain receptor of the target cell. The targeting group is usually covalently bound to the surface of the nanocarrier. For example, dendritic cells are successfully targeted with mannose or trimannose *via* the mannose receptor.[60-61] This has been shown for modified HES-NCs already.[62-63]

2.2.2 Protein corona formation, relevance for biological response to nanocarriers

Once a nanocarrier is incubated with blood, blood plasma or serum, proteins will immediately adsorb to its surface. The resulting layer (or multiple layers) of proteins is commonly referred to as the protein corona.

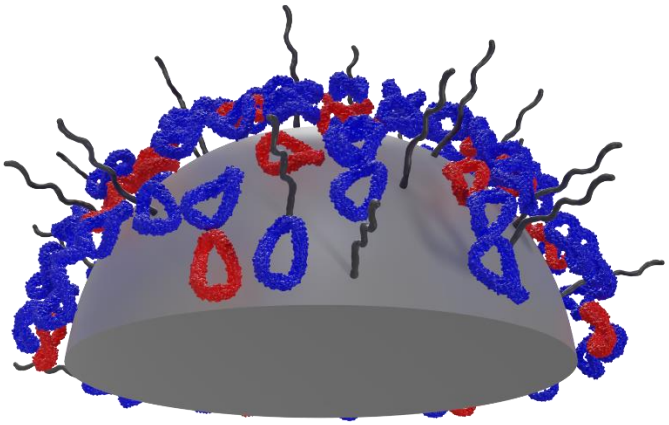

Figure 2.2.2 Protein corona on a PEGylated nanoparticle (illustration). Artwork copyright by [redacted].

The protein corona is the crucial factor for the biological fate, the *in vivo* behavior of a nanocarrier. The nanocarriers "chemical identity", *i.e.* the nature of the surface after synthesis, only plays a minor role when it comes to the biological behavior of nanocarriers.[7] Blood circulation time, specific and unspecific cellular uptake are mainly determined by the protein corona, even targeting capabilities can be compromised by protein adsorption.[64]

The protein corona should not be understood as a static entity, but rather as a dynamic system at the interface. The Vroman effect describes one aspect of this dynamic system: shortly after incubation, the protein corona contains a large number of highly abundant, but weakly bound proteins (*e.g.* human serum albumin, HSA). These are replaced on a longer time scale by low abundant, but strongly binding proteins (*e.g.* apolipoproteins).[65-66] Therefore, the amounts of proteins in the corona can change over time, however the qualitative composition remains constant.[30]

In literature, a differentiation between the so called hard and soft protein corona is made. The hard corona refers to proteins with a high binding affinity to the nanocarrier, which are not washed off upon centrifugation. The soft corona includes more loosely associated proteins with relatively low binding affinities, presumably forming a more diffuse outer layer of the corona, which is stripped off during centrifugation. However, centrifugation conditions are often inconsistent between different groups, so the terms hard and soft corona bear some indeterminacy.

For protein adsorption to nanocarriers, hydrophobic interactions play a major role on a molecular level. Electrostatic interactions and hydrogen bonding are only of minor relevance for protein-nanocarrier-interactions.[67] According to the Gibbs-Helmholtz equation (equation 3.9), the driving force of protein adsorption can be either a loss of enthalpy or a gain in entropy to obtain an exergonic (negative) value for the Gibbs energy ΔG. A gain in entropy is obtained by the release of water molecules forming the hydrophilic shell of the protein and the nanocarrier. When the protein and the

nanocarrier come into contact, the quite ordered state of water molecules bound to their surface is abandoned in favor of freely diffusing water molecules, which goes along with a gain of entropy.

In order to ensure a defined biological response to a nanocarrier, its protein corona needs to be controlled. The presence of certain corona proteins, which may act as opsonins or dysopsonins, is decisive for monocyte uptake and blood clearance. It has been reported that certain apolipoproteins (Apo-A1, CLU) reveal a dysopsonin behavior.[13] The aim for successful drug delivery is to avoid rapid blood clearance and achieve a "stealth effect", *i.e.* non-uptake by monocytes and long blood circulation time of the nanocarriers.

2.2.3 Stealth effect of nanocarriers through PEGylation

A common approach to achieve a stealth effect for nanocarriers is the covalent attachment of poly(ethylene glycol) chains to the surface (PEGylation).[20, 68-69] For PEGylated nanocarriers, PEG-chains form a shell of hydrophilic polymer chains around the surface. PEGylation generally reduces protein adsorption, but does not completely prevent it. The idea of completely oppressed protein adsorption as necessity of a stealth effect has been disproved.[13] In fact, certain proteins in the protein corona mediate the stealth effect by acting as dysopsonins.

As an alternative to PEG, other polymers such as poly(phosphoesters) (PPEs) were grafted to the nanocarrier surface in the past. A similar stealth effect is achieved with these polymers, which are, in contrast to PEG, biodegradable.[13] Thinking of further approaches to a stealth effect, the question about the necessity of covalent binding of the polymer chains to the nanocarrier arises. Simple physical adsorption of appropriate polymers (or oligomers) could also be sufficient. However, the binding affinity of appropriate stealth polymers should be sufficiently high, so upon incubation with proteins, which compete for binding to the nanocarrier, desorption of the stealth polymer can be largely excluded.

2.2.4 Properties of poly(ethylene glycol) and its application as stealth polymer

As described above, the surface modification with PEG is a common method to obtain a stealth effect for different types of nanocarriers. The fact that PEG is a non-toxic, FDA approved compound qualifies it for an application as stealth polymer.[16] The chemical structure of PEG is shown in Figure 2.2.3.

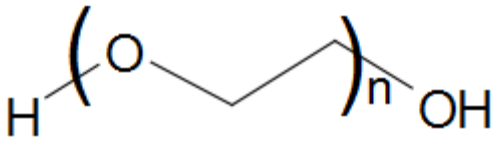

Figure 2.2.3 General structure of PEG, with repeating unit and hydroxyl end group.

PEG is both soluble in water and in nonpolar organic solvents, however the reasons for the hydrophilicity of PEG are still not completely understood.[70] Interestingly, the homologs poly(methylene oxide) and poly(propylene oxide) are not soluble in water.[71] In aqueous solution, PEG chains form a loose coil structure.[72]

Overall protein adsorption is significantly reduced for PEGylated nanocarriers compared to bare ones.[69] For example, it has been shown that a dense layer of PEG-brushes reduces adsorption of fibronectin.[73] Further, the protein adsorption to PEG-nanocarriers depends strongly on the chain length and the PEG chain density on the particle surface.[20] However, the stealth effect of PEG-NPs is not only based on a reduced overall protein adsorption, but on the selective adsorption of a few specific proteins.[13] Strongly reduced macrophage uptake has been observed for presence of specific proteins like Apo-A1 and CLU in the protein corona.

Concerning the biological behavior, stealth nanocarriers bear advantages compared to non-stealth systems. PEG-nanospheres for example show increased blood circulation times and reduced liver accumulation.[69] Increased blood circulation time is connected to reduced phagocyte uptake, which could be observed for PEGylated protein nanocapsules and numerous other PEG-nanocarriers.[20, 74] A long blood circulation time is desirable for specific cell targeting and therefore for successful drug delivery.

2.3 Surfactants for stabilization and surface modification

2.3.1 Colloidal stabilization through surfactants

Colloidal dispersions can undergo aggregation and subsequent sedimentation of the nanoparticles because reduction of the surface is energetically favored. This driving force causes inter-particle attraction and leads to the formation of multi-particle aggregates. The aggregation behavior of nanoparticles in aqueous dispersion is described by the DLVO theory of Derjaguin, Landau, Verwey and Overbeek.

This limitation of colloidal stability is tackled by two approaches: steric (nonionic) and electrostatic (ionic) stabilization. For steric stabilization, bulky polymers are attached to the nanoparticle surface to prevent their close approximation. Electrostatic stabilization is achieved through alike charge of the particles, which results in repulsive electrostatic forces. Both approaches can be realized by the use of appropriate surfactants.

Nonionic surfactants, such as Lutensol® or TWEEN®, consist of a hydrophobic and a hydrophilic block. In an aqueous dispersion of polymeric NPs (*e.g.* hydrophobic PS-NPs), the hydrophobic tail adsorbs to the particle surface and the hydrophilic block reaches into the aqueous phase, providing steric stabilization.

Ionic surfactants like sodium dodecyl sulfate (SDS) or cetyltrimethylammonium chloride (CTMA-Cl) are composed of a hydrophobic tail and charged head group. Their tail adsorbs to the particle material, so the charged head group remains fixed on the surface. This additional charge with like sign on all particles results in electrostatic repulsion, so aggregation is prevented. The zeta potential of a nanoparticle dispersion gives an idea of the surface charge of the particles and therefore represents an indicator for the degree of electrostatic stabilization.

To evaluate and compare the potential of a surfactant, different parameters can be regarded. The critical micelle concentration (CMC) is the threshold above which micelles are formed in aqueous solution. The CMC depends on the nature of the surfactant (ionic/nonionic), the length of the hydrophobic chain and the type of hydrophilic group, among others. Another classification is based on the "hydrophilic-lipophilic-balance" (HLB) by Griffin.[75] The HLB value of a nonionic surfactant is calculated according to the following equation 2.1:

$$HLB = 20\,\frac{M_H}{M_H + M_L} \qquad 2.1$$

with M_H being the mass of the hydrophilic fragment and M_L the mass of the hydropobic fragment. The HLB value is a measure of the hydrophilicity respective hydrophobicity of a surfactant.

2.3.2 Interaction of surfactants with proteins

It is long known that sufficient levels of ionic surfactants, such as sodium dodecyl sulfate (SDS), can denature certain proteins.[38-41] For SDS concentrations above 1 mM, complete denaturation was reported for ovalbumin.[39] In SDS polyacrylamide gel electrophoresis (SDS-PAGE), the process of surfactant denaturation is exploited to unfold and linearize the protein chains, allowing a separation of the proteins by chain length (proportional to mass) on the gel.

For ionic surfactants, typically binding of the surfactants' ionic head groups to charged regions of the protein through electrostatic interaction occurs.[43-45] There might be an additional class of surfactant

binding with low affinity, namely of their hydrophobic tails with hydrophobic pockets of the protein as reported by Nielsen *et al*.[46] Depending on the nature of the surfactant and its concentration, binding to proteins is possible as individual surfactant monomers or as micelle-like clusters.[45] Unfolding rates for charged ionic surfactants are very high, while unfolding occurs rather slowly for nonionic and zwitterionic surfactants.[76] For some proteins, the native state may also be stabilized by surfactant binding and the free energy of denaturation increases.[47,77]

In most cases, ionic surfactants already denature proteins at low concentrations (often below their CMC), while neutral, nonionic surfactants do not tend to denature proteins.[78] In contrast, especially nonionic surfactants are used for stabilization of protein formulations against denaturation and aggregation. [43, 77] Further, surfactants may also increase protein solubility, which may be of importance for pharmaceutical formulations.[43]

Different physicochemical mechanisms have been proposed to describe the binding of ionic surfactants to proteins, so for example the ability of anionic surfactants to interact with lysine residues located in hydrophobic pockets. This process is based on a combination of electrostatic and hydrophobic interactions and is a possible explanation for the increased temperature stability of β-lactoglobulin upon incubation with SDS.[79]

3 Characterization Methods

3.1 Dynamic light scattering

Fundamentals of light scattering have been covered in detail in standard literature.[80-82] In this chapter, only a brief description of the most important aspects is given.

Light as an electromagnetic wave can induce an oscillating dipole in a molecule. This dipole in turn emits an electromagnetic wave of the same wavelength as the incoming wave, which is irradiated isotropically in all directions perpendicular to the oscillating dipole. Figure 3.1.1 shows the scattered wave emitted at an angle θ with the intensity I.

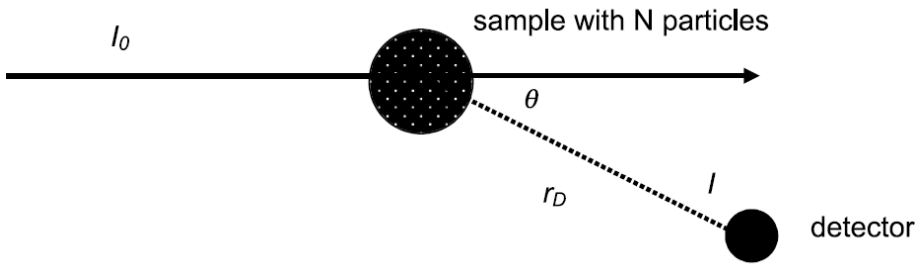

Figure 3.1.1 Schematic principle of light scattering.[80] With permission from Springer Science + Business Media.

A laser is used as the light source in order to obtain coherent, monochromatic light. This enables to monitor small fluctuations of the scattering intensity due to Brownian movement of the scattering centers, as depicted in the top panel of Figure 3.1.2. These fluctuations are analyzed regarding the time intervals τ on which they occur, which leads to the intensity autocorrelation function (bottom panel). From this, the diffusion velocity can be deduced, which in turn is directly correlated with the hydrodynamic radius of the diffusing species *via* the Stokes-Einstein-equation (equation 3.6).

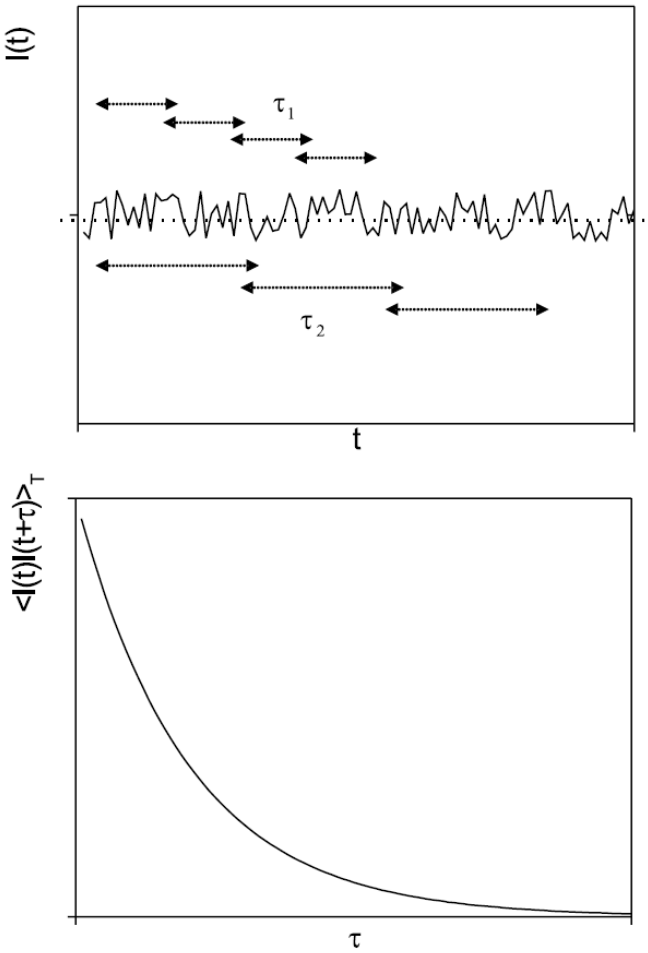

Figure 3.1.2 Principle of DLS data analysis.[80] From fluctuations of the scattering intensity over time (top panel) the intensity autocorrelation function (bottom panel) is derived. With permission from Springer Science + Business Media.

3.1.1 DLS data analysis

To evaluate the formation of nanoparticle aggregates in plasma samples, an analysis according to Rausch *et al.*[83] can be applied. The sum of the autocorrelation functions (ACF) of each individual component (nanoparticles and plasma) is defined as fixed parameters and the respective intensity fractions of the components as well as an additional diffusion process in respect to potentially formed aggregates are used as variables.

For the ACF of plasma, the sum of three exponential terms as given in equation 3.1 is a good approximation:

$$g_{1,P}(t) = a_{1,P}\ \exp\left(-\frac{t}{\tau_{1,P}}\right) + \ a_{2,P}\ \exp\left(-\frac{t}{\tau_{2,P}}\right) + \ a_{3,P}\ \exp\left(-\frac{t}{\tau_{3,P}}\right) \qquad 3.1$$

Amplitudes are denoted by a_i and decay times by $\tau_i = \frac{1}{q^2 D_i}$ with the absolute scattering vector $q = \frac{4\pi n}{\lambda_0} \sin\left(\frac{\theta}{2}\right)$ and the Brownian diffusion coefficient of component i, D_i.

The ACF of pure NPs in dispersion can be fitted by a biexponential function as given in equation 3.2:

$$g_{1,NP}(t) = a_{1,NP}\ exp\left(-\frac{t}{\tau_{1,NP}}\right) + a_{2,NP}\ exp\left(-\frac{t}{\tau_{2,NP}}\right) \qquad 3.2$$

For the analysis of NPs incubated in plasma, a combination of the ACF of plasma and NPs is used in the case of no aggregation. This sum of the individual ACFs, the so-called force fit $g_{1,m}(t)$, contains the intensity contributions f_P for plasma and f_{NP} for nanoparticles and is given in equation 3.3:

$$g_{1,m}(t) = f_P g_{1,P}(t) + f_{NP} g_{1,NP}(t) \qquad 3.3$$

In the case of aggregation, this simple sum of the two components cannot adequately describe the resulting ACF. An supplemental ACF $g_{1,agg}(t)$ with a longer relaxation time $\tau_{1,agg}$ for the larger aggregates needs to be added:

$$g_{1,agg}(t) = a_{1,agg}\ exp\left(-\frac{t}{\tau_{1,agg}}\right) \qquad 3.4$$

This results in the overall correlation function with the intensity contribution of the aggregates f_{agg} in equation 3.5:

$$g_{1,m}(t) = f_P g_{1,P}(t) + f_{NP} g_{1,NP}(t) + f_{agg} g_{1,agg}(t) \qquad 3.5$$

The diffusion coefficient *D* is then extrapolated for $q^2 = 0$. From this value, the hydrodynamic radius R_h is calculated using the Stokes-Einstein-equation:

$$R_h = \frac{k_B\, T}{6\pi\eta D} \qquad 3.6$$

For analysis of multicomponent systems in the framework of this thesis, the software HDRC (programmed by [redacted]) was used.

3.2 Isothermal titration calorimetry

Isothermal titration calorimetry (ITC) is a technique, which allows measuring the enthalpic interaction of two components. The components can be single compounds or mixtures thereof. For interactions between two single compounds, interaction parameters as binding affinity, stoichiometry and binding enthalpy are derived from the ITC data.

The ITC instrument contains a reference cell, filled with deionized water for experiments with aqueous systems, and a measurement cell as depicted in Figure 3.2.1. The measurement cell, which contains compound A, is stirred continuously and the titrant (compound B) is added stepwise by an automatically operated syringe. Experiments are carried out at constant temperature, which is maintained by a Peltier element, and the difference in the heating (respectively cooling) rate between the two cells is recorded.

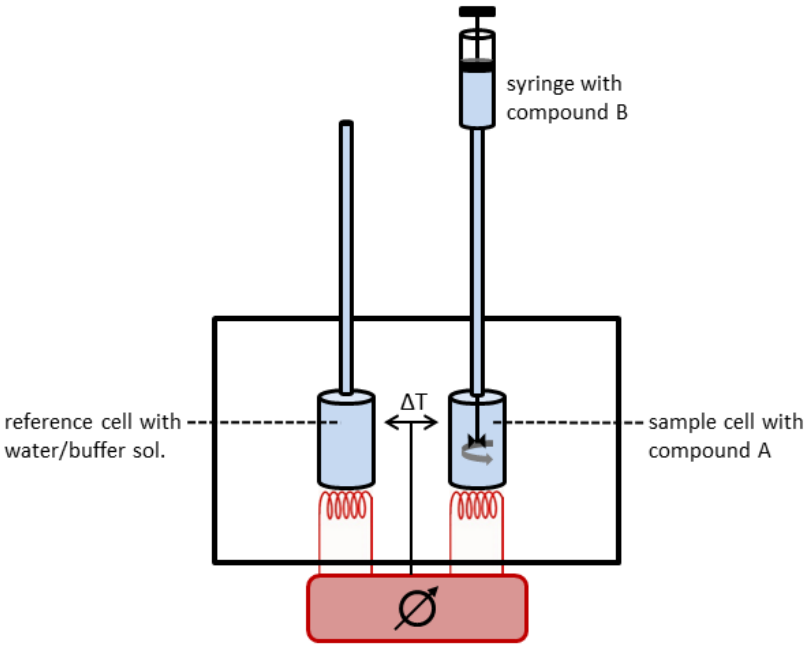

Figure 3.2.1 Schematic illustration of an ITC measurement setup.

The raw data are plotted as heat rate versus time as shown in Figure 3.2.2. For all titration experiments, the heat of dilution of the titrant needs to be considered. Therefore, the measurement cell is filled with water and the titrant (compound B) is added stepwise. This heat of dilution is deducted from the signal of the actual titration experiment of compound A titrated with compound B. The reversed heat of dilution, titrating water into the measurement cell filled with compound A, is usually much smaller and can therefore be neglected.

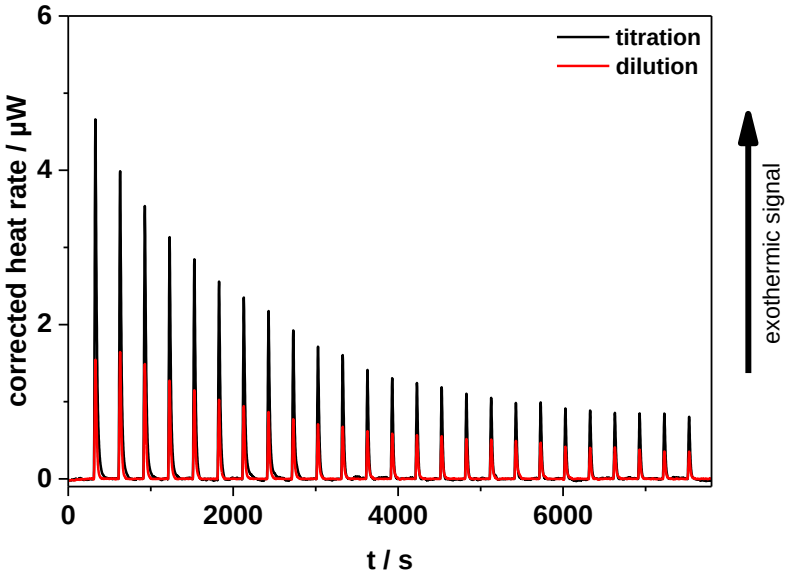

Figure 3.2.2 Raw data in ITC, plot of heat rate versus time. In black, the signal of the actual titration experiment is shown, whereas the red line indicates the signal for a titration of the titrant (compound B) into water.

Integration of the raw data over time and subtraction of the heat of dilution yields the adsorption isotherm. This is plotted as heat versus ratio of the two compounds as shown in Figure 3.2.3 and analysis with a suitable fit function is performed. From the sigmoidal shape of the fit, adsorption parameters are approximated graphically: the stoichiometric ratio n is identified as the x-axis value of the inflection point, the binding affinity K_a corresponds to the slope and the binding enthalpy ΔH is obtained from the difference of the plateaus.

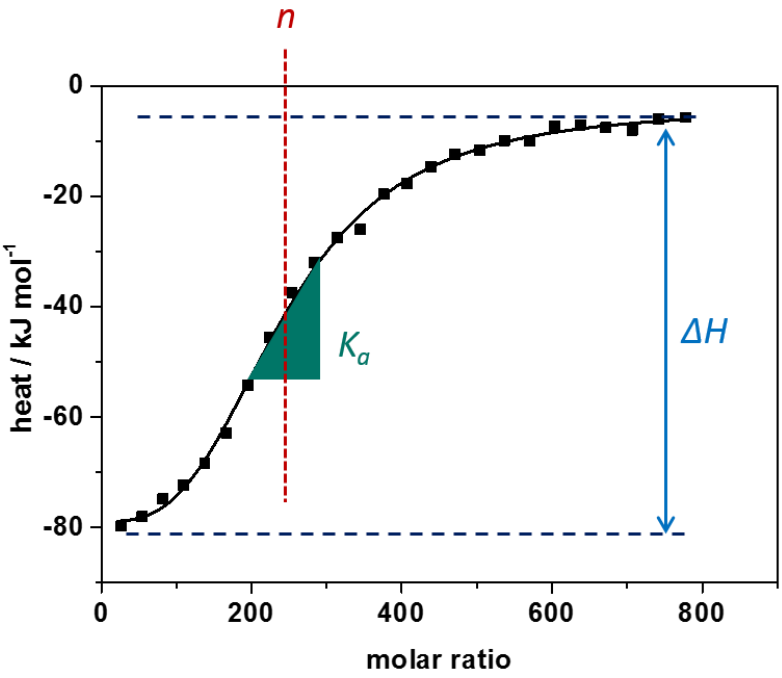

Figure 3.2.3 Adsorption isotherm as obtained from an ITC experiment. An independent binding model fit is shown and the determination of the fit parameters *n*, K_a and *ΔH* is shown schematically.

For a precise mathematical analysis, the adsorption isotherms are analyzed with a fit according to an independent binding model as given in equation 3.7.[84-85] For this model it is assumed that a ligand L binds independently to one site of a macromolecule M without any cooperativity effects.

$$\Delta q = \left(\frac{(n[M]K_a + [L]K_a + 1) - \sqrt{(n[M]K_a + [L]K_a + 1)^2 - 4N{K_a}^2[M][L]}}{2K_a} \right) - [ML]_{n-1}\Delta\mathrm{H}\Delta V_{cell} \qquad 3.7$$

The fit yields values for the parameters n, K_a and ΔH, whereas $[M]$ is given as the concentration of the macromolecule, $[L]$ as the concentration of the ligand, $[ML]$ as the concentration of the formed complex and ΔV_{cell} as the change of the total cell volume during the titration. To calculate the entropy change ΔS of the reaction, the right hand side of the reaction isotherm equation (equation 3.8) was equated with the right hand side of the Gibbs-Helmholtz equation (equation 3.9) and solved for ΔS (equation 3.10).

$$\Delta G = -RT \cdot \ln K_a \qquad 3.8$$

$$\Delta G = \Delta H - T \cdot \Delta S \qquad 3.9$$

$$\Delta S = R \cdot \ln K_a + \frac{\Delta H}{T} \qquad 3.10$$

In these equations, ΔG is the Gibbs free energy, R is the universal gas constant and T the temperature, so the entropy change ΔS can be calculated for known K_a and ΔH.

3.3 Sodium dodecyl sulfate polyacrylamide gel electrophoresis (SDS-PAGE)

Sodium dodecyl sulfate polyacrylamide gel electrophoresis (SDS-PAGE) is used as a method to separate proteins by their molecular mass. A protein mixture is incubated with SDS and heated to denature the proteins to add negative charge in proportion to their masses. The proteins are then loaded on a polyacrylamide gel as matrix and an electric field is applied. Due to their negative charge, proteins migrate through the pores of the matrix towards the anode. Smaller proteins can migrate more easily through the pores of the gel, whereas larger ones are rather retained. Thus, a separation of the proteins by their mass is achieved. As reference, a marker with proteins of known size is run in parallel to the sample. After the electrophoresis, a staining is applied to make the proteins visible. Coomassie Blue and silver staining are common staining reagents, which were used in this work.

3.4 Differential scanning fluorimetry

Differential scanning fluorimetry (DSF) enables to observe the thermal unfolding of a protein. It monitors the fluorescence of tryptophan, which depends strongly on its close surroundings.[86] This method works label-free, as most proteins contain tryptophan or alternatively tyrosine, which shows lower fluorescence though.

In a DSF measurement, protein samples are heated up running a defined temperature ramp and the intrinsic fluorescence is recorded at two wavelengths (350 nm and 330 nm) during excitation with an LED. For analysis, either each single wavelength or the ratio of the two wavelengths are plotted against the temperature. While the single wavelength plot contains information about the course of the absolute fluorescence, the ratio also reveals if a blue- or redshift of the fluorescence occurs. An inflection point in either of the fluorescence curves represents a structural transition (melting point T_m) of a protein. To facilitate data analysis, usually the first derivative of the fluorescence curve is calculated, so inflection points appear as local extrema and are identified more easily as indicated in Figure 3.4.1.

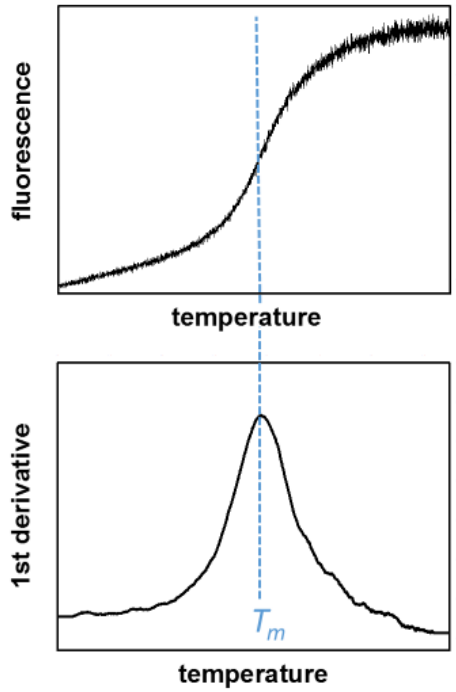

Figure 3.4.1 Illustration of data analysis in DSF.

Subsequent to the unfolding measurement, an optional refolding experiment can be performed by lowering the temperature at a constant cooling rate. For some proteins, again a transition in the fluorescence is observed at the melting point T_m, which indicates (partial) refolding.

3.5 Zeta potential

The zeta potential describes the electrokinetic potential around the surface of a particle in colloidal dispersions. For a charged particle, oppositely charged ions will adsorb electrostatically directly on its surface, forming the so-called 'Stern layer'. For example, a negatively charged particle as shown in Figure 3.5.1 will carry a layer of cations on its surface. More distant to the surface, loosely associated ions form the 'shear plane', which does not move with the particle in an electric field. The potential, which builds up at this 'shear plane', is called the zeta potential.

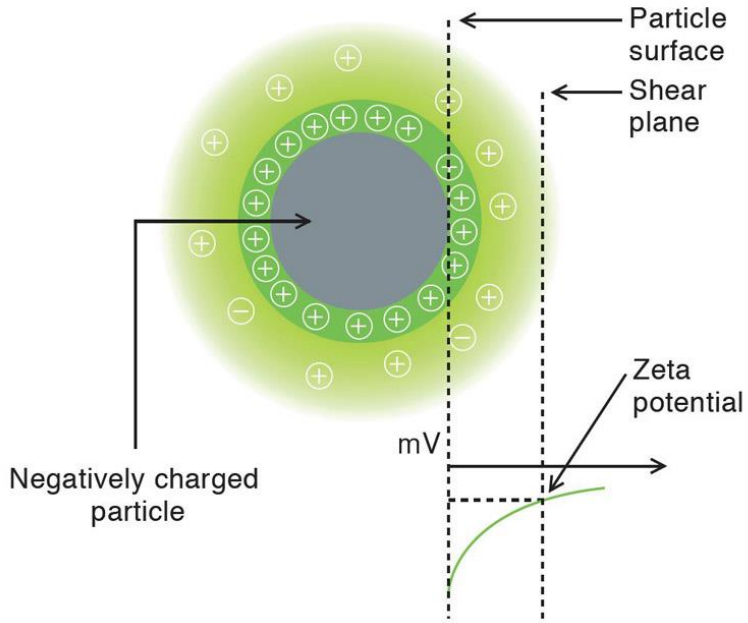

Figure 3.5.1 Charge layers around a particle and illustration of the zeta potential.[87]

Measurement of the zeta potential is possible *via* laser Doppler electrophoresis, where the movement of a particle through an electric field is monitored by the scattered light of a laser beam. With this method, the electrophoretic mobility *U* is determined, from which the zeta potential is calculated using the Smoluchowski equation (equation 3.11):

$$\zeta = \frac{\eta\, U}{\varepsilon} \qquad 3.11$$

The viscosity η and the dielectric constant ε of the sample are typically known. This equation is applied for particles larger than 200 nm dispersed in electrolytes with > 10^{-3} M salt.

The value of the zeta potential is not equal to the surface charge of a particle (as it is not measured directly at the surface), but proportional to it. The zeta potential can be considered as an indicator for the stability of a colloidal dispersion: a high absolute value suggests an electrostatically well stabilized dispersion.

4 Results and Discussion

4.1 Coating nanoparticles with tunable poly(phosphoester) surfactants facilitates control over the protein corona

For a stealth effect of nanocarriers a controlled protein corona with a specific pattern is required. Certain apolipoproteins in the corona of a nanocarrier are responsible for the stealth effect, and special surface modification of the nanocarrier is necessary to promote adsorption of these proteins. PEGylation has been a standard modification procedure to create a stealth effect of nanocarriers. In this chapter, a new approach to stealth nanocarriers is introduced, namely the physical adsorption of surfactants as an alternative surface modification.

Nanoparticles with long blood circulation time are a prerequisite for targeted drug delivery. To make the nanoparticles invisible for phagocytizing cells, functional moieties on the particle surface are necessary to attract specific so-called stealth proteins forming a protein corona. Currently, covalent attachment of those moieties represents the only way to achieve that attraction. However, that approach requires a high synthetic effort and is difficult to control. Therefore, the coating of model nanoparticles with biodegradable polymeric surfactants as an alternative method is investigated.

The results described in this chapter are published in *Biomaterials*, vol. 115, pages 1 – 8 and permission for reproduction was granted by Elsevier. Several persons (all from MPI-P) were involved in this project: [redacted] carried out the synthesis and characterization of the surfactants, [redacted] conducted zeta potential as well as some of the ITC measurements and [redacted] contributed the cellular uptake studies (cell culture and flow cytometry), the protein assay and SDS-PAGE. I planned all and conducted most of the ITC experiments, carried out DLS measurements, created the figures and wrote the manuscript.

4.1.1 Surfactant characterization and adsorption properties

Polystyrene NPs prestabilized with sodium dodecyl sulfate (SDS) were used as a model system to study the interaction with PPE-surfactants and plasma proteins. The NPs were prepared by [redacted] (MPI-P) *via* miniemulsion polymerization as described previously and dialyzed against deionized water for 24 h for purification.[21] Characterization with regards to size and charge was performed by dynamic light scattering and zeta potential measurements. A hydrodynamic diameter of ~108 nm and a narrow size distribution (PDI = 0.028, see Figure 4.1.9) as well as a zeta potential of −49 mV were obtained. The negative zeta potential indicates that even after dialysis there is still a certain small amount of SDS remaining in the dispersion, which is necessary to ensure colloidal stability.

For surface modification of the NPs, two different classes of PPE-surfactants were studied. All surfactants were synthesized by or under the supervision of [redacted] (MPI-P). Surfactants L1 and L2 are the PPE-analog of Lutensol®, a widely used commercial surfactant, as the only difference in structure is the replacement of the PEG block in Lutensol® by a PEEP-block (Figure 4.1.1). In these Lutensol®-analog surfactants, the hydrophobic part was not varied. In the diblock-copolymer surfactants B1 and B2, the hydrophobic as well as the hydrophilic part can be varied by adjusting the length of the respective block (Figure 4.1.1).

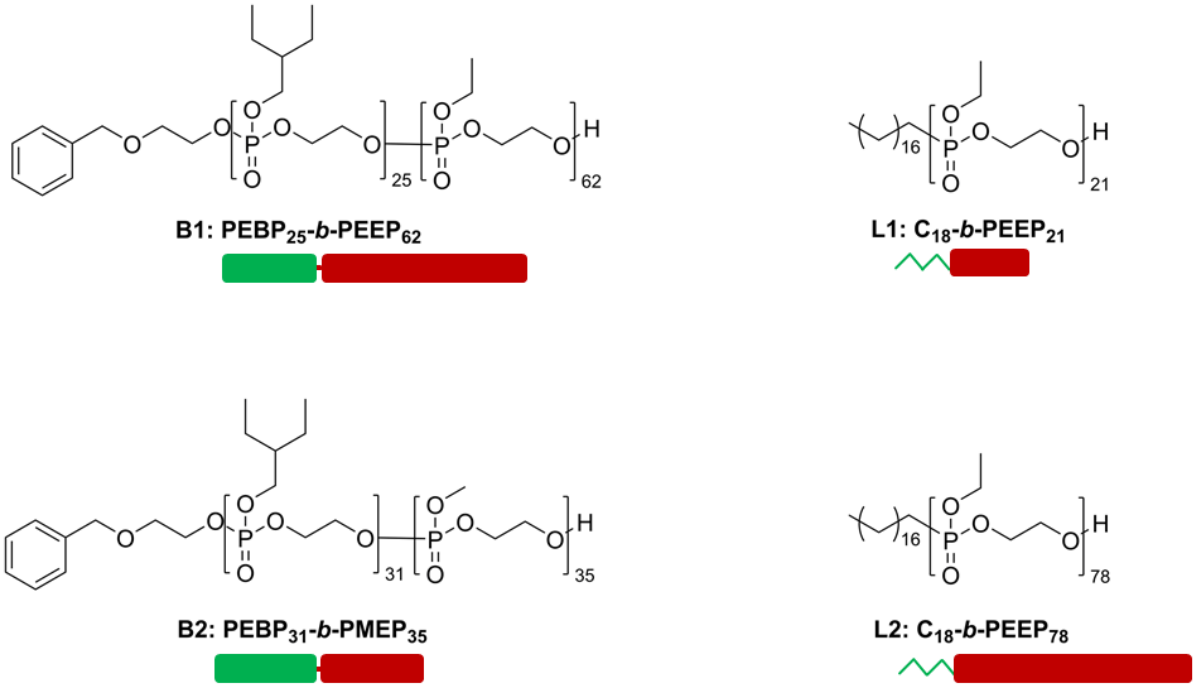

Figure 4.1.1 Chemical structure of PPE-surfactants: Diblock copolymer surfactants (**B1, B2**) and PPEs terminated with a C_{18}-alkyl chain (**L1, L2**) have been used for nanoparticle coating.

To characterize the thermodynamics of surfactant adsorption, isothermal titration calorimetry (ITC) is applied to measure the enthalpy changes arising from the interaction between two different components directly, which makes it a very useful tool in this study. The thermodynamic parameters of surfactant adsorption on polystyrene NPs, such as association constant K_a, binding enthalpy ΔH, and stoichiometry n of surfactant molecules per NP could be determined by ITC by analyzing the heat changes of the adsorption according to an independent binding model (Figure 4.1.2). The results are

displayed in Table 4.1.1. Surfactants with a larger PEEP-block exhibit a higher association constant K_a, whereas the number of surfactant molecules *n* adsorbing to one NP is lower in this case. Particularly for the Lutensol®-analog surfactants L1 and L2 this trend is quite obvious. The fact that less surfactant molecules adsorb to one NP with increasing chain length can be understood intuitively as this is basically a question of space requirements of the hydrophilic block. The values obtained for the surface area per surfactant molecule in Table 4.1.1 have been calculated by dividing the surface area of one NP (~31000 nm²) by the stoichiometric factor *n.* It can clearly be observed that the surface area occupied by one surfactant molecule depends strongly on its structure and chain length respectively.

The variation of the association constant K_a, however, is more difficult to understand and cannot be assigned to the length of the hydrophobic block as it would be expected initially. In fact, longer hydrophilic PEEP-blocks result in an increased K_a. Therefore, it needs to be kept in mind that the PEEP block is not completely hydrophilic and that there might be some hydrophobic interactions, for example of the ethyl side chain with the NP surface.

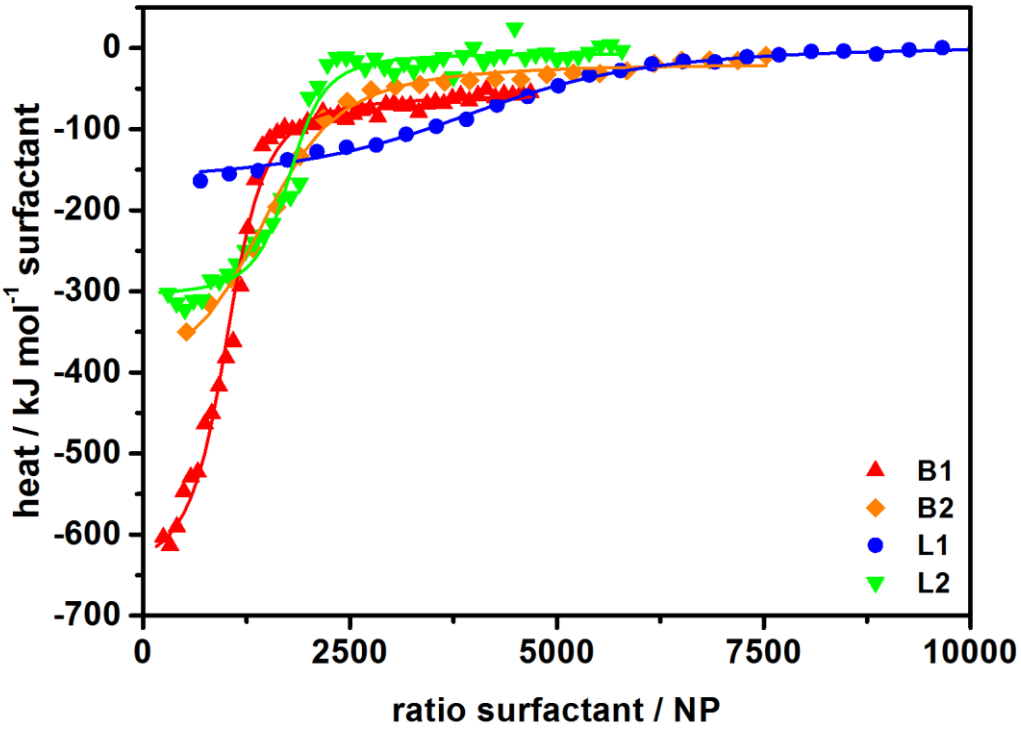

Figure 4.1.2 Exemplary ITC adsorption isotherms of the titration of PS-NPs with four different surfactants B1, B2, L1 and L2 with an independent binding model fit (colored solid lines).

Table 4.1.1 Surfactant adsorption parameters on nanoparticles obtained from ITC measurements applying an independent binding model fit. Mean values of triplicates are given with the standard deviation.

#	structure	K_a / 10^5 L mol^{-1}	n	ΔH / kJ mol^{-1}	ΔS / J K^{-1} mol^{-1}	area per surfactant molecule / nm²
B1		9.5 ± 0.3	1000 ± 30	-594 ± 10	-1878 ± 33	31
B2		3.5 ± 0.3	1530 ± 60	-383 ± 13	-1179 ± 44	21
L1		1.7 ± 0.2	4310 ± 170	-161 ± 7	-439 ± 23	7
L2		16.3 ± 3.9	1350 ± 60	-423 ± 9	-1299 ± 30	23

4.1.2 Impact of surfactant-coating on protein corona

To investigate the effect of surfactant-coating on protein adsorption, the interaction of blood plasma and HSA with surfactant-coated NPs has been studied with ITC. The NPs were loaded with the amount of each surfactant equal to the stoichiometric factor *n* (maximum amount of adsorbed surfactant molecules) determined by ITC for the adsorption of this particular surfactant on the NPs (Table 4.1.1). Diluted plasma (resulting HSA conc. ~8.8 g L^{-1}, total protein conc. 13.4 g L^{-1}) has been titrated to dispersions of surfactant-coated NPs, the respective heat rates are shown in Figure 4.1.3. Analog titrations have been conducted by [redacted] (MPI-P) with pure HSA instead of plasma, the heat rates are displayed in Figure 4.1.4. The integration of the heat rate over time yields the normalized heat *vs*. the molar ratio of plasma proteins per nanoparticle or surfactant shown in Figure 4.1.5. The molar concentration of HSA (which represents about 2/3 of plasma protein[88]) was used as the plasma protein concentration in order to be able to compare the measurements with the titration of pure HSA solution onto NPs. As a control, an aqueous solution of the surfactants without NPs (each with the same amount of surfactant as in the surfactant-coated NP-dispersions) was also titrated with diluted plasma (Figure 4.1.5-B) by [redacted]. Only for two surfactants a distinct enthalpic interaction could be observed, which is significantly lower than the corresponding interaction of diluted plasma with surfactant-coated NPs.

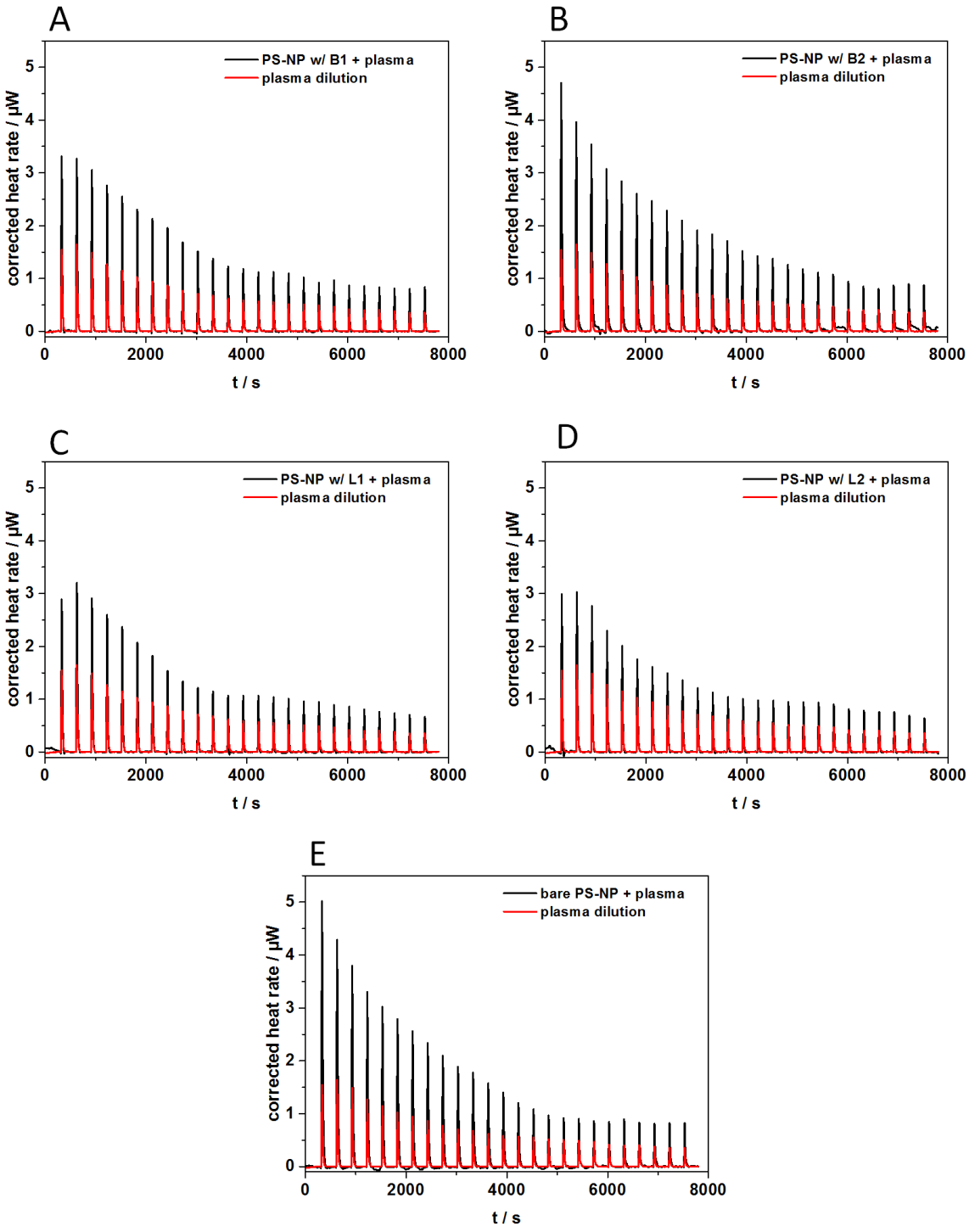

Figure 4.1.3 Heat rates as determined by ITC for the titration of bare (E) and surfactant-coated NPs (A) – (D) titrated with diluted plasma (5x with deionized water). The concentration of the NP dispersions (6 g L^{-1}, $1.5 \cdot 10^{-5}$ mM) was kept constant for all titrations while for the amount of each surfactant added to the NP dispersion, the stoichiometric factor *n* was taken into account. The heat rate of the dilution measurement, *i.e.* titration of diluted plasma into water is shown in each graph (red line –).

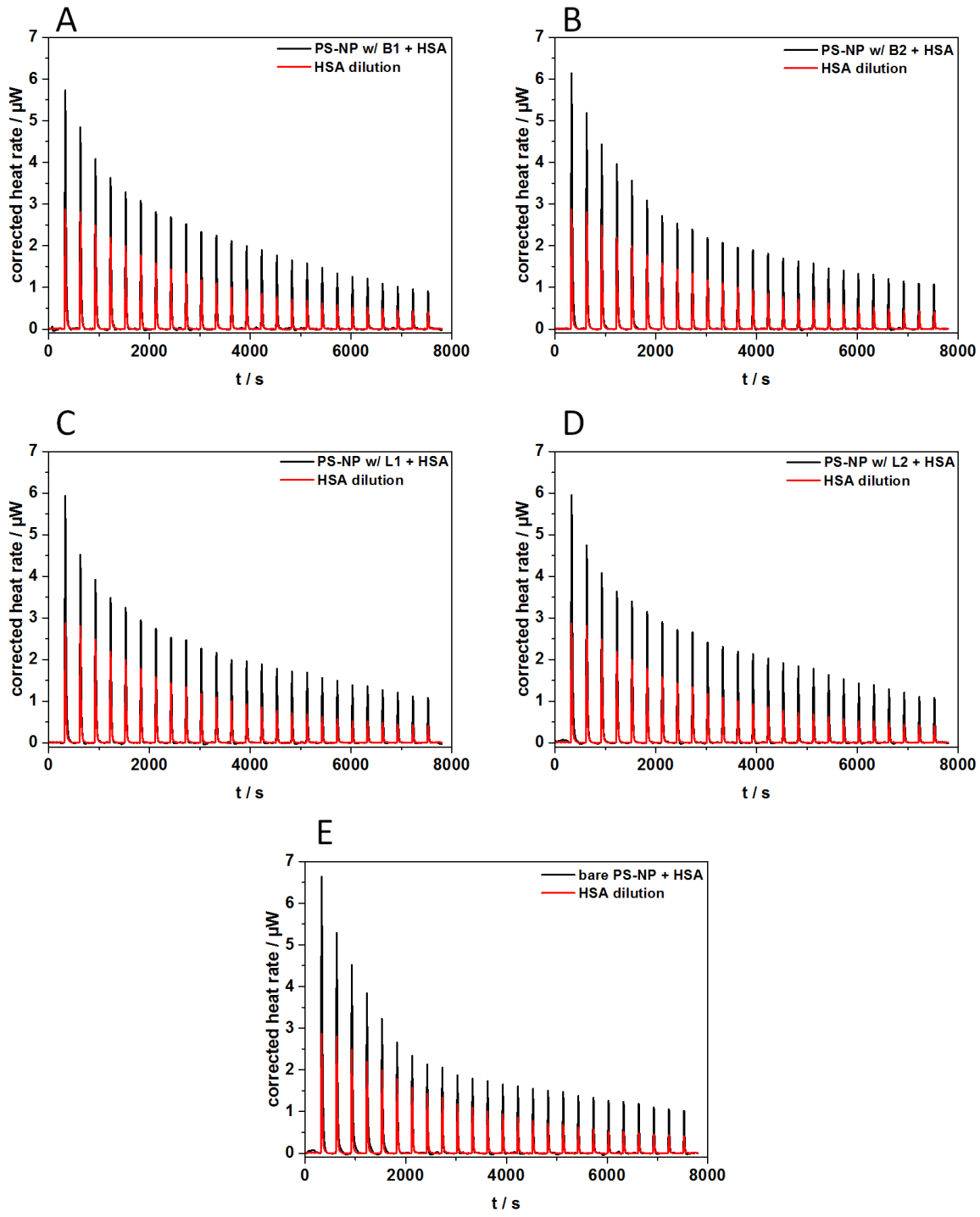

Figure 4.1.4 Heat rates as determined by ITC for bare (E) and surfactant-coated NPs (A) – (D) titrated with HSA in normal saline (9 g L^{-1}). The concentration of HSA (8.8 g L^{-1}, 0.133 mM) and of the NP dispersions (6 g L^{-1}, $1.5 \cdot 10^{-5}$ mM) was kept constant for all titrations. For the amount of each surfactant in the NP dispersions, the stoichiometric factor *n* was taken into account. As above, the heat rate of the dilution measurement (titration of HSA into water) is shown in each graph (red line –). Titrations were conducted by [redacted].

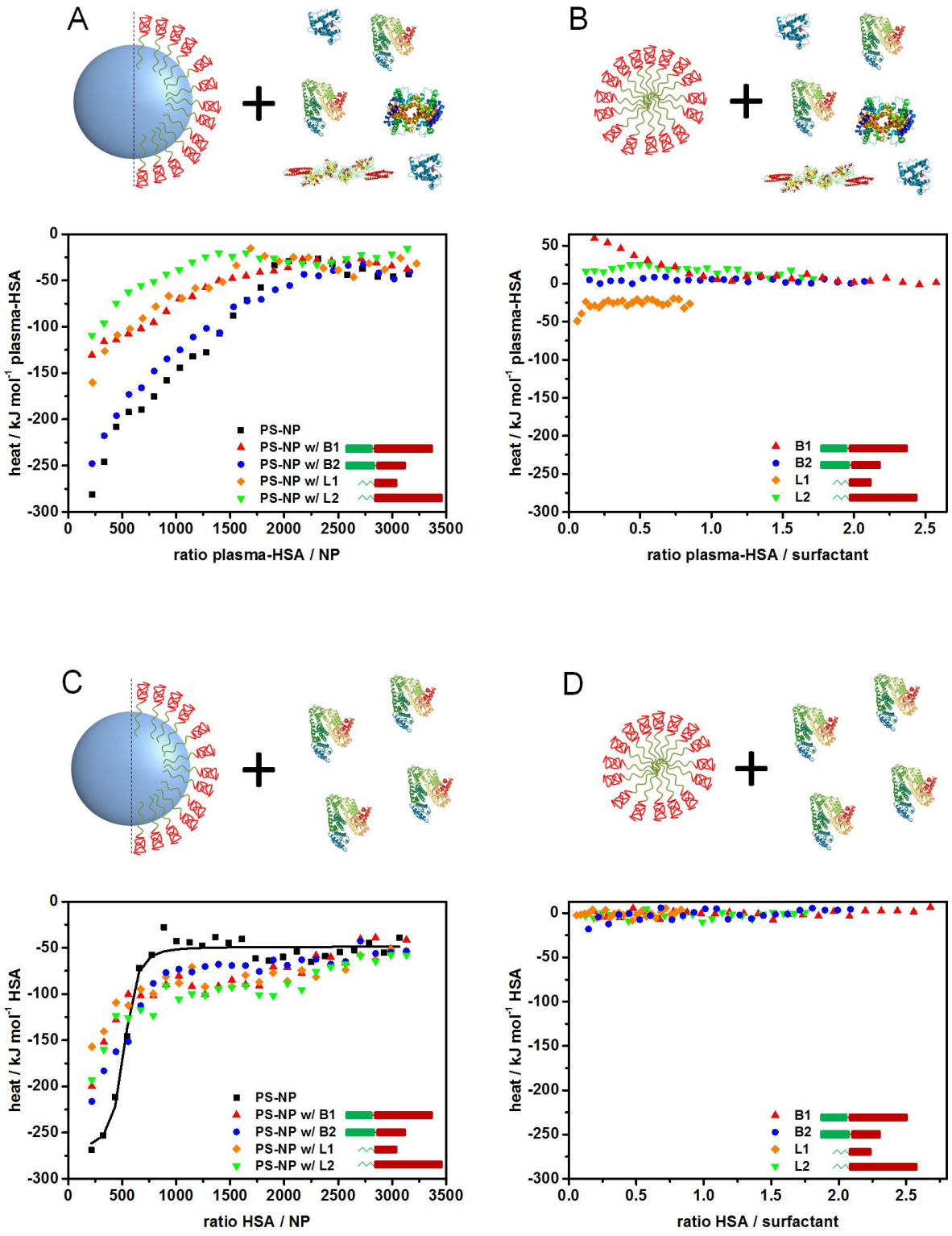

Figure 4.1.5 ITC data (adsorption isotherms) for the interaction of proteins with surfactant-coated NPs. (A) Aqueous dispersion of surfactant-coated and bare NPs titrated with diluted plasma (5x). (B) Aqueous solution of surfactants titrated with 5x diluted plasma. (C) Aqueous dispersion of surfactant-coated and bare NPs titrated with HSA-solution in normal saline. The black line (−) represents the

independent binding model fit. (D) Aqueous solution of surfactants titrated with HSA-solution in normal saline.

For all surfactant-coated NPs, the thermodynamic interaction with diluted plasma is less exothermic and presents a lower binding affinity (slope of the isotherm) than for bare NPs (black squares ■). Interestingly, the data points indicating the smallest heat (green triangles ▼) belong to surfactant L2 with the highest association constant K_a. In general, for both surfactant types the binding affinity decreases with lower block lengths of the hydrophilic block. However, the trend of decreasing protein binding affinity with increasing surfactant affinity is not universal comparing the two different surfactant types, so that it is assumed that the chemical structure itself also plays an important role.

Another aspect to consider is that the heat measured in these ITC experiments does not necessarily have to originate from protein adsorption but can also result from surfactant desorption. Thus, the interaction between proteins and surfactant-coated NPs could potentially involve a (partial) exchange of surfactant molecules by proteins on the surface of the NP. For a surfactant with a high association constant K_a the data suggests that surfactant desorption or exchange with proteins is less likely to occur compared to surfactants with a low association constant.

Similar to the experiment with diluted plasma, NPs coated with a stoichiometric amount of surfactant were titrated with a solution of HSA (8.8 g L^{-1}), as shown in Figure 4.1.5-C. The interaction of an aqueous solution of the surfactants without NPs with HSA was also measured as a control (Figure 4.1.5-D): None of the surfactants showed any specific thermodynamic interaction upon titration with HSA. The integrated heats for the titration of bare NPs with HSA (black squares ■) yield a sigmoidal adsorption isotherm, which is analyzed according to an independent binding model. From the fit, a binding affinity of $K_a = 1.62 \cdot 10^7$ L mol^{-1}, ΔH = -217 kJ mol^{-1} and n = 474 were obtained. However, the integrated heats for the interaction of HSA with surfactant-coated NPs can clearly be distinguished from those obtained for the bare NPs. Even for a lower ratio of HSA per NP, no sigmoidal curve could be observed for surfactant-coated NPs, so the mathematical fit yields no reliable adsorption parameters and is not shown here. From the shape of the curves it can still be concluded that the stoichiometric ratio of HSA per NP is significantly lower for surfactant-coated NPs compared to bare NPs.

To further evaluate the potential 'functional' effect of the surfactant coated NPs, zeta potential measurements of surfactant-coated and bare NPs incubated with pure HSA and full plasma as well as without any proteins were performed by [redacted]. NP-protein mixtures were centrifuged and resuspended in phosphate-buffered saline (PBS) to remove free proteins. In Figure 4.1.6, zeta potentials of nanoparticles without protein corona and with HSA or plasma corona are shown. It can

be seen that the surfactant coating did not change the surface charge of the NP significantly. When NPs are incubated with HSA the value of the zeta potential is increasing (becoming less negative), and even more so for incubation with plasma. As it is already known, adsorbed proteins are shielding the negative surface charge of the nanomaterials.[89] It seems that the negative charge of the bare nanoparticles incubated in HSA is shielded more than for the surfactant coated ones, which resembles the results obtained from ITC. However, comparing the surfactant coated NPs with one another no significant differences in the zeta potential can be noticed. This is probably due to the centrifugation and the removal of the soft protein corona, which results in a leveling of the zeta potential.

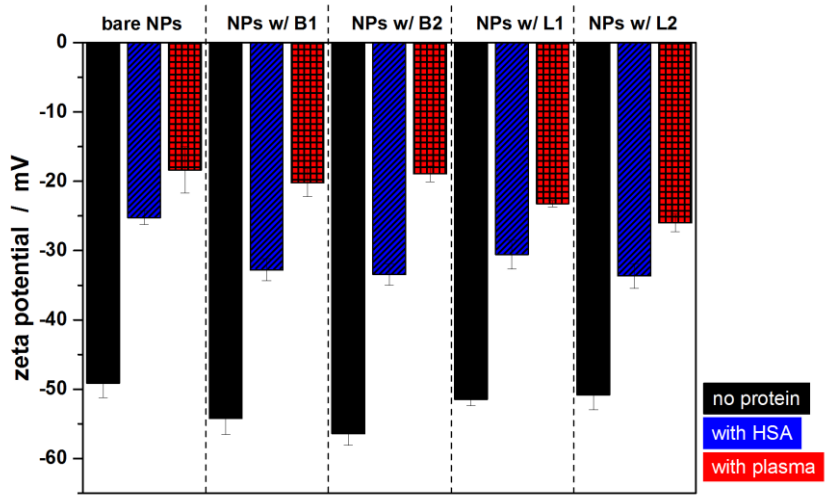

Figure 4.1.6 Zeta potential of NPs coated with stoichiometric amount of different surfactants. The zeta potential of the NP-dispersions was measured without further treatment (black columns) and after incubation with a HSA solution (44 g L^{-1}, blue columns) or undiluted citrate plasma (68 g L^{-1}, red columns). Incubated samples were centrifuged three times to remove excess protein. Sample preparation and zeta potential measurements were conducted by [redacted].

In order to determine the amount of strongly adsorbing proteins – the so-called hard protein corona[89-90] – on bare and surfactant-coated NPs incubated with plasma, a protein quantitation assay was carried out by [redacted] (MPI-P) after three centrifugation steps. The amount of hard corona proteins on bare NPs determined by a Pierce 660 nm protein assay (Thermo Fisher Scientific, Waltham, USA) exceeds the value for surfactant-coated NPs by about a factor of five (Figure 4.1.7). Further, the NPs coated with different surfactants do not show a significant difference in the amount of strongly adsorbed proteins, which – as seen for the zeta potential measurements – is probably a consequence of the centrifugation steps.

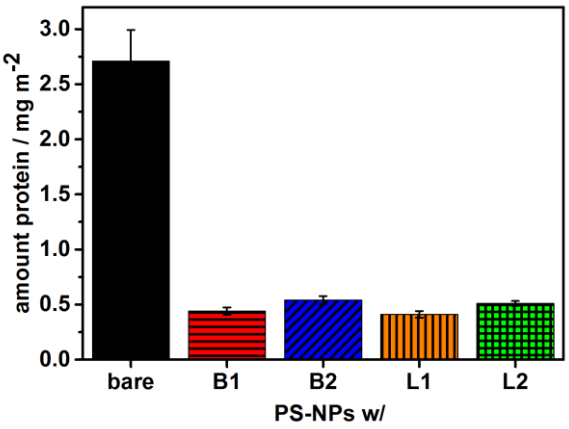

Figure 4.1.7 Total amount of protein recovered from the surface of bare and surfactant-coated NPs after three centrifugation steps determined by a Pierce 660 nm protein assay (mean values of triplicates with standard deviation are shown). Protein assay was carried out by [redacted].

Altogether, the conclusion drawn from the ITC data and zeta potential measurements that the protein adsorption on surfactant-coated NPs after incubation with plasma is decreased could be confirmed. These results are also in good agreement with the decrease of unspecific protein adsorption for many kinds of covalently PEGylated surfaces.

Subsequently, SDS-PAGE analysis was performed by [redacted] to analyze the composition of the hard protein corona on bare and surfactant-coated NPs after incubation with plasma. The NPs were centrifuged three times to remove excess protein and the remaining proteins of the hard corona were desorbed from the NP surface and applied to the gel. The gel with the protein pattern of bare and surfactant-coated NPs incubated with plasma as well as pure plasma as reference is shown in Figure 4.1.8. The most dominant protein bands in pure plasma can be identified as proteins with a high plasma concentration: HSA (~ 44 g L^{-1}, 67 kDa)[88], immunoglobuline G (IgG, ~10 g L^{-1}, heavy chain 50 kDa, light chain 25 kDa)[91] and Transferrin (~ 2.6 g L^{-1}, 75 kDa)[92]. The composition of the protein corona on bare NPs shows the most similarities to the protein pattern of pure plasma as HSA and IgG appear dominantly.

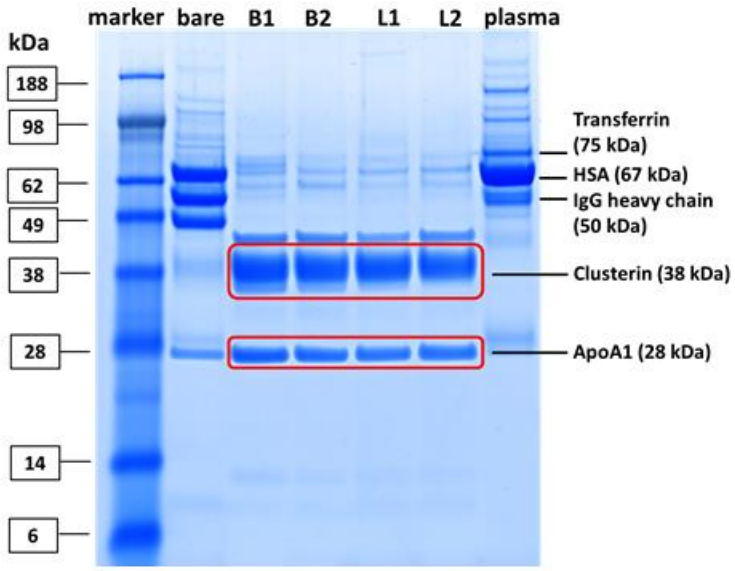

Figure 4.1.8 Protein pattern after SDS-PAGE of the 'hard' protein corona on bare and surfactant-coated NPs incubated with plasma. Proteins were detached from the NP surface after multiple washing steps using an SDS Tris*HCl solution. Pure plasma is given as a reference. The highlighted bands (red boxes) refer to clusterin (38 kDa) and apolipoprotein A1 (28 kDa). SDS-PAGE was performed by [redacted].

For the surfactant-coated NPs, the protein pattern differs significantly. The adsorption of HSA was drastically reduced while a prominent band at 38 kDa appeared (indicated in red). This pattern shows significant similarities to the one on PEGylated NPs reported previously.[5, 13, 19] The band at 38 kDa appears at the same molecular weight range as clusterin (apolipoprotein J), which is known to be one of the most abundant proteins on PS-NPs with PEG and PPE surface modifications although its plasma concentration is quite low.[19] The importance of clusterin for the stealth effect of nanocarriers has been revealed recently by coworkers of our group.[13] Additionally, a band at 28 kDa appears at the same molecular weight range as apolipoprotein A1, which was also found to be enriched on PEGylated particles. Looking at variations between the four surfactants used for coating, the protein patterns for NPs coated with L1 and L2 look very similar. This is comprehensible as these surfactants only differ in the length of the PEEP-block. For B1 and B2 there are some differences in the protein pattern in the 60 – 80 kDa region, which can probably be assigned to the fact that B1 contains a PEEP-block as hydrophilic part whereas B2 contains a PMEP-block.

To evaluate the applicability of the surfactant-coated NPs in biological media and potential risks arising from surfactant desorption, the size of all present species was investigated. For cellular uptake experiments it is very important to minimize the formation of aggregates. The tendency to form additional larger structures (termed 'aggregates' although their nature and origin cannot be

determined) in plasma was evaluated by dynamic light scattering (DLS). For the data analysis the method by Rausch *et al.*[83] has been applied (details see section 3.1.1).

The hydrodynamic radius of the NPs alone, $R_{h,NP}$, was determined to be 50 ± 5 nm for all samples. The hydrodynamic radii R_h of additional larger structures in Table 4.1.2 were calculated from the extrapolated diffusion coefficients by application of the Stokes-Einstein equation and are the z-average $<1/R_h>_z^{-1}$. Figure 4.1.9 shows the autocorrelations functions from DLS measurements of the PS-NPs coated with different surfactants. In Figure 4.1.10, the corresponding data of the diffusion coefficients D vs. the scattering vector q^2 and the extrapolation is shown. Figure 4.1.11 shows the autocorrelation functions of bare and surfactant-coated PS-NPs incubated with plasma. Two different fit functions with and without an additional term for aggregates were applied.

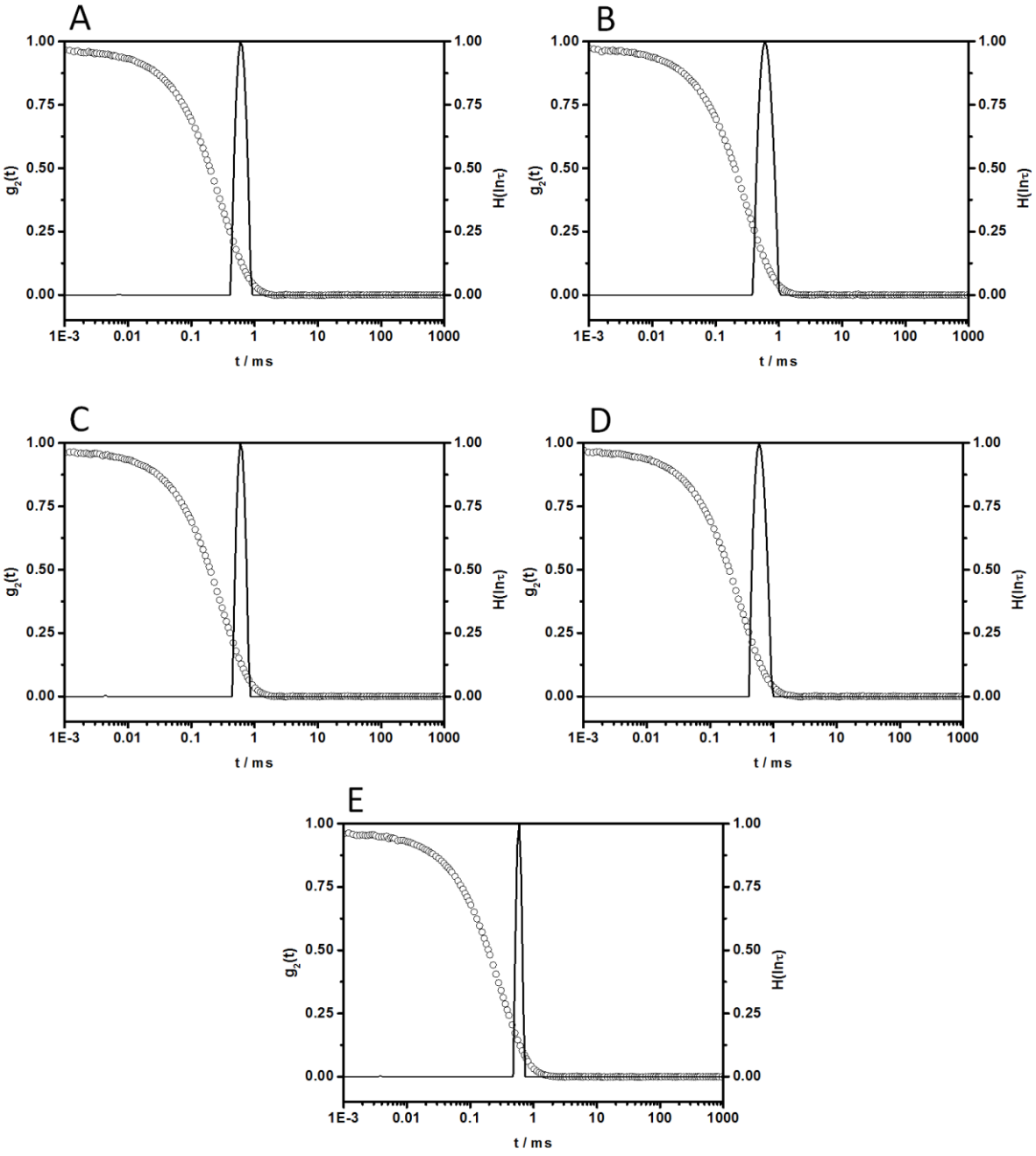

Figure 4.1.9 Autocorrelation functions $g_2(t)$ (black circles o) and the distribution of relaxation times $H(\ln \tau)$ (black line −) calculated by a CONTIN [93-94] data analysis are given for bare and surfactant-coated NPs in water at a scattering angle of 90°. The polydispersity indices (PDIs) obtained from a cumulant fit [95] of the data shown are: (A) PS-NPs with surfactant B1, PDI = 0.037; (B) PS-NPs with surfactant B2, PDI = 0.037; (C) PS-NPs with surfactant L1, PDI = 0.029; (D) PS-NPs with surfactant L2, PDI = 0.030; (E) bare PS-NPs, PDI = 0.028.

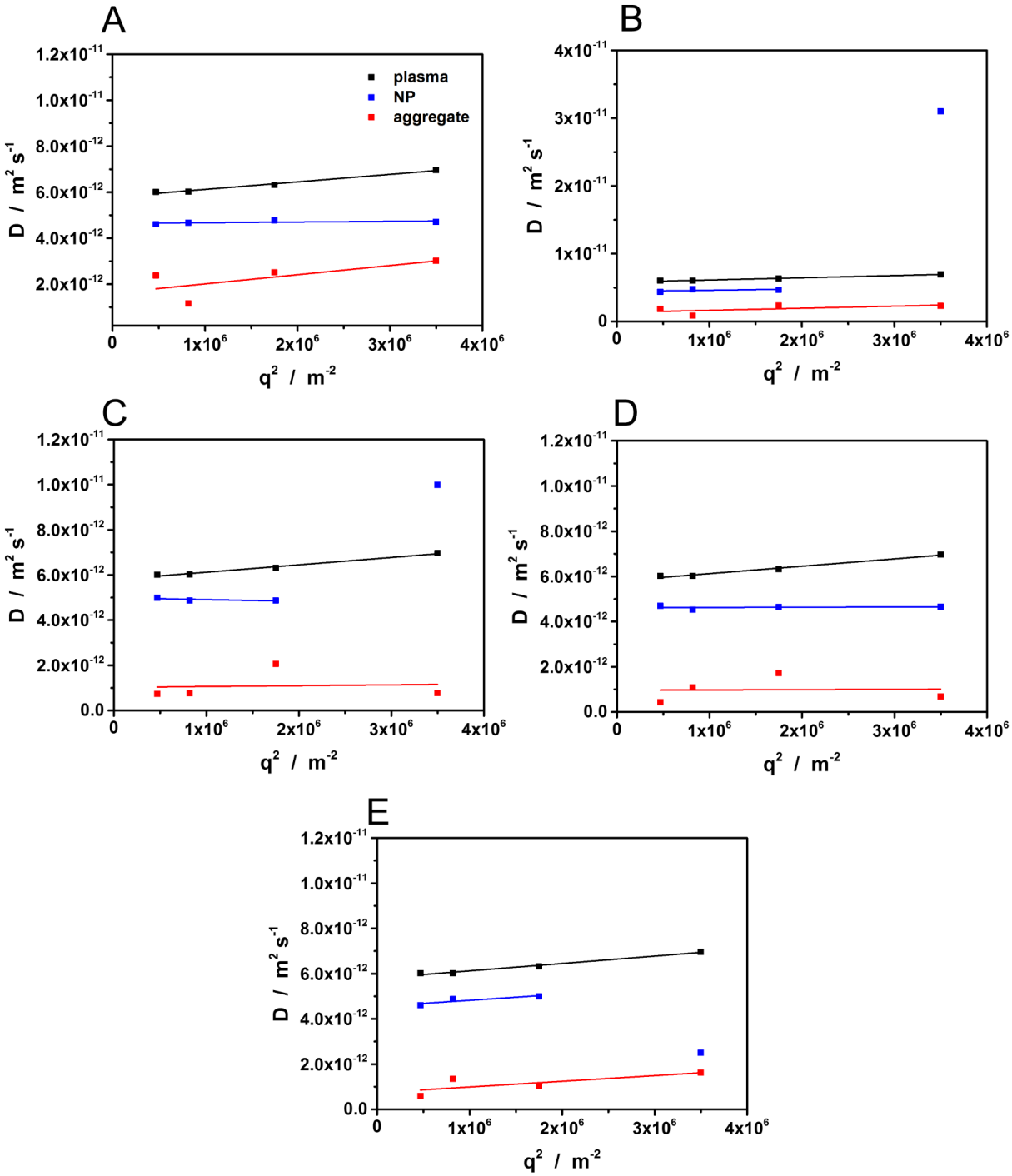

Figure 4.1.10 Plot of the diffusion coefficients *D* of plasma (blue squares), the NP (blue squares) and the aggregate fraction (red squares) versus q^2 obtained from DLS measurements of bare (E) and surfactant-coated NPs (A) – (D) incubated in plasma. Each data set has been approximated by a linear fit. Extrapolation of the fit for $q^2 \rightarrow 0$ yielded the diffusion coefficient from which the hydrodynamic radius R_h of the aggregates given in Table 4.1.2 was calculated using the Stokes-Einstein equation.

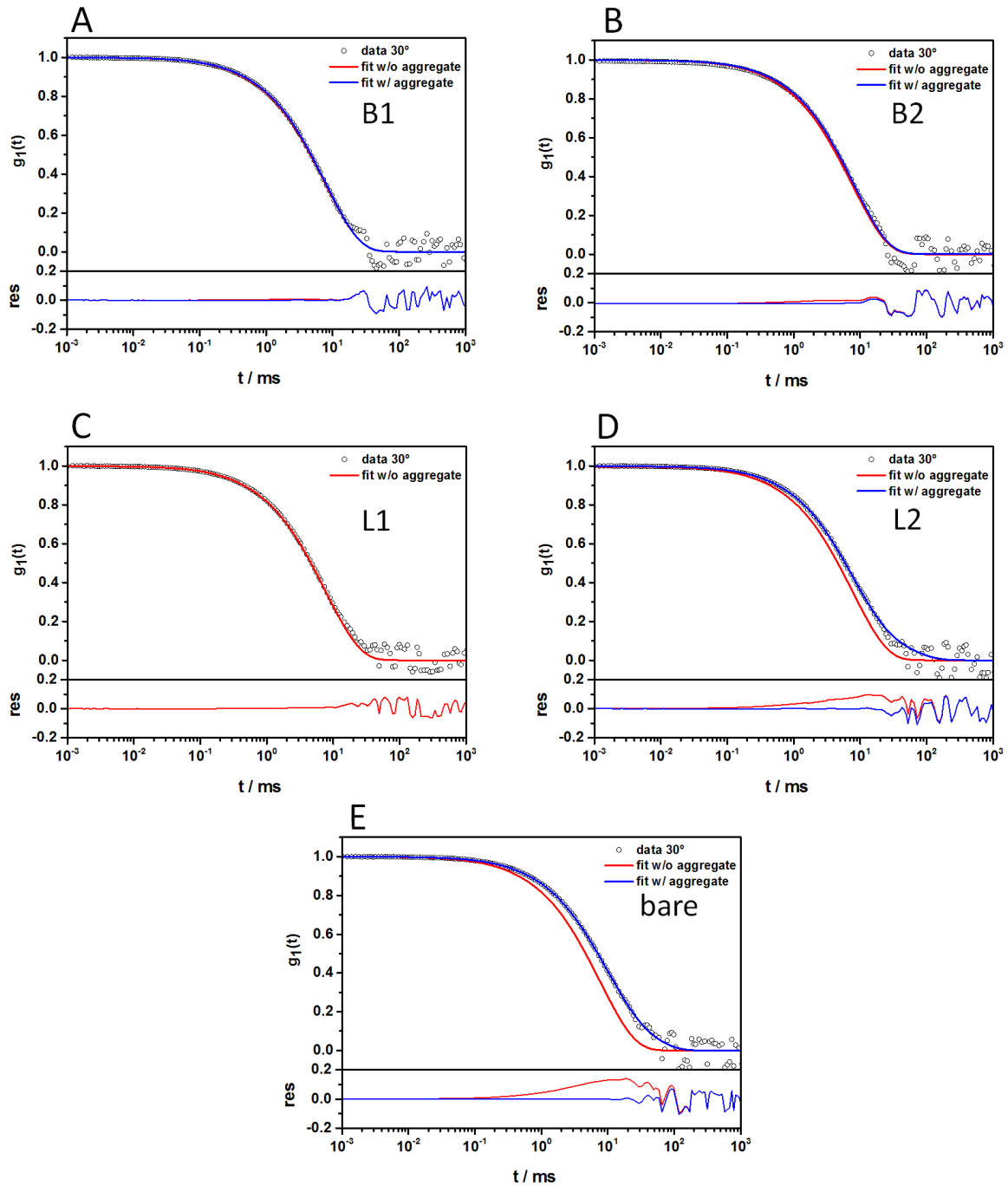

Figure 4.1.11 Autocorrelation functions (ACFs) for NP-dispersions with four different surfactants and for bare NPs in plasma. NPs coated with a stoichiometric amount of surfactant (A) B1, (B) B2, (C) L1, (D) L2 and (E) without surfactant. Upper graphs: ACF $g_1(t)$ (black circles o) for a scattering angle of 30° with a forced fit consisting of the sum of the two individual components (red line –) and a fit with an additional aggregate function where necessary (blue line –). Lower graphs: Residuals resulting from the difference of the data and the corresponding fits.

The bare NPs without any additional surfactant coating are forming additional larger structures in concentrated plasma detectable at scattering angles of 30°, 60° and 90°. The respective intensity fraction of the additional larger structures f_{agg} is pictured in Figure 4.1.12. Ideally, further surfactant coating should aim at the same or a better result while featuring the desired protein adsorption characteristics. The NPs stabilized with surfactants B1 and B2 are forming additional larger structures with a moderate size increase in plasma, the intensity fractions are ranging between 5 and 15% for all measured scattering angles (Figure 4.1.12). The corresponding ACFs (Figure 4.1.11-A and -B) cannot be described by a fit without an additional aggregate function. Due to the size of the additional larger structures those additional fractions can not only be a result of a size increase after protein corona formation.

Table 4.1.2 Hydrodynamic radii of additional larger structures formed from bare and surfactant-coated NPs in plasma determined by DLS.

surfactant	structure	R_h / nm
-	bare NPs	330 ± 33
B1	$PEBP_{25}$-*b*-$PEEP_{62}$	151 ± 15
B2	$PEBP_{31}$-*b*-$PMEP_{35}$	183 ± 18
L1	C_{18}-*b*-$PEEP_{21}$	238 ± 24
L2	C_{18}-*b*-$PEEP_{78}$	254 ± 25

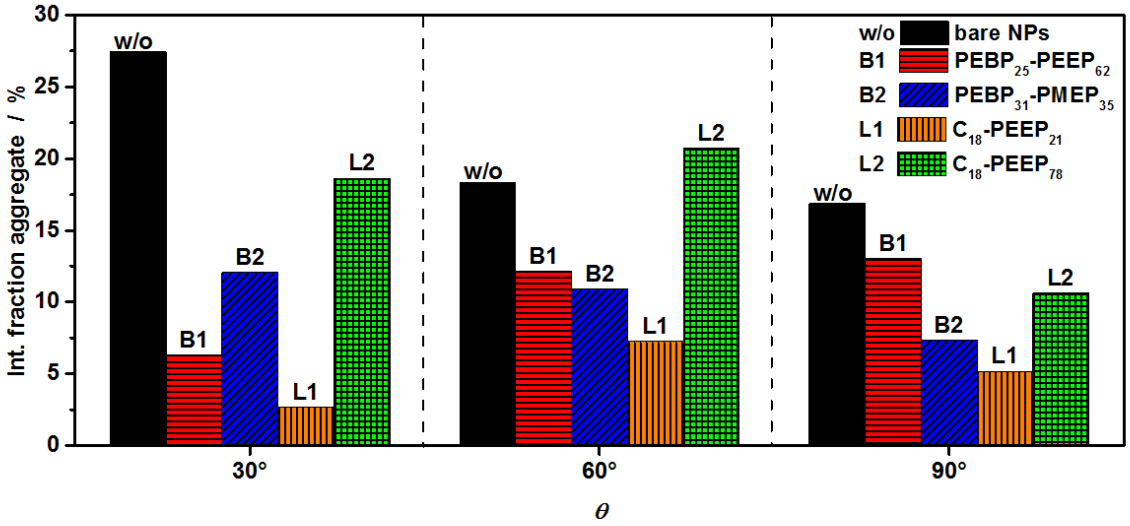

Figure 4.1.12 DLS intensity fractions of the additional larger structures for different scattering angles.

For the Lutensol®-analog surfactant L1 the data is approximated well by a fit without an additional aggregation function. Still, when applying equation 3.5 for L1, a low-intensity aggregate fraction could be detected, which exhibits a R_h of approximately 240 nm, as it is depicted in Table 4.1.2. For surfactant L2, nearly the same R_h could be detected, while the intensity fraction of the aggregate is higher.

It can be summarized that the different surfactants keep their stabilizing effect on the NP even after incubation in plasma and thereby aggregate formation is reduced depending on the surfactant. This is deducted from the generally lower intensity fraction and the smaller hydrodynamic radius R_h of the aggregates for surfactant-coated NPs compared to bare NPs. In this case the obtained sizes imply that the samples can be further used in cell experiments since the species are not too large for cell uptake.

In order to prove that the obtained protein pattern indeed results in a 'stealth' behavior of the nanoparticles, the cell uptake into macrophages (RAW 264.7) was exemplarily tested for particles coated with surfactant L1 by [redacted]. For this surfactant, the intensity fraction of additional larger structures found in DLS experiments (Figure 4.1.12) was the lowest of all surfactants, suggesting good prospects concerning its applicability. Cellular uptake of bare, L1 and L1 + plasma coated particles was analyzed by flow cytometry (Figure 4.1.13). Bare and L1-coated nanoparticles were highly taken up by macrophages. Incubation of L1 coated nanoparticles with plasma, however, reduced cellular uptake by 94%, proving the 'stealth' properties of L1 coated nanoparticles. Since coating with all surfactants resulted in a similar hard corona pattern shown in Figure 4.1.8, this uptake behavior is presumed for all PPE-containing surfactants.

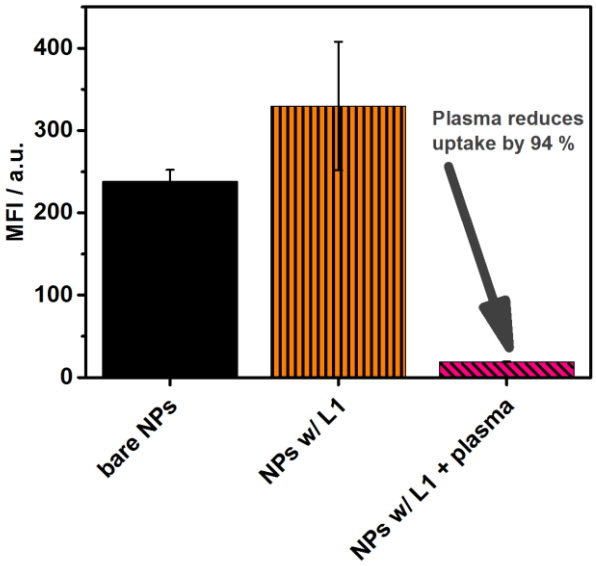

Figure 4.1.13 Flow cytometry analysis of bare, L1 and L1 + plasma coated nanoparticles. RAW264.7 cells were incubated with nanoparticles (75 µg mL^{-1}) in cell culture medium without FBS for 2 h and cellular uptake was analyzed by flow cytometry. The obtained median fluorescence intensity (MFI) with the standard deviation of three independent triplicates is shown. Experiments were conducted by [redacted].

4.1.3 Discussion

Our results reported here show that the surface functionalization of polystyrene NPs by adsorption of tunable PPE-surfactants significantly reduces unspecific protein binding. A major advantage to conventional covalent PEGylation is the simplified attachment of the polymer chains to the NP-surface *via* physical adsorption instead of covalent binding. In addition, PPE chemistry allows a straightforward adjustment of hydrophilicities in homopolymers or the controlled synthesis of amphiphilic block copolymers.[96] Nevertheless, it needs to be ensured that free surfactant in blood plasma does not cause macroscopic aggregation or cell toxicity. This can be realized by the choice of the surfactant and adjustment of length and hydrophilicity of the blocks, respectively, to obtain a strong binding affinity between surfactant and nanomaterial. For example, for surfactant L2 with 78 PEEP-units an association constant K_a of $1.6 \cdot 10^6$ L mol^{-1} for the adsorption to PS-NPs was determined, which indicates rather strong binding compared to the other surfactants. For all surfactants a correlation between the length of the hydrophilic block and the binding affinity was observed as K_a increased with the number of PEEP/PMEP units for either one of the surfactant types. Additionally, the hydrophobic chain also seems

to play an important role. L1 and L2 possess higher binding affinities than the diblock-copolymer surfactants B1 and B2. The reason could be that the alkyl chain in L1 and L2 is more hydrophobic than the PEBP-block in B1 and B2 and thus by itself exhibits a higher binding affinity towards the hydrophobic polystyrene surface. By adjusting the surfactant structure and properties, the binding affinity to a nanoparticle surface and with it the behavior in a physiological environment can thus be tailored.

In relation to those surfactant properties, we intensively studied the interaction of plasma proteins with surfactant-coated PS-NPs with complementary methods to determine their different effects on the protein corona and a possible application as a 'stealth' material. Analysis of the 'soft corona' was carried out with ITC and DLS while the 'hard corona' was investigated with SDS-PAGE and measurements of the zeta potential. 'Soft corona' refers to a diffuse shell of rather loosely attached proteins around the NP while 'hard corona' describes a stable layer of proteins with high binding affinities on the surface of the NP, which is not removed during centrifugation.

A significantly reduced interaction with plasma and HSA could be observed for most surfactant-coated NPs compared to bare NPs in ITC experiments. As anticipated, the steric repulsion of the surfactants' PPE-chains forming a hydrophilic shell around the surface of the NP leads to a generally reduced protein binding affinity. Further, the data suggests that the binding affinity of surfactants to NPs is related to their interaction with plasma and HSA respectively. With increasing surfactant binding affinity, the interaction with proteins (more specifically their K_a) decreases for surfactants with similar chemical structures. For example, NPs coated with the Lutensol®-analog surfactant L2, which has the highest association constant K_a, exhibit the lowest enthalpic interaction with plasma and HSA respectively. If the surfactant is adsorbed strongly to the NP surface, desorption and replacement by proteins upon incubation with plasma is unlikely. Instead, the surfactant-coating inhibits protein adsorption to a large extent, so a lower enthalpic interaction can be observed in ITC. To summarize, for surfactants with an increasing association constant the affinity of surfactant-coated NPs to plasma decreases by trend.

To assess the intended functional properties of the surfactants, the amounts of protein as well as the protein patterns were analyzed to determine the types of proteins adsorbed before and after surfactant coating. The amount of protein adsorbed was found to be similar for all surfactant coated NP samples but lower than on the bare NPs. This supports the results obtained from ITC, although the differences between the individual surfactants probably cannot be resolved due to the centrifugation steps during sample preparation. Gel electrophoresis revealed the presence of clusterin in the hard corona of all surfactant-coated NPs in contrast to the bare NPs, which has been identified before as a key protein in the corona of stealth PEGylated-/PPEylated nanocarriers.[13, 62] The overall protein pattern

is similar to the pattern for PEGylated NPs for which a stealth effect has been shown. This indicated that the intended function of the surfactants as 'stealth' surfactants could indeed be obtained.

The formation of additional larger structures in plasma was mostly reduced by surfactant coating compared to bare NPs as observed in DLS measurements. However, a reliable interpretation of this 'aggregation behavior' is non-trivial, as several different processes can occur in parallel: As an example, surfactant desorption could take place (especially for surfactants with low binding affinity) and might or might not provoke the aggregation of plasma proteins. Moreover, the formation of multi-particle aggregates might occur. Thus, the 'aggregation behavior' of surfactant-coated NPs cannot be directly correlated with the binding affinity of the surfactants and the origin of the formed aggregates is not known yet.

To verify their effect on cellular uptake, further studies have exemplarily been conducted on macrophages with the surfactant-coated nanoparticle system featuring the lowest aggregation tendency. The reduced cell uptake was observed as expected and can be presumed for all other used PPE-surfactant types since a similar protein pattern was obtained. As the desired functionality was given by all of the surfactants, a suitable type is chosen by its properties: a high association constant for PS-NPs, a low interaction of surfactant-coated NPs with plasma/HSA as well as minor/no aggregate formation of surfactant-coated NPs in plasma and thus most likely no significant surfactant desorption.

Accordingly, the surfactants could be further optimized by variation of the chain length and by chemical modification of the pendant chain at the phosphorus center to achieve the optimum protein adsorption properties, aggregation behavior and protein patterns. Also, the amount of surfactant used for the nanoparticle coating can be adjusted to yield the optimum protein adsorption properties. However, as a basis for tailored functional surfactants inducing a 'stealth' effect, the alkyl-terminated PPEs are excellent candidates.

4.1.4 Conclusion

In conclusion, surfactants based on structurally versatile poly(phosphoester)s are predestined to be used for a non-covalent surface modification of model nanocarriers providing an easier approach than covalent linkage. The amount and types of proteins identified on the PPE-surfactant-coated nanocarriers after incubation in human plasma resemble previously reported covalently PPEylated nanocarriers and result in a similar stealth functionality. Thus, non-covalent coating with surfactants facilitates tailoring the protein adsorption on nanoparticles and their behavior in a biological environment. Since for coating no initial surface functionalization is required, this approach can potentially be applied to any type of nanocarriers.

4.2 Beyond the Protein Corona – Lipids Matter for Biological Response of Nanocarriers

In the previous chapter, NPs coated with PPE-surfactants were introduced, which showed controlled protein adsorption and a stealth effect after incubation with full plasma. While the main focus was on the proteins, it should not be forgotten that plasma also contains other species such as lipids, which can also potentially adsorb to nanocarriers. Therefore, the role of lipids on the stealth effect will be investigated further.

The work presented in this chapter is accepted for publication in the journal *Acta Biomaterialia*. Parts of the experiments were conducted by [redacted] in the framework of his Master thesis under my supervision. Moreover, [redacted] conducted LC-MS measurements as well as cellular uptake studies (cell culture and flow cytometry), and [redacted] made all TEM experiments. I planned the experiments related to ITC, cholesterol assay and SDS-PAGE, and carried out these experiments with the lipoprotein fractions. Further, I conducted DLS experiments, created figures and wrote the text.

The interaction of nanocarriers with blood plasma components influences the biological response and therefore needs to be controlled. Whereas protein adsorption to nanocarriers has been investigated to a large extent, the role of lipid interaction for drug delivery and its biological impact is not yet clear. However, lipids represent an important constituent of blood plasma and are usually bound in the form of lipoproteins. Since already for many nanocarriers systems an enrichment of apolipoproteins in their protein corona was reported, we examine the interaction of lipoproteins with nanocarriers. If interaction occurs in terms of lipoprotein adsorption, two scenarios are possible: adsorption of intact lipoprotein complexes or disintegration of the complexes with adsorption of the single components. To investigate the interaction and clarify which scenario occurs, polymeric model nanoparticles and different lipoprotein types have been studied by isothermal titration calorimetry, transmission electron microscopy and other methods.

4.2.1 Adsorption behavior of lipoproteins

As stated above in the theory section, different types of lipoproteins are distinguished by their density: high density lipoproteins (HDL) have a density between 1.06 and 1.21 g cm^{-3}, low density lipoproteins (LDL) between 1.02 and 1.06 g cm^{-3} and very low density lipoproteins (VLDL) between 0.95 and 1.01 g cm^{-3}.[35] In order to ensure conditions close to an *in vivo* situation for the interaction with nanoparticles, lipoproteins were isolated directly from human plasma. A lipoprotein fractionation kit was used to obtain an HDL-fraction and a LDL/VLDL-fraction from human citrate plasma. However,

with the fractionation kit it is not possible to separate LDL and VLDL. To be able to distinguish also between LDL and VLDL, three different commercially available lipoproteins (HDL, LDL, VLDL; Lee Biosolutions, Metro Ct, USA) were used additionally. Figure 4.2.1-A shows the different types of lipoproteins used in this study with their physico-chemical properties.

A

	R_h / nm	ζ / mV	c (Chol.) / g L^{-1}	Main Apolipoprotein(s) [a]	ρ [a] / g cm^{-3}
HDL comm.	12 ± 1	-10 ± 1	0.38 ± 0.06	Apo-A1	1.06 - 1.21
LDL comm.	21 ± 2	-14 ± 1	0.60 ± 0.09	Apo-B100	1.02 - 1.06
VLDL comm.	42 ± 4	-22 ± 2	0.68 ± 0.10	Apo-B100, Apo-E	0.95 - 1.01
HDL-fraction	13 ± 1	-5 ± 1	0.35 ± 0.05	Apo-A1	1.06 - 1.21
(V)LDL-fraction	25 ± 3	-6 ± 1	0.57 ± 0.09	Apo-B100, Apo-E	0.95 - 1.06

[a] Information taken from literature.[35]

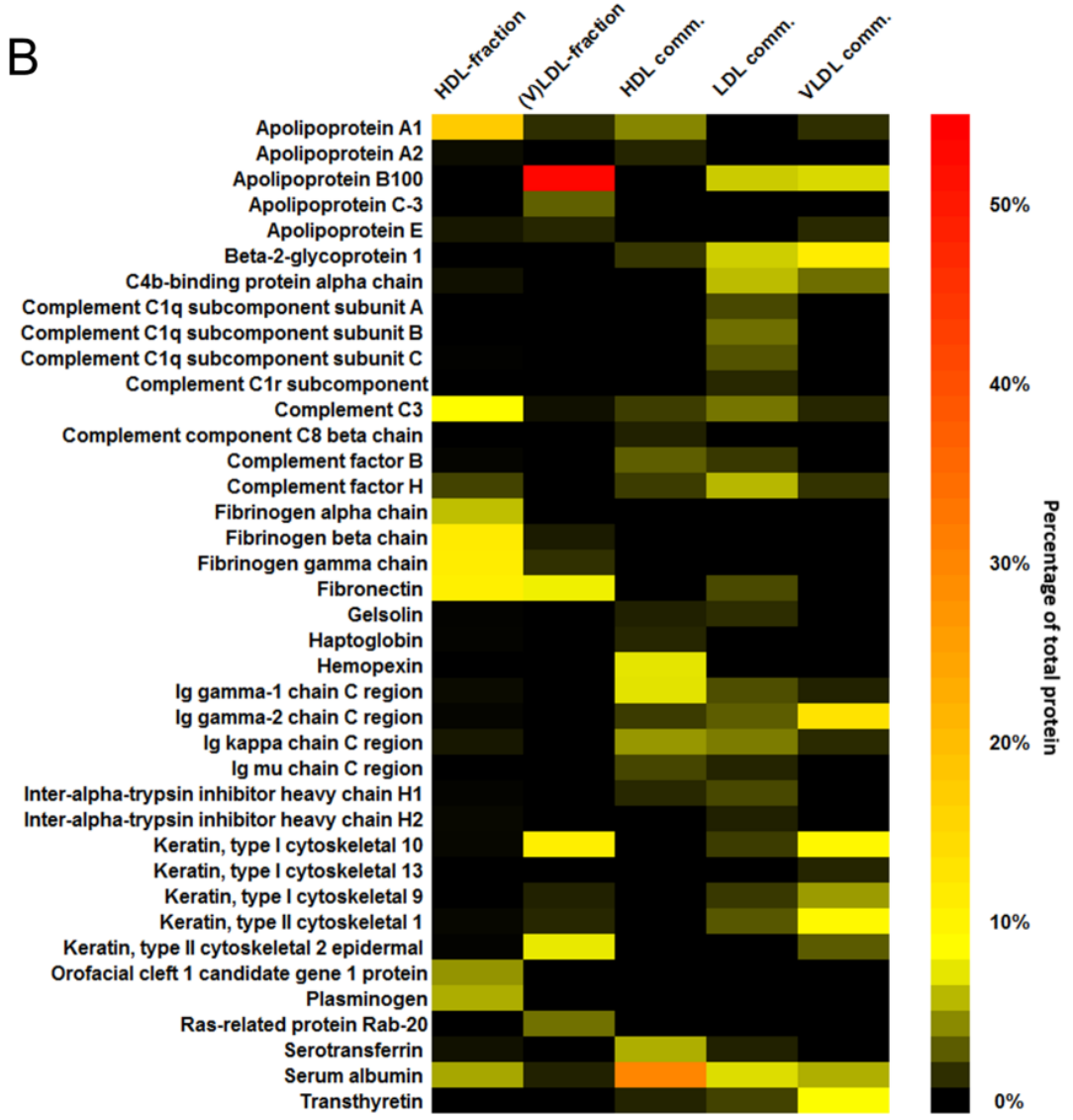

Figure 4.2.1 Physico-chemical properties and protein composition of different commercial lipoprotein samples and lipoprotein fractions. (A) Characterization of different lipoproteins used in this study. Hydrodynamic radii were determined by DLS and are in good agreement with literature values.

Concentrations of cholesterol were determined by a cholesterol assay. (B) Proteins identified in lipoproteins by LC-MS. The LC-MS identifies all the proteins and gives their absolute values based on Hi3 approach. From the list of amounts of all proteins (in fmol), their relative molar percentage was calculated. Displayed are only proteins with > 1% abundance in at least one of the samples. LC-MS experiments were performed by [redacted].

Average hydrodynamic radii R_h were determined by dynamic light scattering (DLS) of pure lipoprotein samples. With decreasing density of the lipoproteins their hydrodynamic radii increase, with VLDL forming the largest complex with a hydrodynamic radius of 42 nm. The general trend of the experimental data is in good agreement with previous findings for the size of lipoproteins, as the values with their error range correspond well with literature values.[35] The hydrodynamic radius of the (V)LDL-fraction was determined to be 25 nm, which is in between the values of pure LDL and VLDL, however closer to the value of LDL. This is plausible, as it contains a mixture of LDL and VLDL.

In Figure 4.2.1-B, proteins detected by liquid chromatography-mass spectrometry (LC-MS) in the different lipoprotein samples are shown (measurements performed by [redacted]). All lipoprotein samples contain different plasma proteins in low to medium concentrations and an enriched amount of apolipoproteins, Apo-A1 and Apo-B100 in particular. The MS data thus confirm the presence of apolipoproteins reported from literature (listed in the table in Figure 4.2.1-A) in the lipoproteins used herein. Compared to the fractionated lipoproteins, the commercial lipoproteins contain numerous different plasma proteins, so their purity can be considered lower than the purified fractions. Especially the relatively high levels of human serum albumin, the most abundant protein in blood plasma, are noticeable.

For investigating their interaction with nanoparticles, polystyrene nanoparticles (PS-NPs) with a hydrodynamic radius of 52 nm and a narrow size distribution (see Figure 4.2.2) were used as a model system. In isothermal titration calorimetry (ITC) experiments, an aqueous solution of each of the five different lipoprotein samples was titrated stepwise to an aqueous PS-NP dispersion. The lipoprotein-fractions were used with a concentration as obtained after isolation from plasma. The concentration of the commercial lipoproteins was adjusted to blood plasma level according to manufacturer's instructions. Titrations with commercial lipoproteins were conducted by [redacted]. The measured heat obtained from integrating the corrected heat rates (see Figure 4.2.3) is plotted against the ratio of lipoprotein complexes per PS-NP in Figure 4.2.4-A to -E. The ratio was calculated by the number of apolipoproteins per lipoprotein. As reference, titrations of single apolipoproteins (Apo-B100 and Apo-E) were conducted in the same manner and are shown in the respective graphs of

lipoproteins, in which they naturally occur. The titrations with Apo-A1 and Apo-B100 are shown in Figure 4.2.5 with an adjusted scale. All binding isotherms were fitted according to an independent binding model.[97] Although the adsorption process is probably not reversible for all compounds involved, we consider this independent binding model as most suitable from the fit models available for this technique.

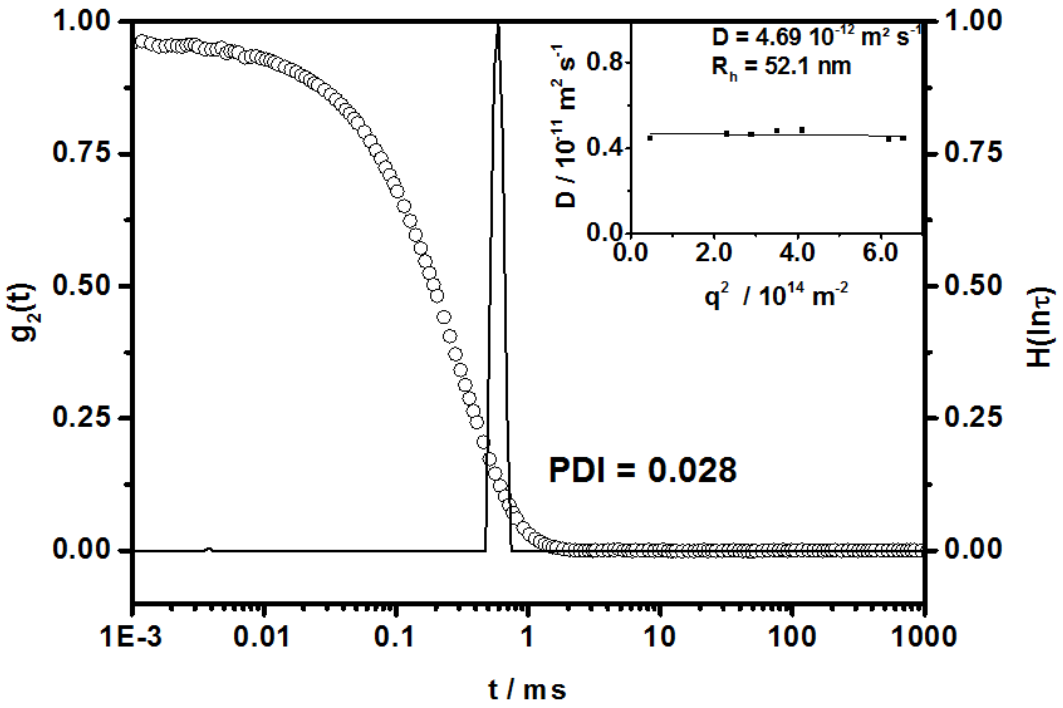

Figure 4.2.2 Dynamic light scattering autocorrelation function and distribution of relaxation times of PS-NPs for a scattering angle of 90°. Top-right corner: diffusion coefficient *D* against scattering vector squared q^2. The distribution was calculated using the CONTIN model, the polydispersity index (PDI) was identified *via* a cumulant fit model. The diffusion coefficient *D* was determined using a biexponential fit model.[94] The sample shows a monodisperse distribution, the PDI was determined to be 0.028. From the extrapolated diffusion coefficient, a value of 52 nm was obtained for the hydrodynamic radius using the Stokes-Einstein-equation.

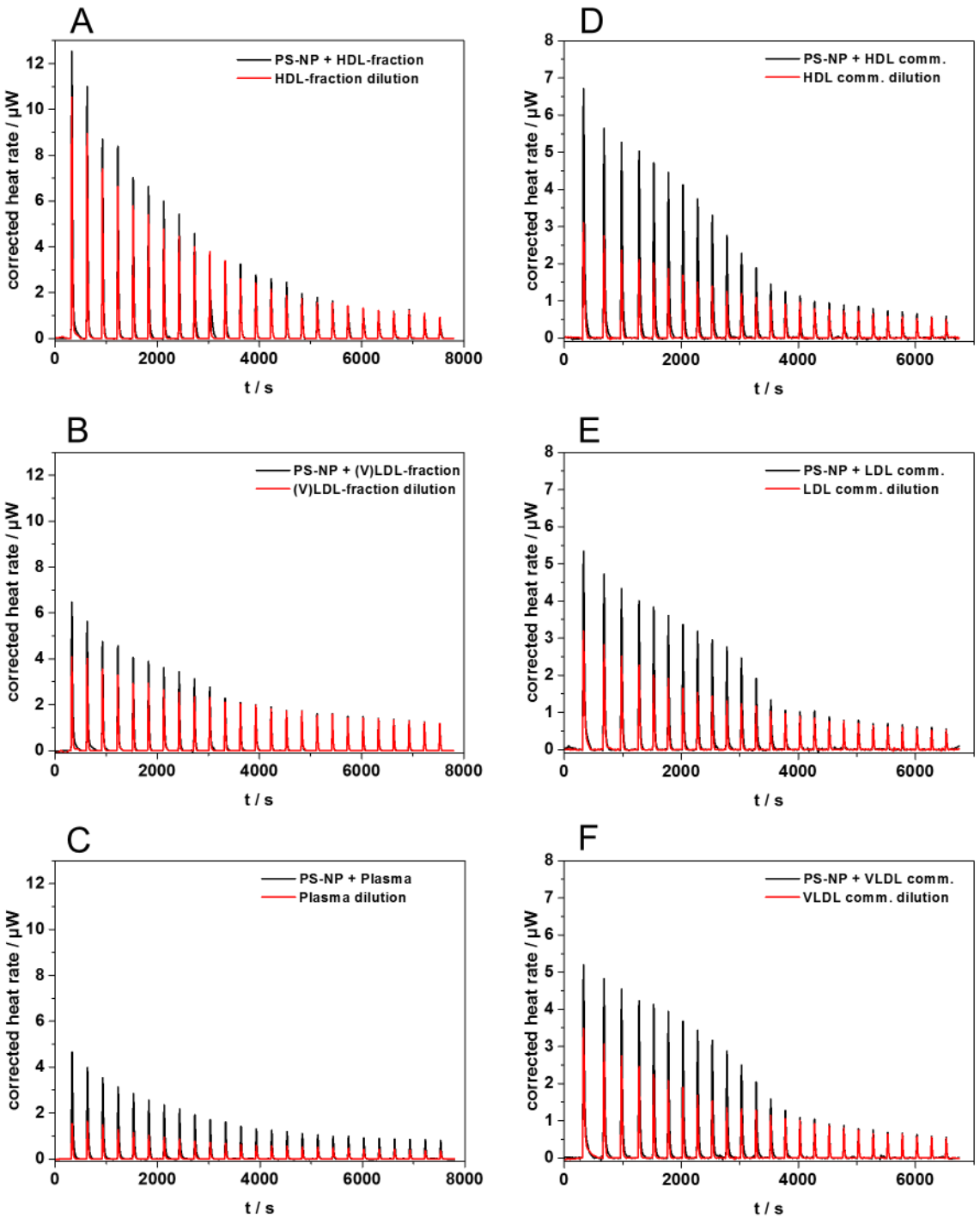

Figure 4.2.3 ITC raw heat rates of the titration of PS-NPs with different lipoprotein sources. The signal of the titration of the respective lipoprotein into water (heat of dilution) is shown in red. In the graphs shown in Figure 4.2.4 and in Figure 4.2.5, the heat of dilution was subtracted from the original signal. Titrations with plasma and commercial lipoproteins were conducted by [redacted].

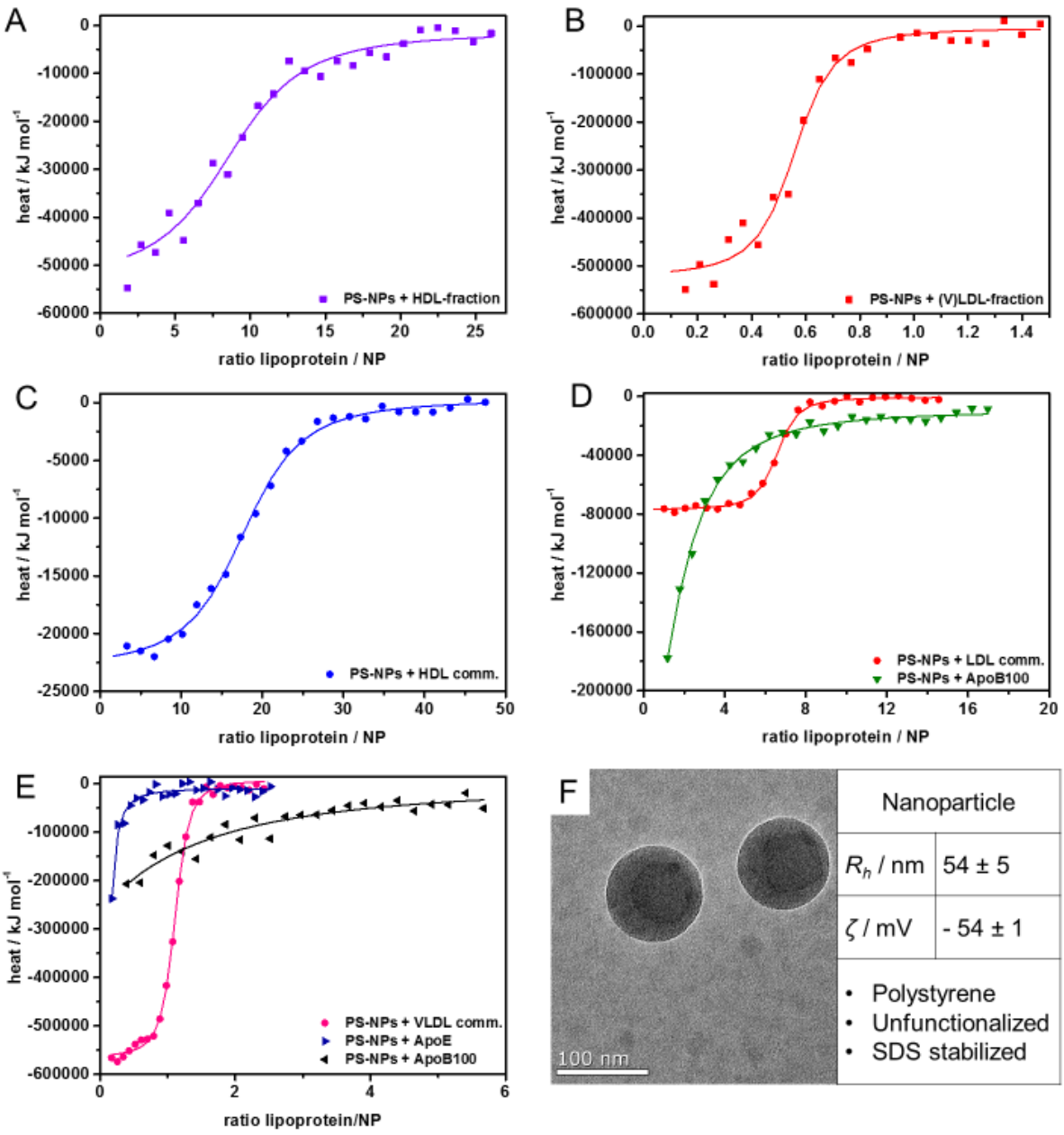

Figure 4.2.4 Adsorption isotherms of lipoproteins on NPs (referred to complete lipoprotein complexes) as observed in isothermal titration calorimetry (ITC) and NP-properties. (A) – (E) Integrated heats of the (lipo)protein - PS-NP titrations fitted with an independent binding model (solid lines). The contribution of the respective present apolipoproteins examined in separate control titrations (displayed as triangles ▼,◀,▶ in (D) and (E)). (F) TEM micrograph of the PS-NPs used in this study. Titrations with plasma and commercial lipoproteins were conducted by [redacted], TEM micrograph by [redacted].

In Table 4.2.1, the values for the association constant K_a, the binding enthalpy ΔH and the stoichiometric ratio n of lipoproteins (LPs) per nanoparticle obtained from the independent binding model fit are displayed.

All binding affinities K_a of lipoproteins to PS-NPs are in the range of 10^8 M^{-1} and above, which represents very strong binding. When the lipoproteins become larger in size (HDL < LDL < VLDL), they tend to exhibit a higher value of K_a. Thus, it is likely that lipoproteins immediately adsorb to available nanoparticle surfaces and do not, or only in negligible extent, diffuse freely in solution.

Table 4.2.1 Adsorption parameters obtained from ITC experiments.

	K_a / 10^8 M^{-1}	ΔH / MJ mol^{-1}	ΔS / kJ mol^{-1} K^{-1}	n (LPs per NP)	# lipid-like molecules in LP [a]	ΔH per lipid-like molecule / kJ mol^{-1}	A per lipid-like molecule / nm^2
HDL-fract.	1.7 ± 0.2	-51.0 ± 6.0	-172 ± 20	8.4 ± 0.4	460	-110.9 ± 0.1	7.3
(V)LDL-fract.[b]	195.0 ± 64.0	-538.0 ± 76.0	-1800 ± 250	0.6 ± 0.1	4100	-131.2 ± 18.5	13.3
HDL comm.	1 ± 0.1	-23.3 ± 0.2	-78 ± 5	18.0 ± 0.3	460	-50.7 ± 0.4	3.4
LDL comm.	34.9 ± 3.6	-76.1 ± 1.2	-255 ± 4	6.4 ± 0.1	4100	-18.6 ± 0.3	1.1
VLDL comm.	141.9 ± 13.8	-582.0 ± 6.2	-1950 ± 21	1.0 ± 0.1	120000	-4.9 ± 0.1	0.3

[a] For lipid-like molecules an average molar mass of 600 g mol^{-1} was assumed and literature values were used for the mass of lipoproteins. For further details see Experimental section.

[b] For the (V)LDL-fraction, 100% of LDL were assumed for the calculation of lipid-like molecules, as DLS and TEM results suggest clear predominance of LDL.

The binding enthalpies ΔH of lipoproteins titrated to PS-NPs are in the range of megajoule per mol, which seems unusually high at first glance. The heat detectable in the titrations with apolipoproteins is significantly lower compared to the corresponding lipoproteins in most cases. Only in the case of commercial LDL the titration with apolipoprotein-B100 shows heats within the same range. Taking into account that the fit parameters refer to complete lipoprotein complexes, which consist of a large

number of small molecules/lipids (and few proteins), explains why the values for *ΔH* are so large. The heats are most probably a result of all different molecules interacting with the particle surface. This is a first hint that not only protein-NP interactions are occurring. Possible protein denaturation upon adsorption on PS-NPs cannot explain a negative *ΔH* of several megajoule per mol. The denaturation process of a protein is endothermic and only driven by the entropy gain upon unfolding.[98] The enthalpy of denaturation for an 'average' protein reported in literature is +33.5 J g^{-1}, which leads to an endothermic molar value of several hundred kilojoule to few megajoule, depending on the molecular weight of the protein.[99] Thus, protein denaturation cannot be the driving force for the examined adsorption processes.

For further analysis, the number of lipid-like molecules (all molecules except the proteins) in one lipoprotein was approximated (details in Experimental section, chapter 5.4.6) and the enthalpy *ΔH* per lipid-like molecule was calculated. In the case of disintegration of the lipoprotein complexes and adsorption of the single components, a relation of the adsorption parameters to these single components would be more meaningful. The values for *ΔH* per lipid-like molecule are in the range of kJ per mole, which is a typical range for adsorptive interactions to nanoparticles. This can be interpreted as first evidence that in fact disintegration of the lipoprotein complexes takes place. This would include an exothermal adsorption process of lipids contained in the lipoproteins on the PS-NPs. The chemical structure of the lipids suggests a hydrophobic interaction between lipids and nanoparticle, which settles in the highly negative *ΔH*.

Calculating the change in entropy *ΔS* gives slightly negative values per lipid-like molecule, which means that the order of the system increases during the interaction. This matches the process of complete lipoprotein adsorption onto the NP surfaces. For example, the value for *ΔS* per lipid-like molecule for commercial LDL is -62 J mol^{-1} K^{-1}, which is exceeded by the corresponding value for *ΔH* per lipid-like molecule (-18.6 kJ mol^{-1}, Table 4.2.1) by a factor of 300. The driving force of the adsorption process therefore is the adsorption enthalpy *ΔH*.

The stoichiometric ratio *n* describes how many lipoproteins interact with one PS-NP. It clearly shows a dependency on the size of the lipoprotein: for the rather small HDL 18 lipoproteins interact with one NP, while for the large VLDL only about one lipoprotein interacts with one NP. For the extracted lipoprotein fractions the obtained stoichiometry was in the same order of magnitude. For the V(LDL)-fraction a ratio *n* of 0.6 was detected, which either is a result of concentration errors or means that bigger clusters of lipoproteins and NPs are formed. In general, the ratio of lipoproteins per NP is rather low considering the dilution of nanocarriers in the blood stream in an *in vivo* situation and the physiological blood level of the lipoproteins. In that case, a comparably small number of nanocarriers faces a huge excess of lipoproteins, independent of the blood level fluctuations of lipoproteins. It is

thus likely that fluctuations of the lipoprotein level may not cause major changes in the lipoprotein pattern adsorbing to the NP surface.

Additionally, the available surface area for one lipid adsorbing to a NP was calculated, subtracting the space needed for apolipoproteins. Although the values show some variation, their order of magnitude suggests that the available surface space is sufficient for a monolayer of lipid molecules (assuming that a disintegration of lipoproteins takes place). The numbers do not give any evidence for the formation of multilayers of lipids on the nanoparticles. For the calculations, as number of apolipoproteins contained in the lipoproteins three Apo-A1 in HDL, one Apo-B100 in LDL, one Apo-B100 and one Apo-E in VLDL were used according to Berg *et al.*[35] In titrations with the respective apolipoproteins (see Figure 4.2.5-A, -B, -C, -D with the axis scale adjusted to the apolipoprotein ratio) much smaller exothermic heat is evolved through interaction of the apolipoproteins with the PS-NPs compared to the titrations with the corresponding lipoproteins. Therefore, most of the heat shown in the graphs of Figure 4.2.4 does originate from adsorption of lipids to NPs. This supports the assumption that the strong adsorption of lipoproteins on PS-NPs is mainly driven by interaction of the lipids rather than of the apolipoproteins. All measurements were corrected by the heat of dilution of the corresponding lipoprotein/apolipoprotein sample (Figure 4.2.3).

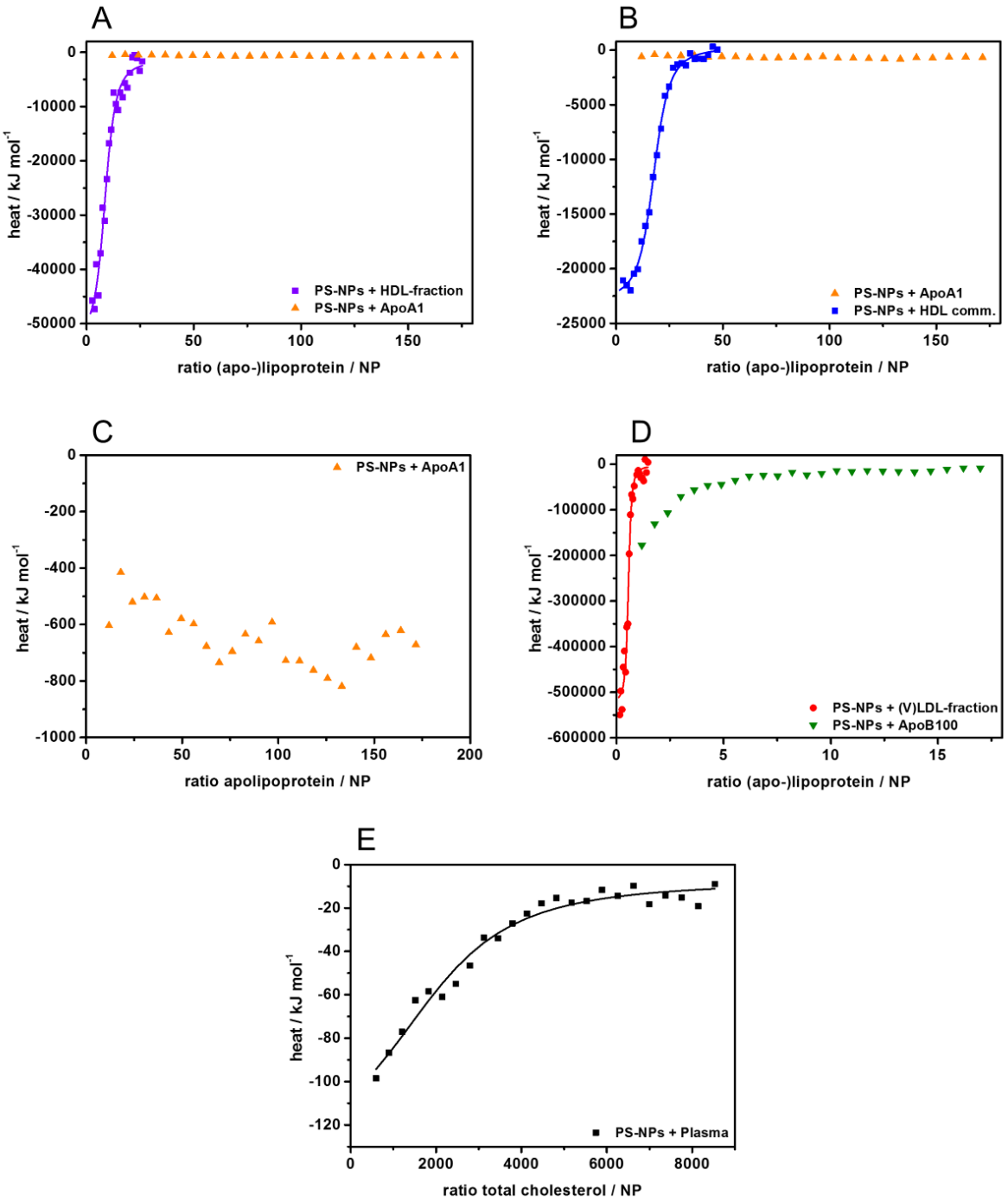

Figure 4.2.5 (A) – (D) ITC experiments of PS-NPs with lipoproteins (HDL-, (V)LDL-fraction, HDL comm.) and apolipoproteins as reference. For each lipoprotein, the respective apolipoprotein is shown in the same graph, with the x-axis adjusted to the ratio of apolipoprotein per NP. (E) ITC titration of PS-NPs with centrifuged plasma. For the plasma, the mass concentration of total cholesterol as determined by a cholesterol assay (see Figure 4.2.8 and Table 4.2.3) was divided by the average molar mass of cholesterol and cholesteryl esters (600 g mol^{-1}). This, together with the respective concentration of the nanoparticles, enables calculation of the ratio of total cholesterol per nanoparticle at each point of the titration.

In an *in vivo* situation, where numerous different proteins compete for adsorption to the NPs, lipoproteins will most likely show a different adsorption behavior than in pure NP dispersions as applied in these experiments. Probing lipoprotein adsorption in full plasma, which would be the most realistic scenario, is not possible directly as lipoproteins are already present in plasma. Therefore, additional experiments were carried out with PS-NPs precoated with HSA by [redacted]. This most abundant protein in blood plasma was chosen to create a situation close to the conditions in plasma. The heat rate measured for these titrations and the respective heat of dilution is shown in Figure 4.2.6.The adsorption isotherms obtained from these experiments are shown in Figure 4.2.7, the parameters from the respective fits are listed in Table 4.2.2.

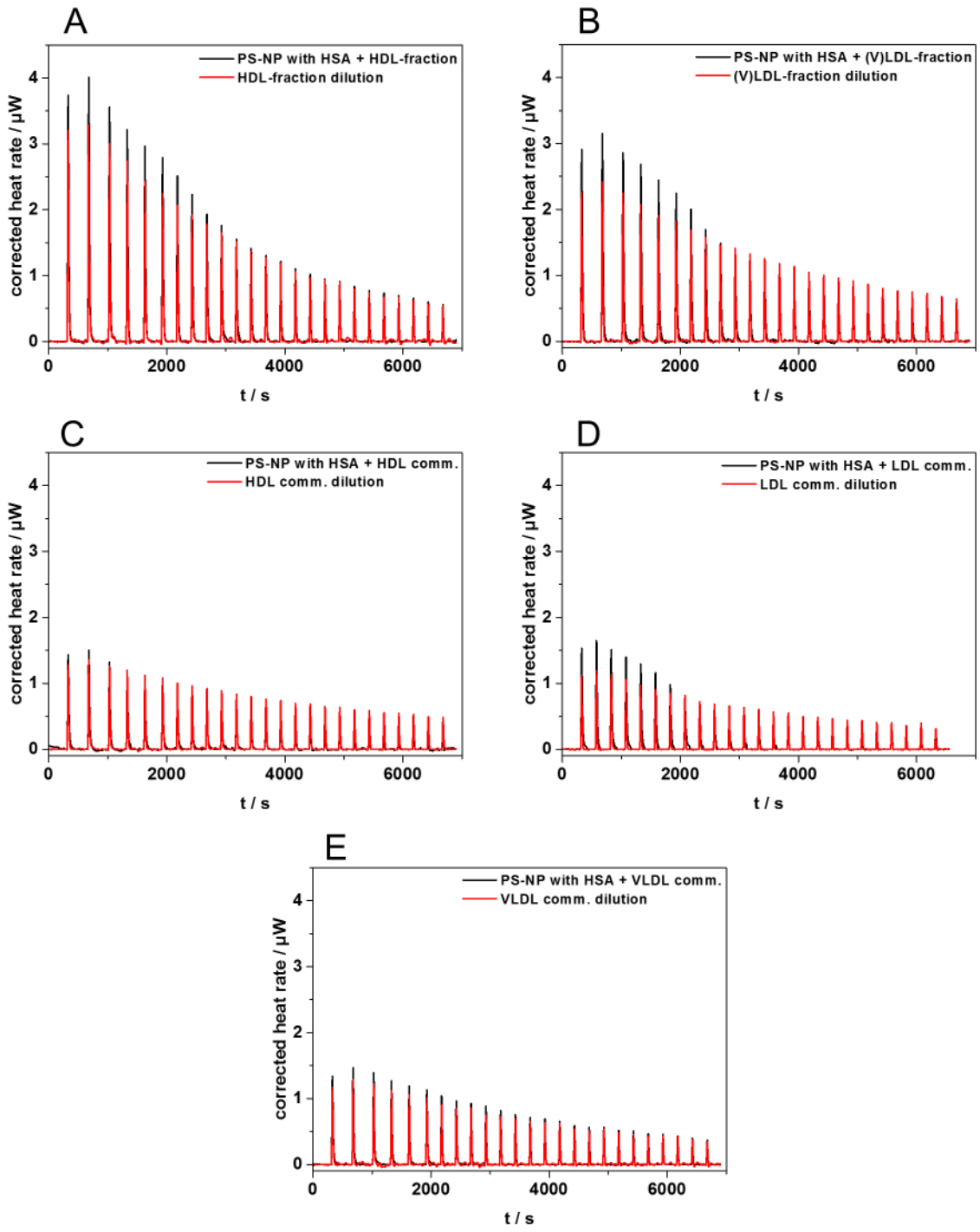

Figure 4.2.6 ITC raw heat rates of the titration of HSA-precoated PS-NPs with different lipoproteins. The red line corresponds to the titration of the respective lipoprotein into an aqueous HSA solution with the same amount as added to precoat the PS-NPs. In the graphs shown in Figure 4.2.7, this heat of dilution was subtracted from the original signal. Titrations were conducted by [redacted].

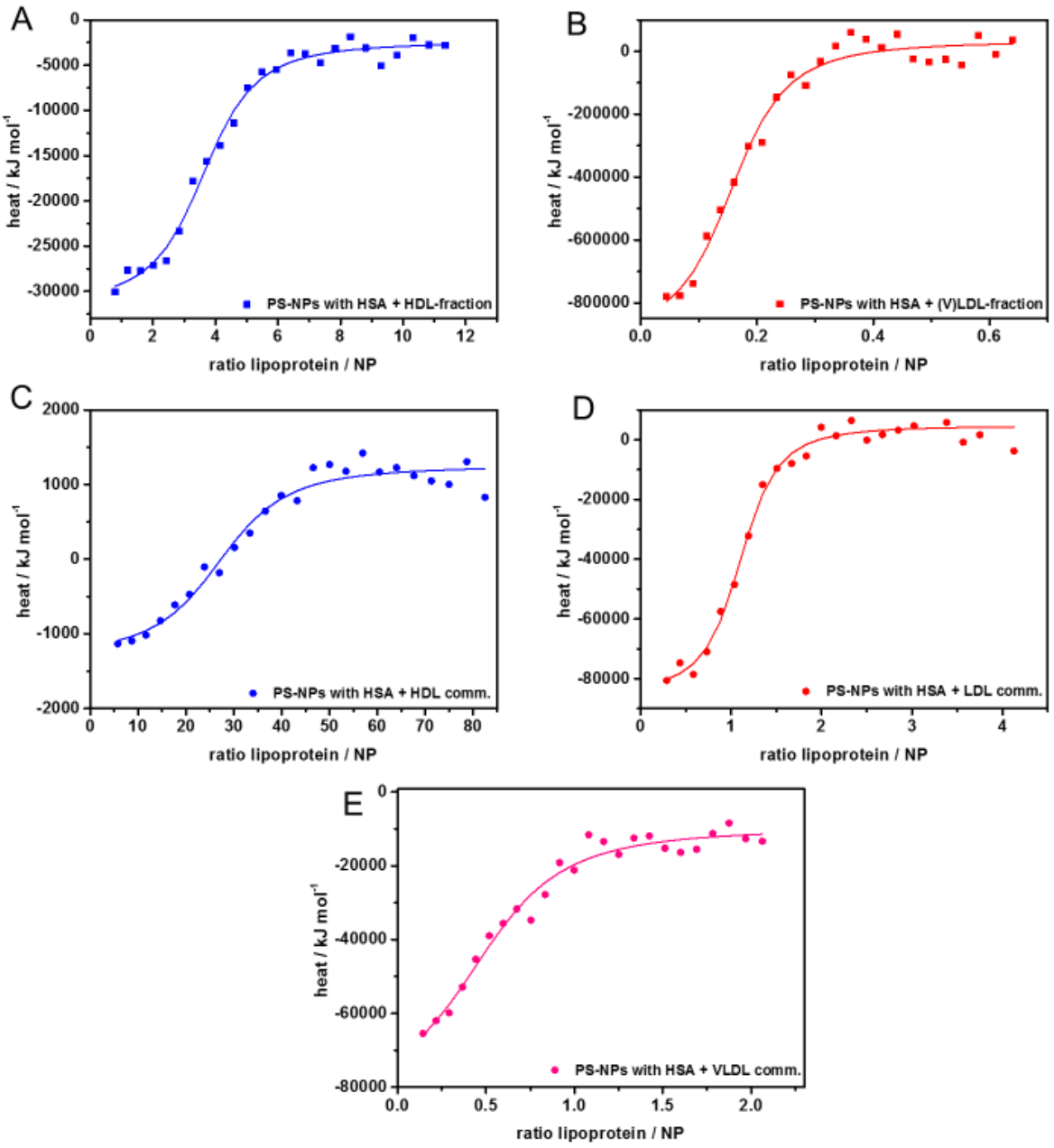

Figure 4.2.7 Adsorption isotherms from ITC experiments of PS-NPs precoated with HSA and titrated with lipoproteins. Lipoprotein fractions (A), (B) and commercially available lipoproteins (C) – (E) were used. The PS-NPs were precoated with a stoichiometric amount of HSA as determined in previous ITC experiments. Titrations were conducted by [redacted].

For each of the lipoproteins, an exothermal interaction with rather large signal intensities could be observed. The binding affinities K_a in Table 4.2.2 are in the range of 10^8 M^{-1}, the values are by trend slightly lower or the same as the K_a obtained for the titrations without HSA (Table 4.2.1). Only the HDL-fraction shows a higher value than in the previous titrations. The stoichiometry n for (assumed) complete lipoprotein complexes is in most cases significantly lower than for the adsorption on bare

nanoparticles (Table 4.2.1). This is comprehensible as the NP surface is already partly covered with HSA, so less free space is available for lipoprotein adsorption. However, it remains unclear, if HSA desorbs when the lipoproteins come into play. It is imaginable that a kind of dynamic equilibrium is reached at some point. The binding enthalpy *ΔH* detected for lipoprotein adsorption on HSA precoated PS-NPs is approximately in the same range (several MJ per mol) as the values displayed in Table 4.2.1. There are some deviations to the values of *ΔH* determined in the previous ITC experiments, but it is not possible to derive a general trend (lower/higher) here. The uncertainty of the fate of HSA regarding desorption could be a possible explanation for deviations observed for *ΔH*.

Following the high absolute values for *ΔH* in the MJ range, it can still be concluded that disintegration of the lipoprotein complexes also occurs in the presence of other proteins.

Table 4.2.2 Adsorption parameters obtained from ITC experiments of PS-NPs (pre-incubated with HSA) and the respective lipoproteins.

	K_a / 10^8 M^{-1}	*ΔH* / MJ mol^{-1}	*ΔS* / kJ mol^{-1} K^{-1}	*n* (LPs per NP)	# lipid-like molecules in LP [a]	*ΔH* per lipid-like molecule / kJ mol^{-1}
HDL-fract.	5.0 ± 1.8	-32.6 ± 2.5	-110 ± 9	3.8 ± 0.5	460	-70.9 ± 5.4
(V)LDL-fract.[b]	115.2 ± 30.0	-1289.4 ± 472.8	-4324 ± 1587	0.17 ± 0.01	4100	-314.5 ± 115.3
HDL comm.	0.9 ± 0.4	-2.5 ± 0.3	-8.3 ± 1.0	24.9 ± 2.6	460	-5.4 ± 0.7
LDL comm.	30.5 ± 7.7	-101.2 ± 17.6	-339 ± 59	1.1 ± 0.2	4100	-24.7 ± 4.3
VLDL comm.	24.7 ± 10.2	-70.8 ± 3.0	-237 ± 10	0.5 ± 0.1	120000	-0.6 ± 0.1

[a] For lipid-like molecules an average molar mass of 600 g mol^{-1} was assumed and literature values were used for the mass of lipoproteins. For further details see Experimental section.

[b] For the (V)LDL-fraction, 100% of LDL were assumed for the calculation of lipid-like molecules, as DLS and TEM results suggest clear predominance of LDL.

4.2.2 Lipoprotein corona analysis

In ITC measurements, the protein corona is probed *in situ*, without any further manipulation than constant stirring. However, in common corona preparation procedures, centrifugation is applied to remove free proteins before analysis.[13] In order to analyze quantitatively how centrifugation affects lipoproteins' cholesterol in the biomolecular corona, an enzymatic assay was used. The idea is to clarify how much cholesterol is washed off during centrifugation, how much remains on the NPs and can then be compared to the ITC data.

A common corona preparation procedure implies incubation of nanoparticles with an excess of lipoprotein solution and five subsequent centrifugation steps. After each step, the pellet is resuspended in 1 mL of phosphate-buffered saline (PBS) (see Experimental section). With the enzymatic assay, blood plasma, pure lipoprotein samples as well as the lipoprotein corona formed on PS-NPs were analyzed. Further, the supernatant after each centrifugation step during lipoprotein corona preparation was analyzed in order to track possible removal of cholesterol from the NPs surface during centrifugation steps (Figure 4.2.8). In the supernatant after the first centrifugation step, most cholesterol is found, usually in the same range as in the initial solution incubated with lipoproteins. Further centrifugation steps do not release significant amounts of cholesterol. By desorption of the remaining 'hard corona', a certain amount of cholesterol adsorbing to the PS-NPs is finally released and can be detected with the assay. The number of molecules of total cholesterol (TC; free cholesterol and cholesteryl esters) retrieved from the corona of the PS-NPs was then compared to the number of TC molecules calculated from the previously discussed ITC experiments. In order to calculate the number of TC molecules, an average molar mass of 600 g mol^{-1} was assumed.

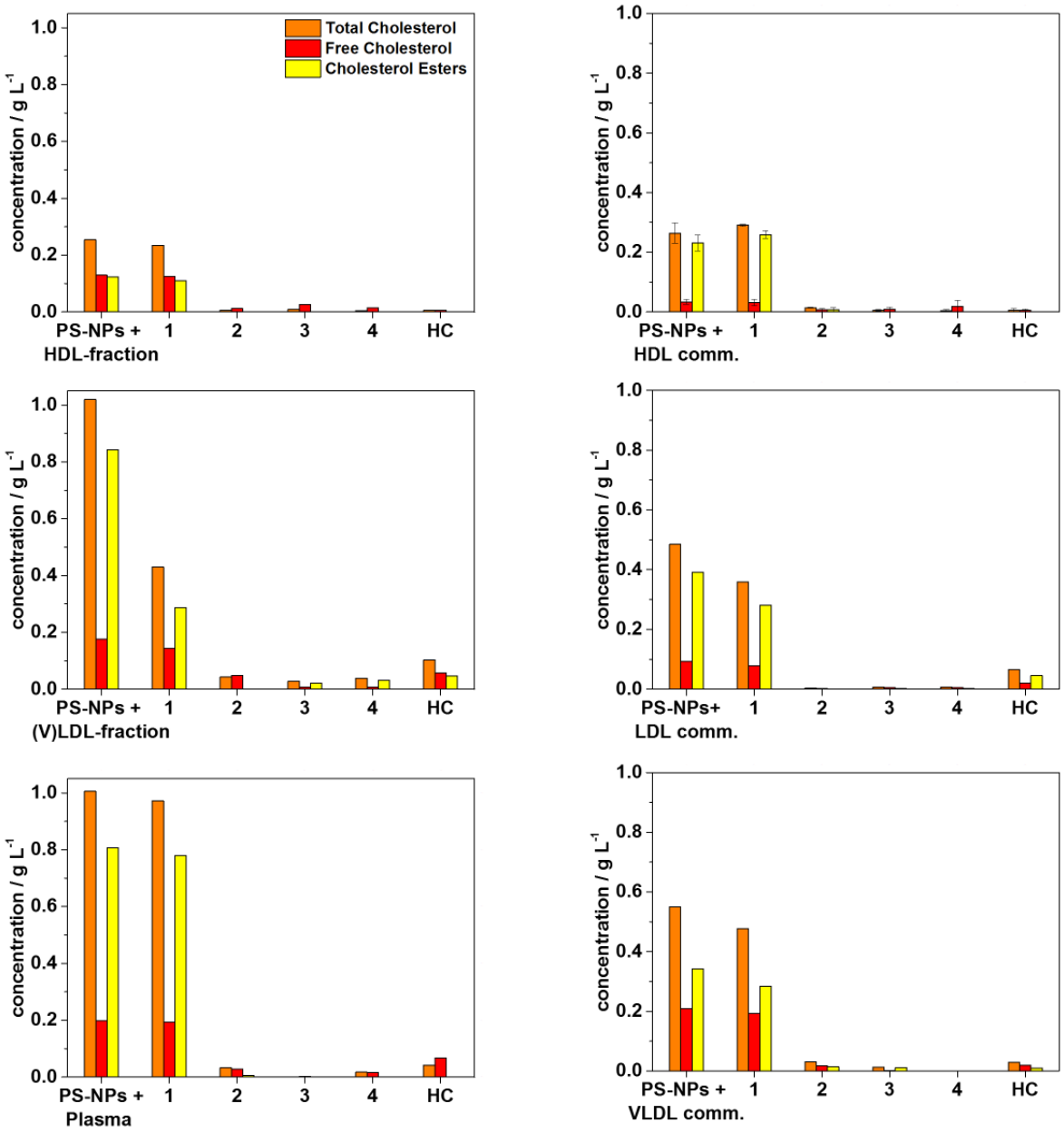

Figure 4.2.8 Cholesterol assay of PS-NPs incubated with different lipoprotein samples. The numbers 1 – 4 indicate after which centrifugation step the supernatant was analyzed, 'HC' refers to the hard corona remaining on the PS-NPs after five centrifugation steps. Experiments with plasma and commercial lipoproteins were conducted by [redacted].

As expected, most of the excessive cholesterol was discarded in the first washing step, only minor amounts of cholesterol are found in the supernatant of the following washing steps (see Figure 4.2.8). However, significant amounts of cholesterol were found on the surface of the PS-NPs after four washing steps (see Table 4.2.3). This already suggests that the cholesterol molecules exhibit a high binding affinity towards the NP surface. Even for the incubation with plasma, where numerous other biomolecules (such as proteins) compete for adsorption on the NP surface, cholesterol was detected

in the biomolecule corona. Furthermore, the amount of TC molecules per NP as determined *via* the cholesterol assay matches the number of TC per PS-NP determined by ITC experiments well (see Table 4.2.3). Only in the case of the (V)LDL-fraction the calculation of the number from ITC does not take into account the high amount of cholesterol in VLDL, which leads to an underestimation of TC molecules. Following this, cholesterol and cholesteryl esters must adsorb rather strongly on the nanoparticles' surface during interaction as they cannot be discarded during centrifugation, which suggests them to be rather strongly adsorbing corona components. This is also in accordance with the high association constants observed in the previously discussed ITC experiments between complete lipoproteins and PS-NPs. Interestingly, the number of TC molecules found on the nanoparticles after plasma incubation is in the same order of magnitude as after incubation with pure lipoprotein fractions. This suggests that the strong interactions between the lipoproteins and nanoparticles also take place under physiological conditions. Though it would also be desirable to directly probe the adsorption of pure cholesterol or cholesteryl esters on PS-NPs by ITC, this is precluded by the insolubility of these compounds in water.

Table 4.2.3 Number of TC molecules adsorbed per PS-NP, data obtained from cholesterol assay and ITC experiments.

	m (TC) per NP / 10^{-17} g (chol. assay)	# TC molecules per NP (chol. assay)	# TC molecules per NP (ITC)
Plasma	3.0 ± 0.5	30000 ± 5000	2420 ± 610 [a]
HDL-fraction	0.4 ± 0.1	4000 ± 1000	3860 ± 180
(V)LDL-fraction	7.4 ± 1.1	74000 ± 11000	2260 ± 380 [b]
HDL comm.	0.7 ± 0.1	7000 ± 1000	3900 ± 70
LDL comm.	5.0 ± 0.8	50000 ± 8000	15000 ± 230
VLDL comm.	2.1 ± 0.3	21500 ± 3000	13200 ± 1320

[a] For details on calculation see Figure 4.2.8.

[b] For the ITC experiments concerning the (V)LDL-fraction, 100% of LDL were assumed for the calculations, as DLS and TEM results suggest clear predominance of LDL.

Besides the lipids contained in lipoproteins, the protein fraction of the corona formed by lipoproteins was also analyzed in order to get a full understanding of the lipoprotein-NP-interaction. To identify

proteins in the different lipoprotein-corona samples, liquid chromatography-mass spectrometry (LC-MS) measurements (performed by [redacted]) as well as sodium dodecyl sulfate polyacrylamide gel electrophoresis (SDS-PAGE) experiments (see Figure 4.2.9) were carried out. As expected, in commercial HDL (and in the HDL fraction), a band attributed to Apo-A1 at 28 kDa is observed; the same applies to the respective coronae. The molecular weight of apolipoprotein B-100 as reported in literature is 550 kDa, which is out of range of the marker. For commercial LDL, VLDL and the (V)LDL-fraction, still a similar pattern at high molecular weights is detected. A band at 34 kDa attributed to apolipoprotein E can be found in commercial VLDL and its corona.

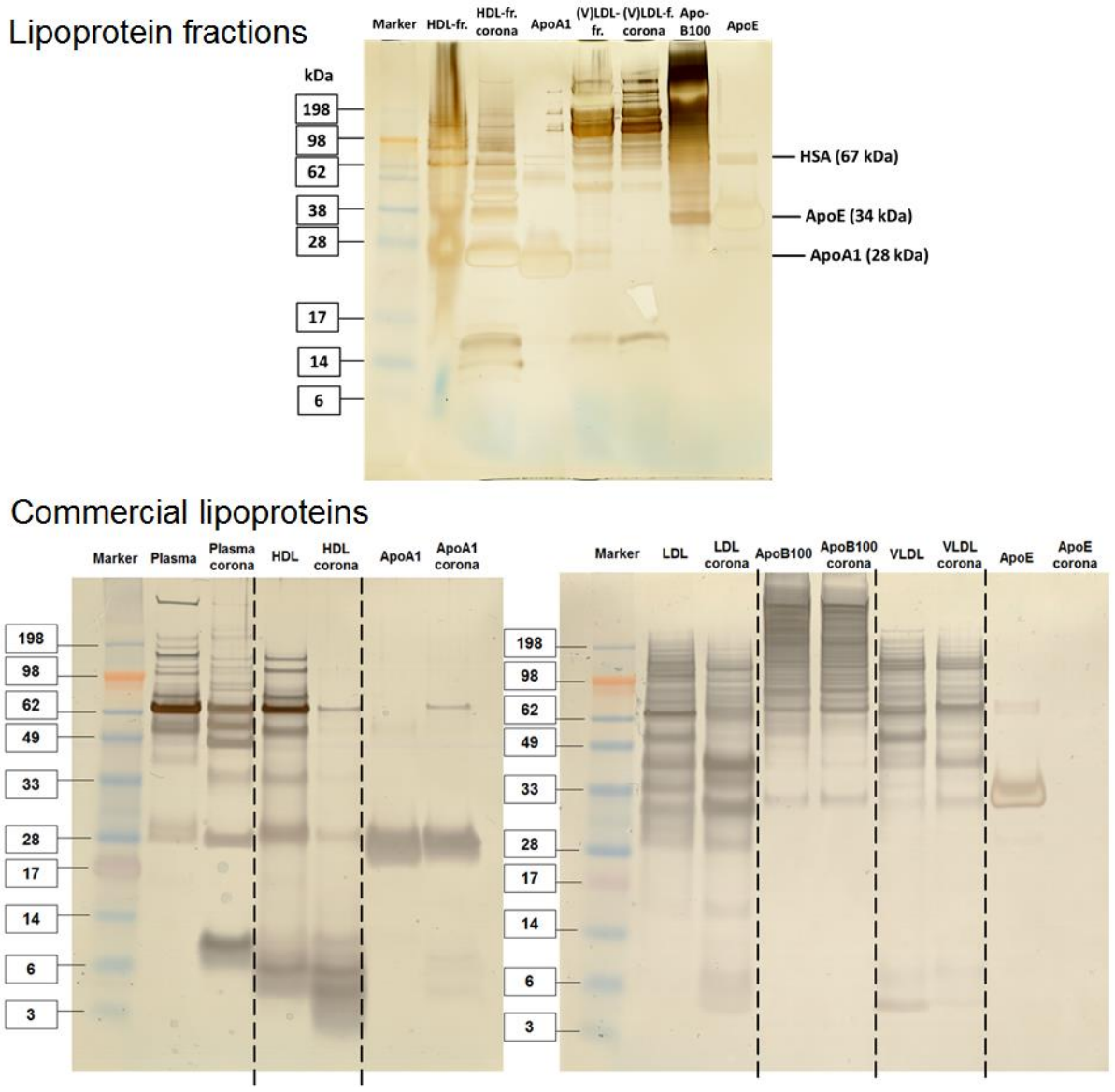

Figure 4.2.9 Sodium dodecyl sulfate polyacrylamide gel electrophoresis (SDS-PAGE). Proteins present in lipoproteins alone and in the lipoprotein corona of PS-NPs were separated by size. For reference, single apolipoproteins were applied to the gel and full plasma as well as a corona on PS-NPs prepared

thereof were applied as well. SDS-PAGE of the commercial lipoproteins (lower panel) were performed by [redacted].

Figure 4.2.10 shows the proteins with a fraction of > 1% in the biomolecular corona of NPs incubated with lipoproteins as determined by LC-MS (experiments performed by [redacted]). In HDL- and (V)LDL-fractions, the most abundant proteins are Apo-A1 and Apo-B100 proteins, respectively. Apo-B100 appears also in commercial LDL and commercial VLDL coronae, ending up as the second most abundant protein. In addition, Apo-A1 and Apo-B100 were the main protein representatives of HDL- and (V)LDL-fractions, as it can be seen in Figure 4.2.1. LC-MS analysis reveals also some proteins (*e.g.*, serum albumin) not characteristic to HDL and (V)LDL. The presence of those proteins was already shown in the lipoprotein samples before corona formation and is a result of the challenging purification process. The protein identification of the corona samples contains a significant amount of apolipoproteins, suggesting that also proteins of the lipoproteins have a high affinity to the PS-NPs and not only the lipids.

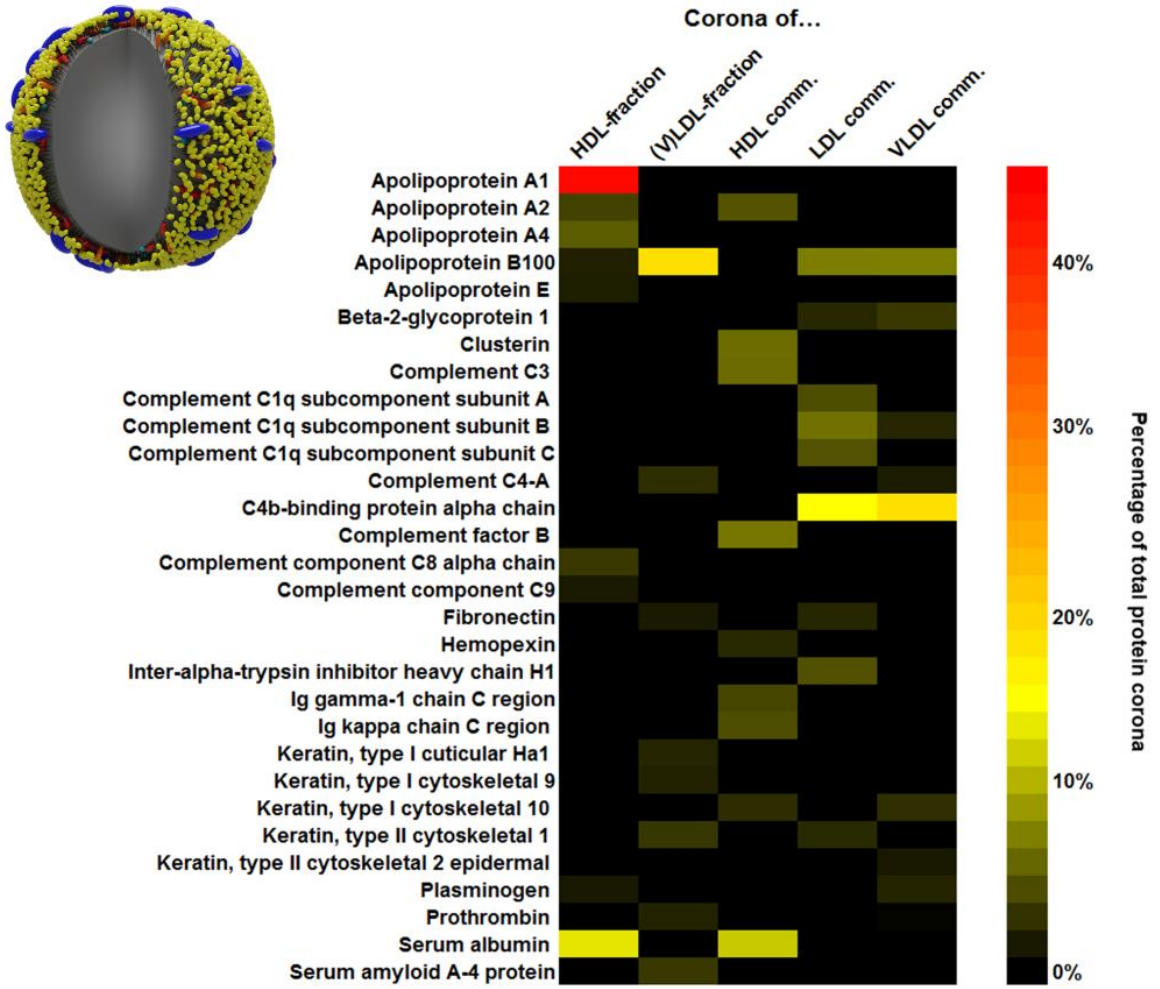

Figure 4.2.10 LC-MS analysis of the protein coronae of PS-NPs after incubation with different lipoproteins. Proteins with an abundance of > 1% are presented as a heat map. LC-MS experiments were conducted by [redacted].

Transmission electron microscopy (TEM) was used to visualize the structure of the lipoprotein corona forming around the PS-NPs (experiments performed by [redacted]). Lipoproteins and nanoparticles were embedded in a layer of trehalose containing heavy metals (uranyl acetate), providing additional contrast. This preparation method, which was recently presented by Kokkinopoulou *et al*., allows to preserve the morphology of adsorbed proteins on PS-NPs better than measurements in dry state and enables the visualization of the proteins.[100] In the control micrographs in Figure 4.2.11, lipoproteins are visible as bright spots. As expected, their size increases from HDL over LDL to VLDL. When the PS-NPs were incubated with a lipoprotein concentration according to ITC stoichiometry, no complete lipoprotein complexes (bright spots) were visible anymore. However, if a ten-fold excess of lipoprotein is used, again complete unbound lipoproteins were detected. Using a ten-fold excess, the lipoprotein/NP ratio comes closer to the realistic physiological situation of NPs in

blood (few NPs facing a large excess of lipoproteins) than using the ITC stoichiometry does. This clearly indicates that a relevant interaction between the two components takes place well below physiological ratios. The fluctuation of the lipoprotein levels *in vivo* will accordingly not have therapeutic relevance. Even a lipoprotein level at the lower threshold of the physiological range would represent a very large excess to the NPs, so an increased lipoprotein level will not change this situation significantly. The absence of intact lipoproteins incubated with NPs at ITC stoichiometry, together with the high binding enthalpy observed in ITC, leads to the conclusion that lipoproteins disintegrate upon contact with PS-NPs. Once all available surface of PS-NPs is saturated, lipoprotein complexes will stay intact, which is the case for the ten-fold excess incubation.

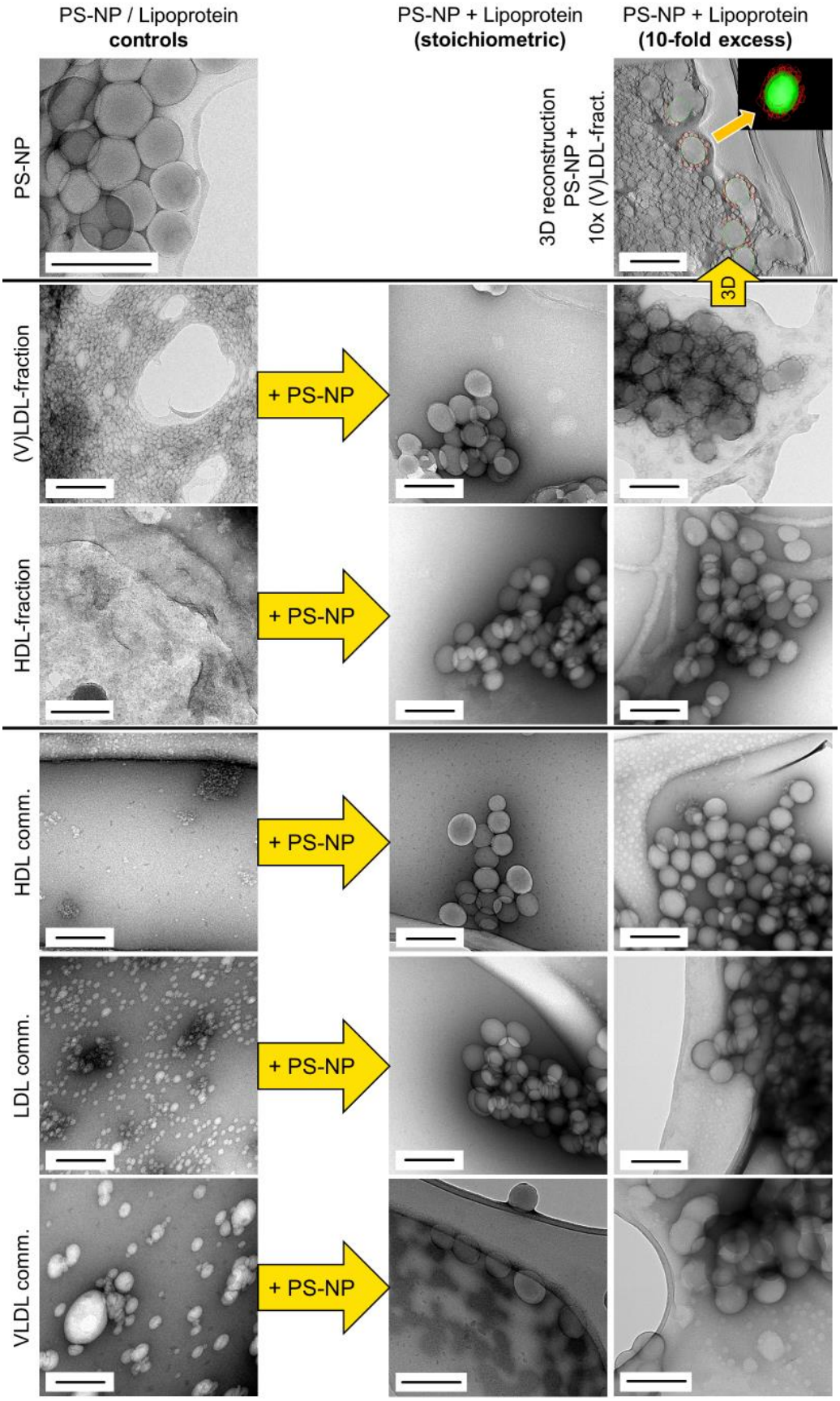

Figure 4.2.11 TEM micrographs of PS-NPs, lipoproteins and mixtures of both. The samples were embedded in trehalose and negatively stained with uranyl acetate. Two different concentrations of lipoproteins were applied: stoichiometric ratio *n* obtained from ITC (Table 4.2.1) and 10-fold excess of

stoichiometric ratio *n* (indicated by arrow). A snapshot from 3D reconstruction of a PS-NP with 10-fold excess of the (V)LDL-fraction is shown in the right column. Scale bars are 200 nm. TEM experiments were performed by [redacted].

For the lipoprotein fractions, it is observed that in ten-fold excess, also complete lipoproteins complexes stick to the surface of PS-NPs, probably on top of a layer of adsorbed lipids. In the case of stoichiometric incubation, this does not occur, so disintegration and adsorption of lipids also takes place for the lipoprotein fractions. For the sample containing intact lipoproteins attached to the NP surface Image J was used to calculate the size distribution after adsorption.[101] The diameter of the additional corona was estimated to be 26 nm (see Figure 4.2.11, magnification in Figure 4.2.12, and Table 4.2.4).

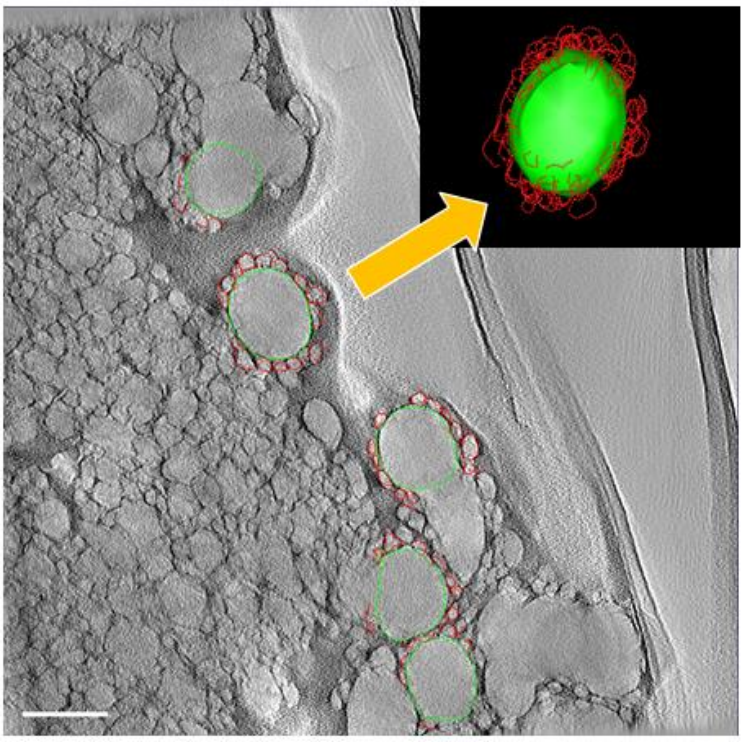

Figure 4.2.12 TEM 3D reconstruction. Snapshot from 3D reconstruction of a PS-NP incubated with 10-fold excess of the (V)LDL-fraction. It seems that most of the surface of the PS-NP was covered by the lipoproteins in the TEM micrograph. In the model, the surface of PS-NPs was not fully covered due to the missing wedge when collecting the tilt series at the microscope. Scale bar: 100 nm.

Table 4.2.4 Size distribution (NPs with 10-fold ITC stoichiometry) from TEM micrographs of NPs incubated with the (V)LDL-fraction analyzed with ImageJ.[101]

sample	diameter / nm
PS-NP	89 ± 12
(V)LDL-fraction	19 ± 4
PS-NP + (V)LDL-fraction	115 ± 18

This gives a rough idea of the size of the biomolecule corona formed on the PS-NPs and matches well with the size of LDL particles. Moreover, for the same sample the corona was visualized and analyzed using a 3-D reconstruction model. This is also pictured in Figure 4.2.11. It seems that most of the surface of the PS-NP is covered by the lipoproteins. Note that a part of the surface cannot be visualized due to the missing wedge when collecting the tilt series. Comparing this to the observations reported in literature, we think that the intact lipoproteins found in other studies could also be a result of an excess of lipoproteins and that a surface coverage with disintegrated lipoproteins underneath cannot be completely ruled out. However, this might also be dependent on the initial nanoparticle material, so that more hydrophilic surfaces could eventually hinder disintegration.

Nanoparticles bearing a biomolecular corona on their surface can exhibit drastically different behavior in comparison to naked nanoparticles, *e.g.* during cell-nanoparticle interaction and subsequent cellular uptake. This statement is true also for macrophages, a type of immune cells that play major role in the removal of foreign particles from the blood. Fluorescently labeled SDS-stabilized PS-NPs coated with HDL- or (V)LDL-fractions were analyzed with regard to their uptake by a murine macrophage-like cell line, namely RAW264.7, by [redacted]. As shown in Figure 4.2.13 all particles covered either with HDL or (V)LDL showed a huge decrease of cellular uptake similar to PS-NPs incubated in full plasma in contrast to those of naked nanoparticles (called “Water”). This stealth effect (*i.e.* the decrease of the unspecific uptake) can only be attributed to the biomolecular corona, which covers the surface of the nanoparticles.

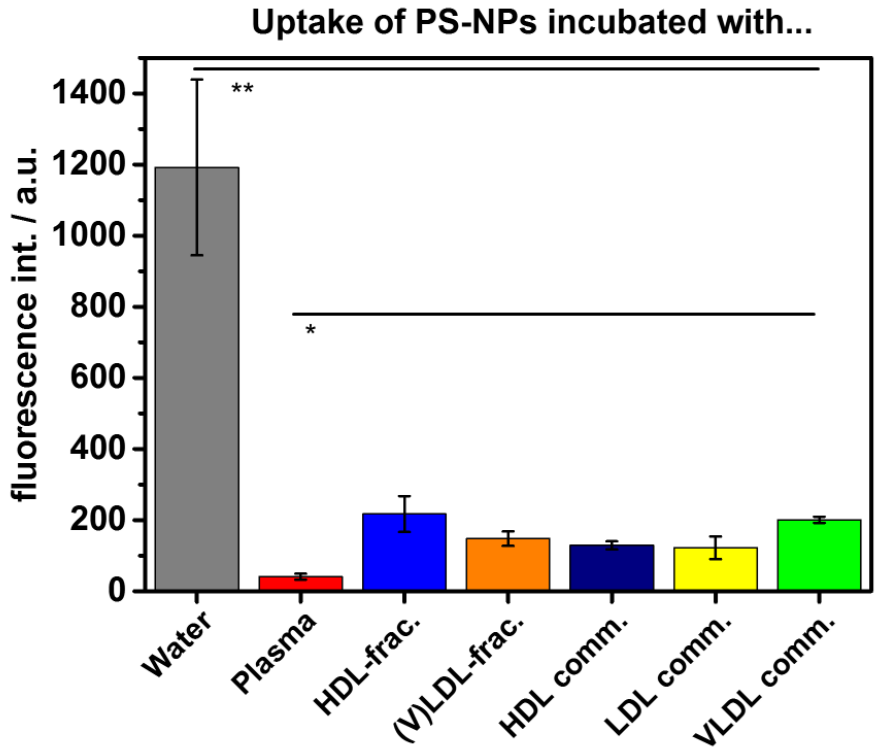

Figure 4.2.13 Cellular uptake of nanoparticles covered by different lipoprotein-coronae. The nanoparticles were incubated with HDL- and (V)LDL-fractions either purified from plasma or purchased commercially and centrifuged afterwards. Lipoprotein-coated nanoparticles were subsequently subjected to cellular uptake by mouse RAW264.7 macrophages. Fluorescence intensity values are expressed as mean ± SD (n = 3). The uptake of naked PS-NPs ("Water") and plasma-incubated PS-NPs ("Plasma") were used as controls. Cellular uptake experiments were performed by [redacted]. * $p < 0.05$, ** $p < 0.01$.

As we have reported earlier, when preparing the biomolecular corona from the incubation of nanocarriers modified with poly(ethylene glycol) in plasma, apolipoproteins were found to be highly enriched and responsible for a significantly reduced cell uptake.[13] Here, we have a similar effect on cell uptake when exposing the nanoparticles to pure lipoproteins, which could also mean that upon apolipoprotein enrichment the other lipoprotein components are present as well. It is still not clear, if the lipids themselves could be responsible for the decreased uptake, but this study supports that theory. The stealth effect in general increases the blood circulation time of the nanoparticles, thus giving the nanocarriers a higher probability to successfully reach their target (*e.g.* cancer cells). However, now in the case of lipoproteins it should also be considered that lipoprotein adsorption could also decrease the uptake into actual target cells. For successful drug delivery, the interaction of nanocarriers with lipoproteins thus needs to be carefully considered, as fluctuating cholesterol levels (and thereby lipoprotein concentrations) potentially affect the biological response. Besides our

findings, it was reported very recently that reconstituting the hydrophobic core of LDLs with fatty acids enables effective targeting of cancer cells.[57] Thus, coating of nanocarriers with lipoproteins might present a different strategy to provide a stealth effect and at the same time deliver cargo to cells exhibiting lipoprotein receptors.

4.2.3 Conclusions

In this study, we evaluated the thermodynamic aspects of the interactions between different lipoproteins and polymeric nanoparticles, which implied adsorption of not only the apolipoproteins but also the lipid-like molecules of the complexes, indicating that the adsorption process is not only driven by proteins. All lipoproteins adsorbed with a very high binding affinity, which is further supported by the fact that a significant amount of cholesterol is still bound to the particles even after centrifugation. Additionally, by applying TEM imaging the interaction mechanism was explored in detail: First, the three lipoproteins seem to disintegrate and cover the nanoparticle surfaces completely until saturation is reached. Subsequently, the adsorption of additional intact lipoproteins can be detected in some cases. Finally, the formed 'biomolecule' corona after lipoprotein adsorption significantly decreased the cell uptake into macrophages, leading to a similar effect as already reported for apolipoproteins. This means that for drug delivery studies with nanocarriers it is essential to also consider lipoproteins and not only proteins. Additionally, the strong adsorption affinity of lipoproteins towards nanocarriers might be exploited to create new "smart" delivery systems.

4.3 Denaturation *via* surfactants changes composition of protein corona

It has been shown in the previous chapter that lipoprotein adsorption to nanocarriers is an aspect of the biological response that should not be neglected. It was shown that amphiphilic lipids have an impact on the stealth effect. Previously, the effect of a PPE-surfactant coating of nanocarriers on the protein corona has been investigated.

Now, another aspect of common surfactants, which are usually present in NP dispersions, to the protein corona will be examined: How do these surfactants interact with proteins, which concentrations can induce denaturation and how does this affect formation of the protein corona? It is long known that amphiphilic surfactants, especially ionic ones, can denature proteins. This issue is likely to have consequences for the stealth effect of nanocarriers.

The content of this chapter was submitted as a full paper to the journal Biomacromolecules. Contributions to this work were made by other persons: [redacted] conducted LC-MS, SDS-PAGE as well as cellular uptake experiments, and [redacted] isolated CLU. I carried out ITC, DSF, zeta potential and DLS measurements, created figures and wrote the manuscript.

Surfactants can have different effects on the structure of proteins, as discussed in chapter 2.3.2. This can possibly affect the interaction of proteins with nanocarriers. However, it remains unknown how the adsorption behavior of proteins to nanoparticles and the composition of the protein corona is exactly affected by surfactants. Therefore, we analyzed the types of proteins adsorbing to nanoparticle dispersions with different surfactant concentrations after incubation with plasma and investigated how certain single proteins are affected/denatured by the surfactant.

In this chapter, isothermal titration calorimetry (ITC), differential scanning fluorimetry (DSF) and liquid chromatography-mass spectrometry (LC-MS) were applied to analyze the impact of surfactant-induced denaturation on the protein corona. Among others, ITC, differential scanning calorimetry (DSC) and DSF are suitable methods to study the interaction of surfactants with proteins and the denaturation of the latter.[45] We investigated how surfactants promote denaturation and influence the adsorption of apolipoproteins to model polystyrene nanoparticles (PS-NPs). The degree of denaturation depends strongly on the type of the protein itself, so different types of proteins are affected by surfactants to variable extent. Our results on two important corona proteins suggest that clusterin (CLU, also known as apolipoprotein-J) is more sensitive to surfactant denaturation than apolipoprotein-A1 (Apo-A1). These two apolipoproteins were chosen because they occur in the protein corona of stealth NPs in disproportionately high amounts and thus are of particular importance for the stealth effect.

4.3.1 Results and Discussion

The aim of this chapter is to investigate how surfactants influence protein adsorption to nanoparticles (NPs) and to which extent the composition of the protein corona is altered. Therefore, cetyltrimethylammonium chloride (CTMA-Cl), which is a standard surfactant for the stabilization of NPs in aqueous media, has been added in different, but still relatively small concentrations (between 0.01 wt% and 0.3 wt%) to NP-dispersions and the protein corona after incubation with plasma has been analyzed by LC-MS and SDS-PAGE.

Two different types of polystyrene nanoparticles introduced in Figure 4.3.1 were used in this study. The first NPs, referred to as PS-Lut, were stabilized by the nonionic surfactant Lutensol® AT50, which contains a poly(ethylene glycol) (PEG)-block. The only surface functionalization of PS-Lut was PEG adsorbed in the form of Lutensol®. The other NPs, called PS-PEG, were functionalized with covalently bound PEG-chains of a molecular weight of 5000 g mol^{-1} and were stabilized beforehand by the cationic surfactant cetyltrimethylammonium chloride (CTMA-Cl).

	PS-Lut	PS-PEG
R_h / nm	82 ± 8	67 ± 7
ζ / mV	− 8 ± 1	+ 13 ± 1
Functionalization	PEG adsorbed	PEG covalently bound
Surfactant	Lutensol (PEG-based)	CTMA-Cl
SEM	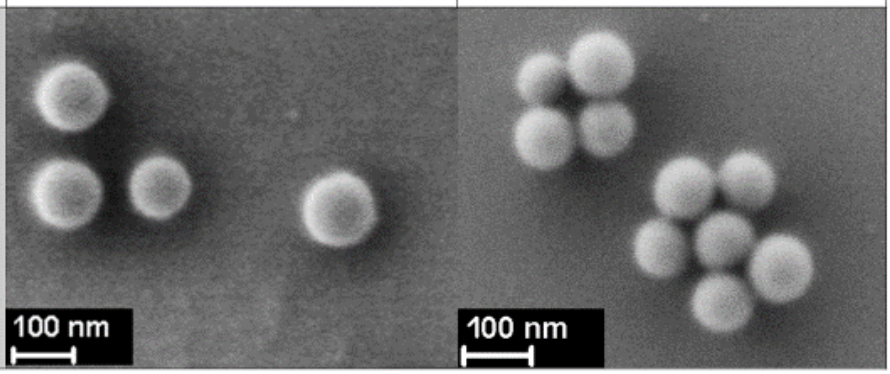	

Figure 4.3.1 Characteristics of the nanoparticles, with scanning electron microscopy (SEM) micrographs. Lutensol-stabilized polystyrene nanoparticles (PS-Lut) and PEGylated polystyrene nanoparticles (PS-PEG) with covalently attached PEG-chains (M_n = 5000 g mol^{-1}) of similar diameters were used in this study.

Dispersions of PS-Lut with different amounts of CTMA-Cl were prepared and each sample was incubated with human citrate plasma (experiment scheme see Figure 4.3.2-A). After preparation of the hard protein corona by applying several centrifugation steps for the removal of excessive free proteins, (see Experimental Section), LC-MS and SDS-PAGE were carried out by [redacted]. In Figure 4.3.2-B, the amounts of the most abundant corona proteins identified by LC-MS are given for the different concentrations of CTMA-Cl in PS-Lut dispersions. Interestingly, the relative amount of CLU was reduced for CTMA-Cl concentrations > 0.01%. The amount of Apo-A1, however, increased for increasing CTMA-Cl concentrations. A significant amount of vitronectin appeared at a concentration of 0.1% CTMA-Cl and further increases for higher concentrations. The total amount of all adsorbing proteins also rose upon addition of CTMA-Cl.

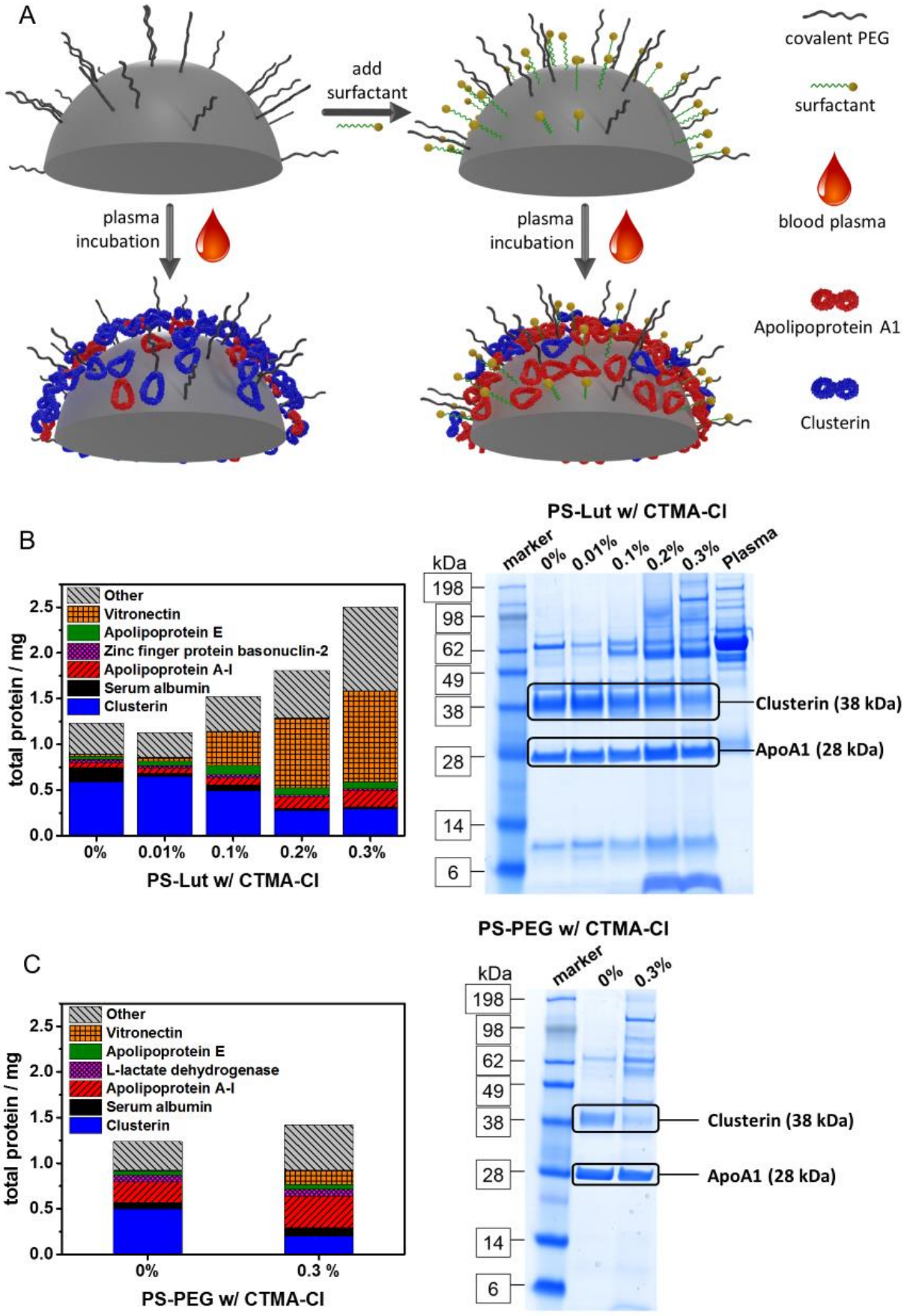

Figure 4.3.2 Protein corona composition of PS-NPs with different amounts of surfactant, as observed after incubation with plasma. (A) Schematic illustration of the experiment resulting in an enrichment

of apolipoprotein-A1 (red) in the protein corona of PEGylated nanoparticles with additional surfactant (not drawn to scale). (B),(C) Total amounts of protein identified by LC-MS and Pierce 660 nm protein assay in the protein corona of nanoparticles (PS-Lut and PS-PEG) with additional surfactant (CTMA-Cl) incubated with blood plasma and SDS-PAGE of the same samples. Artwork copyright by [redacted]. LC-MS experiments and SDS-PAGE were conducted by [redacted].

SDS-PAGE confirmed the findings from LC-MS. Strong bands at 38 kDa are attributed to CLU, other prominent bands at 28 kDa to Apo-A1. Moreover, the difference of the corona composition compared to plasma is quite apparent: human serum albumin (66 kDa) is highly abundant in plasma, but made up only a small fraction of the protein corona.

To investigate whether this effect also occurs for other types of nanoparticles, a similar experiment was conducted with covalently PEGylated NPs. As for PS-Lut the most pronounced effect was observed for the highest concentration of CTMA-Cl, only 0% and 0.3% CTMA-Cl were tested for PS-PEG. Indeed, similar observations were observed in LC-MS and SDS-PAGE for the respective experiment with PS-PEG dispersions, as shown in Figure 4.3.2-C. While the protein corona of bare PS-PEG contained more CLU than Apo-A1 and no vitronectin, for PS-PEG with 0.3% CTMA-Cl more Apo-A1 than CLU were detected, as well as additional vitronectin. Also, the overall amount of proteins showed a slight increase. Figure 4.3.2-A sums up the findings of Figure 4.3.2-C schematically: When extra CTMA-Cl was added to PS-PEG particles before incubation with plasma, more Apo-A1 than CLU was found in the corona.

For PS-Lut, four other concentrations of CTMA-Cl were tested additionally. No significant difference of the protein corona composition was observed in SDS-PAGE for these concentrations of CTMA-Cl below 0.1%, (see Figure 4.3.3).

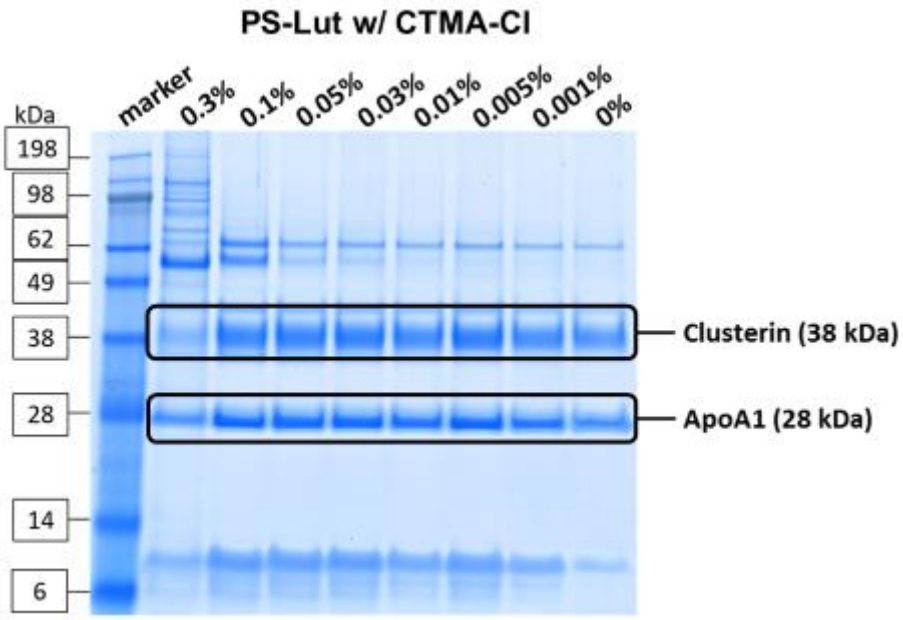

Figure 4.3.3 SDS-PAGE of PS-Lut with additional CTMA-Cl concentrations, as supplementation to Figure 4.3.2. SDS-PAGE was conducted by [redacted].

To get a better understanding of the role of CTMA-Cl, the theoretical maximum number of CTMA-Cl molecules binding to the NP surface has been calculated and found to be 212000 molecules per NP for PS-Lut and 141000 for PS-PEG (assuming a required area of 0.4 nm² per molecule CTMA-Cl). For the samples prepared with additional CTMA-Cl, this means that for concentrations larger than 0.01%, a significant amount of CTMA-Cl was freely diffusing in the NP-dispersions.

The zeta potential of the dispersions correlated with the amount of CTMA-Cl adsorbed to the NP surface, as additional positive charge was added to the NPs. The zeta potential of PS-Lut (see Table 4.3.1) changes from a negative to a positive value upon CTMA-Cl addition. As saturation of the NP surface is reached with 0.01% of CTMA-Cl, the zeta potential does not increase further at higher concentrations.

Table 4.3.1 Zeta potential of NP-dispersions with different amounts of additional CTMA-Cl (samples of Figure 4.3.2).

	PS-Lut					**PS-PEG**	
CTMA-Cl	0%	0.01%	0.1%	0.2%	0.3%	0%	0.3%
ζ / mV	−8 ± 4	22 ± 8	26 ± 8	24 ± 9	26 ± 9	13 ± 6	15 ± 7

The hydrodynamic diameters of the NPs loaded with additional CTMA-Cl were measured by DLS. In Table 4.3.2, the results are displayed. Considering the error range, no significant differences in size between the NPs without and with additional CTMA-Cl was found. This meets the expectations, as the size increase by adsorption of a surfactant monolayer is marginal and within the error range of DLS. Beyond that, a formation of surfactant multilayers is unlikely.

Table 4.3.2 Hydrodynamic diameters of NPs with added CTMA-Cl as determined by DLS.

	PS-Lut					**PS-PEG**	
CTMA-Cl	0%	0.01%	0.1%	0.2%	0.3%	0%	0.3%
D_h **/ nm**	119 ± 27	111 ± 19	122 ± 23	115 ± 43	116 ± 15	114 ± 30	141 ± 56

As Apo-A1 and CLU proved to be dominant in the protein corona, these two apolipoproteins were analyzed in detail with further analytical methods. In differential scanning fluorimetry (DSF), the auto-fluorescence of a protein, mainly caused by the tryptophan residues, is recorded during controlled heating of the sample. No fluorescent dye is required for this method. It allows to monitor protein unfolding and to detect the proteins 'melting temperature', *i.e.* its point of denaturation.

Unfolding of the protein goes along with a change of the vicinity of the tryptophan residues and therefore a change of the proteins' intrinsic fluorescence.[102] DSF experiments were conducted with CLU and Apo-A1 samples with different CTMA-Cl concentrations. The respective unfolding and refolding curves and the associated first derivatives are shown in Figure 4.3.4.

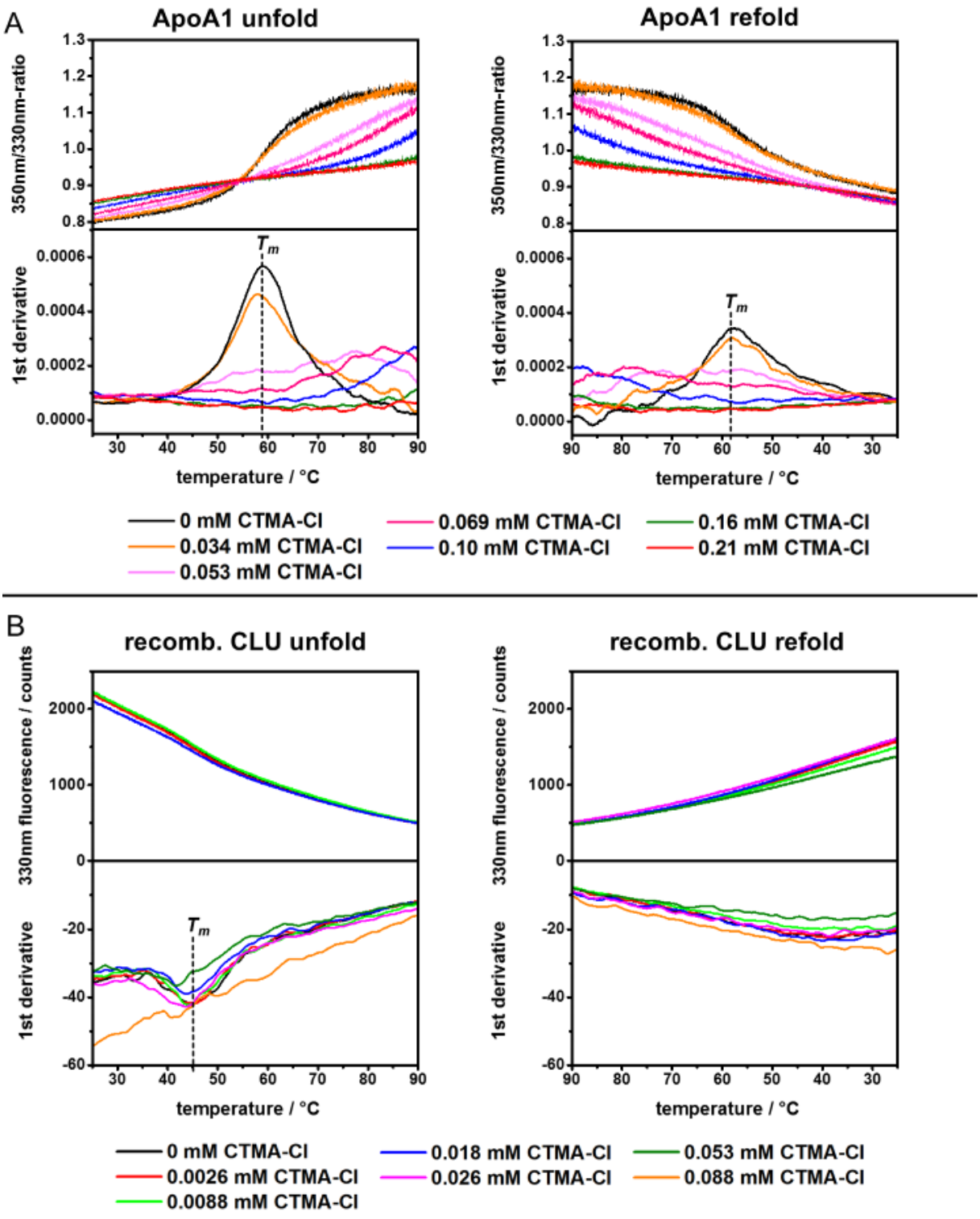

Figure 4.3.4 Differential scanning fluorimetry (DSF) of Apo-A1 and recombinant CLU with CTMA-Cl in different concentrations showing the protein unfolding (heating) and refolding (cooling). (A) 350 nm/330 nm ratio of fluorescence of Apo-A1 with CTMA-Cl together with the first derivative (B) 330 nm fluorescence of CLU with CTMA-Cl together with the first derivative.

For Apo-A1, the ratio of the fluorescence recorded in two wavelength channels (350 nm and 330 nm) and the respective derivative is depicted in Figure 4.3.4-A.

The sample of native Apo-A1 (black line **–**) shows a distinct transition at approximately 59 °C (maximum in the first derivative), indicating unfolding of the protein at this temperature. This unfolding or 'melting' temperature T_m is observed for native Apo-A1 and the lowest concentration of CTMA-Cl. For concentrations higher than 0.034 mM CTMA-Cl, this transition cannot be detected that clearly anymore, suggesting that the protein is already denatured by the surfactant to a large extent. In a refolding experiment run subsequently to the initial unfolding experiment, a transition of Apo-A1 is found at about the same temperature for the native protein and 0.034 mM CTMA-Cl sample. Apo-A1 therefore seems to have the capability to fold back into the native state.

For DSF, the quality of the curves obtained for the different wavelengths varies between different proteins depending on the mechanism of the respective unfolding. Thus, in Figure 4.3.4-B, the single wavelength fluorescence at 330 nm of CLU is plotted, because of a better signal-to-noise ratio than the ratio of two wavelength channels. Native CLU exhibits a transition at approximately 45 °C (minimum in the 1st derivative), which is shifted to lower temperatures upon addition of CTMA-Cl, for example to 42 °C for 0.053 mM CTMA-Cl. For 0.088 mM CTMA-Cl, no transition is observed anymore, so complete denaturation by the surfactant has occurred. Unlike for Apo-A1, no transition is detected in the subsequent refolding experiment, which means that CLU does not fold back once it has been denatured.

Denaturation of CLU in DSF experiments occurs at significantly lower concentrations than for Apo-A1, so obviously CLU is more sensitive to denaturation by CTMA-Cl than Apo-A1.

For NP-dispersions with additional CTMA-Cl (as in Figure 4.3.2), it therefore needs to be assumed that CLU is denatured by free CTMA-Cl. Since Apo-A1 is less prone to denaturation by CTMA-Cl, it is therefore conceivable that it can take over the free binding sites on the NP surface from CLU. This is a possible explanation of the observation from Figure 4.3.2 that more Apo-A1 than CLU adsorbs to NPs with an increase of additional, free CTMA-Cl.

As a control experiment, an aqueous solution of pure CTMA-Cl at a high concentration was measured (Figure 4.3.5). The fluorescence recorded is about one order of magnitude below the level typically measured for the protein samples with CTMA-Cl. The surfactant therefore has no significant contribution to the fluorescence in the DSF measurements of proteins presented above.

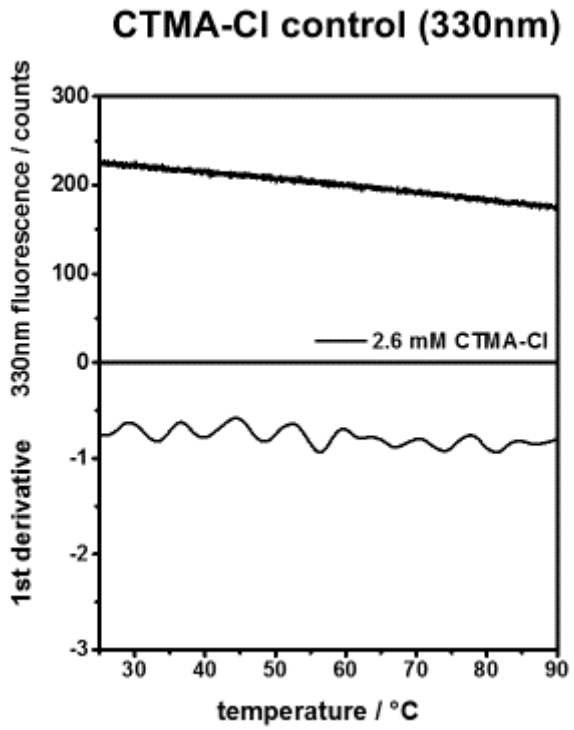

Figure 4.3.5 DSF experiment of pure CTMA-Cl in water as control experiment.

To further characterize the interaction (respectively the denaturation) of apolipoproteins by CTMA-Cl, the proteins were titrated with the surfactant in isothermal titration calorimetry (ITC) experiments. Figure 4.3.6 depicts the heat rates (raw data) of the experiments. The plots of heat versus molar ratio are shown in Figure 4.3.7-A and -B, including an independent binding model fit. In Figure 4.3.7-A, a linear blank was combined with the independent binding model fit to adequately describe the descending slope, in Figure 4.3.7-B a constant blank was sufficient as an upper plateau is observable.

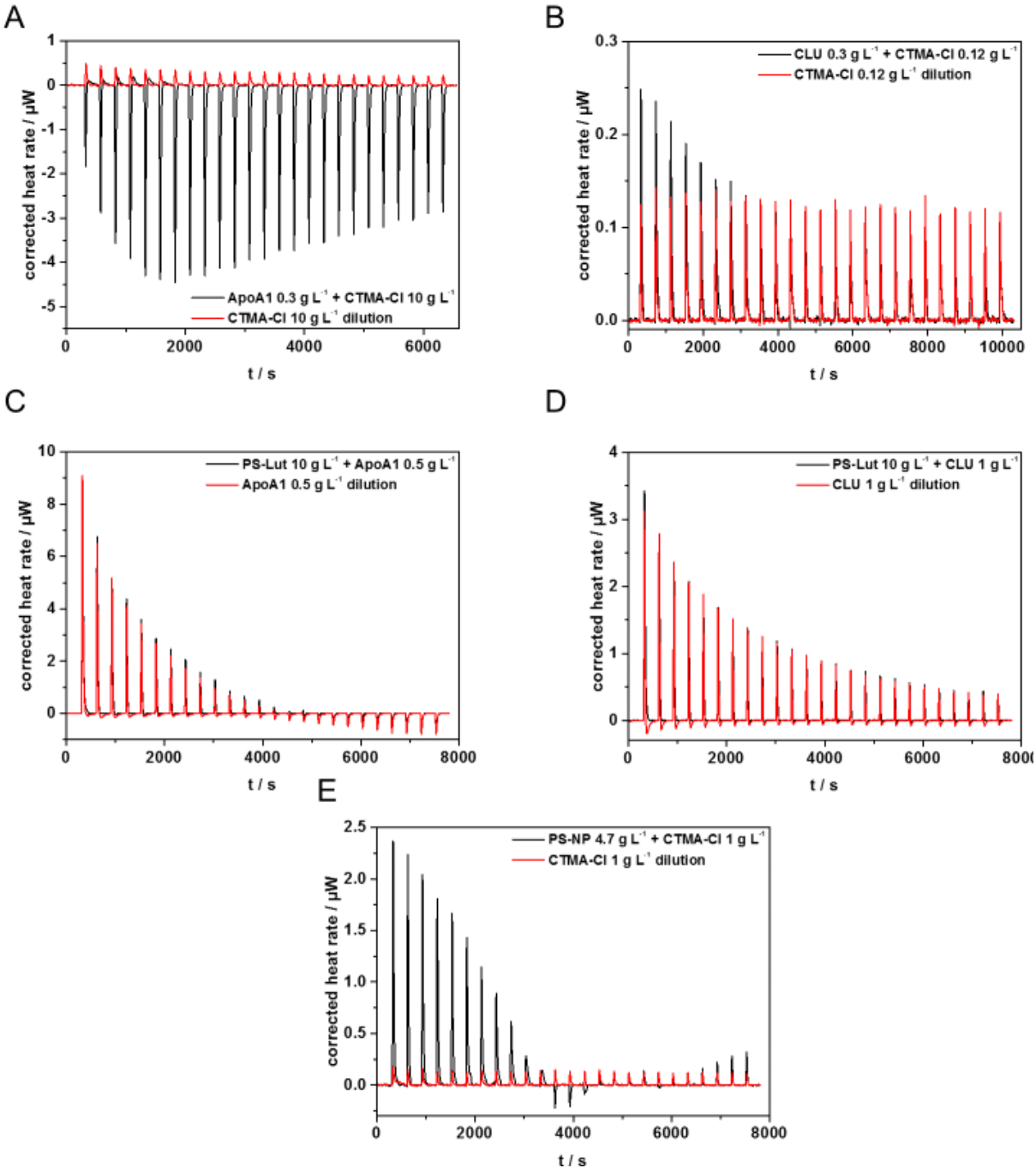

Figure 4.3.6 Heat rates (raw data) of ITC experiments displayed in Figure 4.3.7 and Figure 4.3.8. The black line (**–**) shows the heat rate for the respective titration experiment and the red line (**–**) indicates the heat rate of the dilution experiment (titration of the titrant into Milli-Q water).

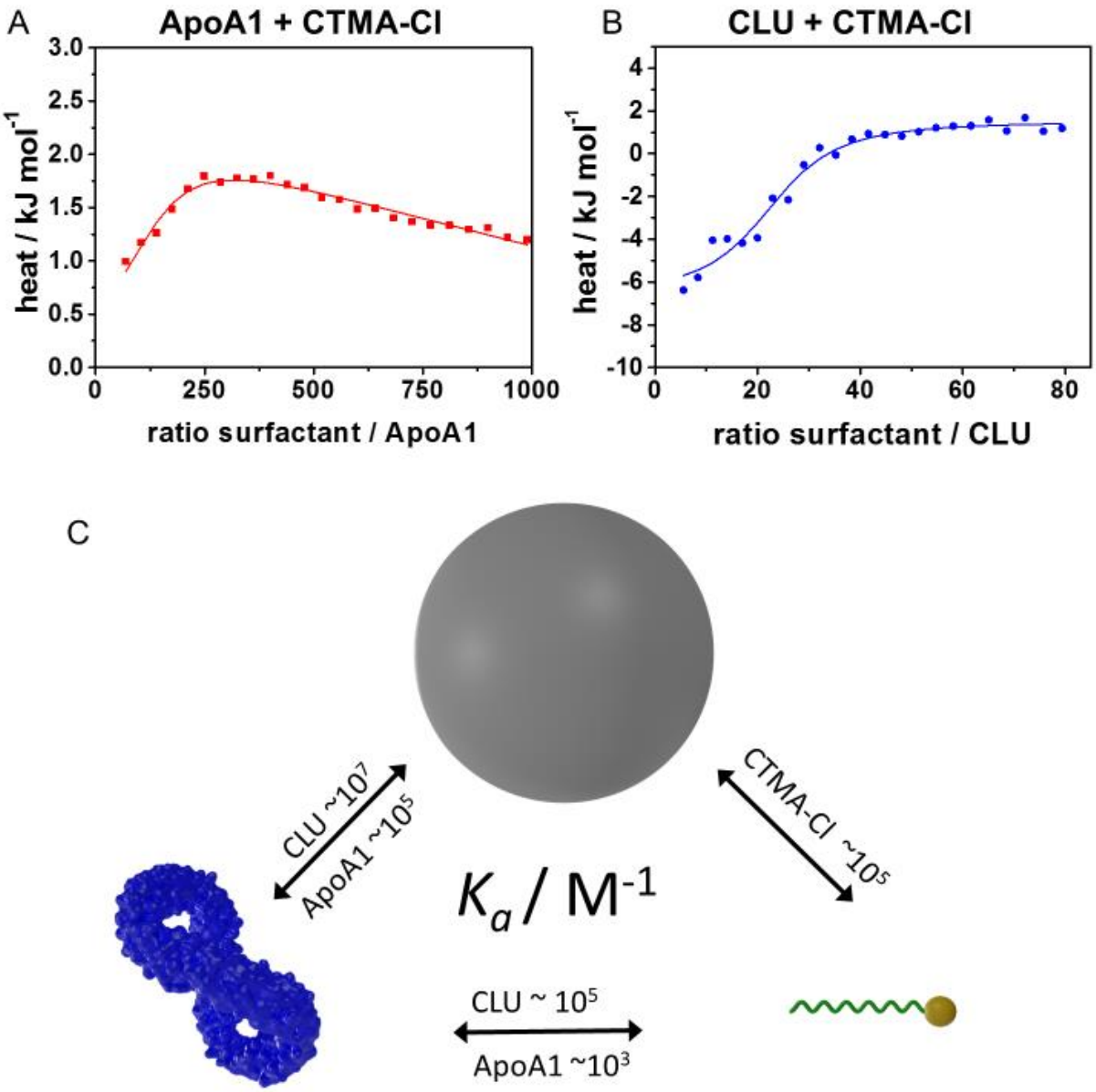

Figure 4.3.7 Isothermal titration calorimetry (ITC) experiments of Apo-A1 and recombinant CLU with CTMA-Cl together with a schematic comparison of binding affinities K_a obtained for the different components of the nanoparticle-protein-system. (A) Titration of Apo-A1 with CTMA-Cl together with an independent binding model fit (red line –) (B) Titration of recombinant CLU with CTMA-Cl together with an independent binding model fit (blue line –).

For the interaction of Apo-A1 with CTMA-Cl (Figure 4.3.7-A), an endothermal response is observed after subtracting the heat of dilution (Figure 4.3.6), while for CLU and CTMA-Cl (Figure 4.3.7-B) an interaction occurs mainly in the exothermal range. The change of entropy ΔS was determined from the fit (Table 4.3.3) as ΔS = 61 J K^{-1} mol^{-1} for Apo-A1 and ΔS = 79 J K^{-1} mol^{-1} for CLU. This increase of entropy can possibly be attributed to the denaturation process of the protein, which involves a loss of the

(ordered) native protein structure and thus increases the rotational freedom of the protein backbone. The corresponding values for the enthalpy change ΔH (Table 4.3.3) are comparably small, so the interaction of surfactant with the proteins is described as entropy-driven.

In Figure 4.3.7-C, the orders of magnitude of the binding affinities K_a for all the components (NP, CTMA-Cl, CLU, Apo-A1) are given. The precise values of K_a and other fit parameters with standard deviation (where available) of these and of additional ITC experiments are listed in Table 4.3.3. The ITC graphs of additional experiments with PS-Lut nanoparticles and Apo-A1/CLU, as well as PS-NPs with CTMA-Cl are shown in Figure 4.3.8. The binding affinity of CTMA-Cl to CLU ($4 \cdot 10^7$ M^{-1}) exceeds the value for CTMA-Cl to Apo-A1 ($3.7 \cdot 10^3$ M^{-1}) by two orders of magnitude. This higher affinity between protein and surfactant can be interpreted as the driving force for the denaturation of CLU occurring at lower CTMA-Cl concentration compared to Apo-A1. Moreover, the binding affinity of CLU to PS-Lut particles is in the order of 10^7 M^{-1}, while the one of Apo-A1 is only about 10^6 M^{-1}. This supports the observation from Figure 4.3.2-A that initially significantly more CLU than Apo-A1 adsorbs to PS-Lut without additional CTMA-Cl. The affinity of CTMA-Cl to PS-NPs with minimal amount of CTMA-Cl (after dialysis, see experimental section) was determined to be about 10^5 M^{-1}, so in the case of competition between free surfactant and apolipoproteins, the proteins will rather adsorb to the nanoparticles (or possibly even replace CTMA-Cl from the surface).

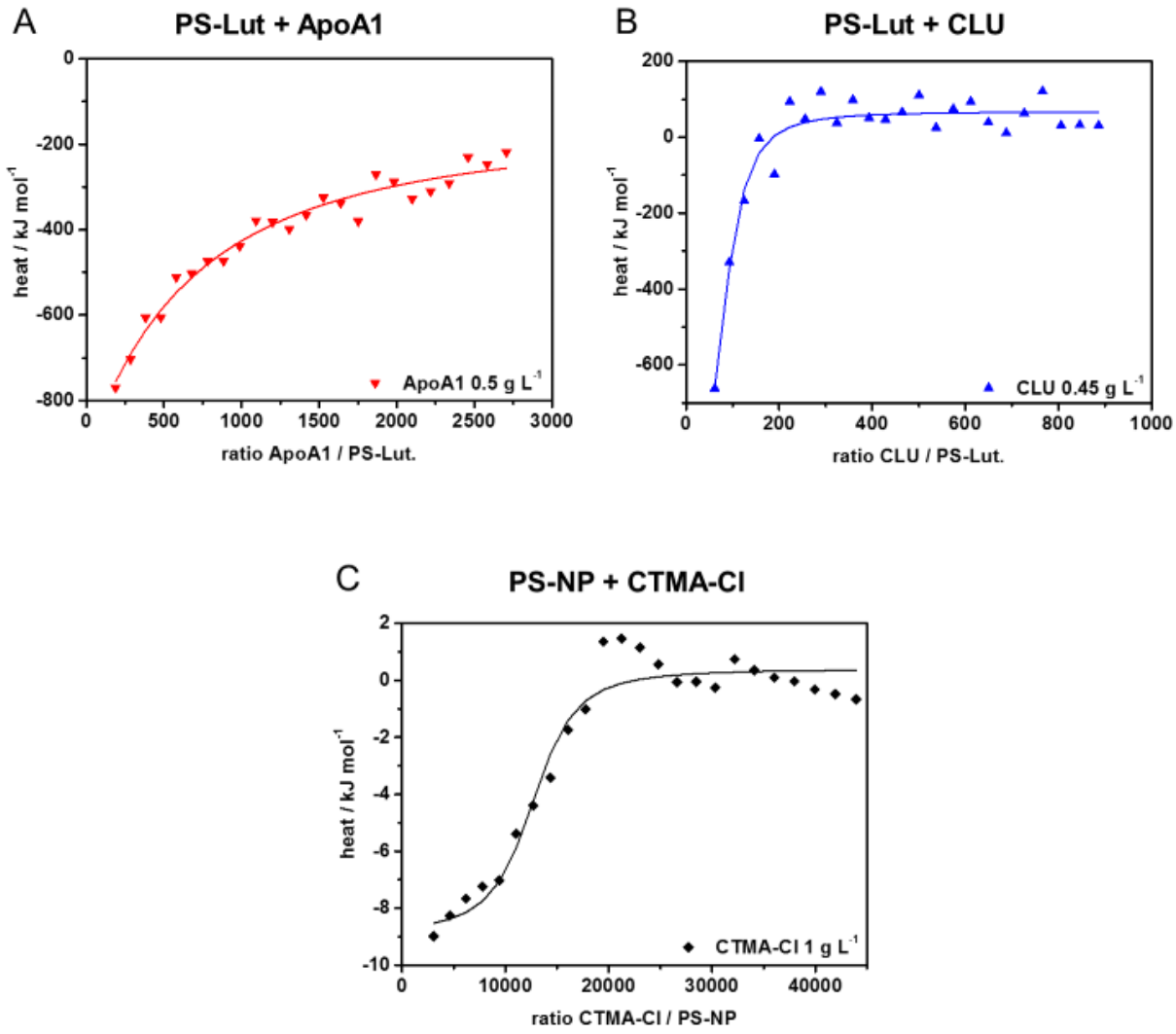

Figure 4.3.8 Additional ITC graphs. (A) Titration of a PS-Lut dispersion (10 g L^{-1}) with Apolipoprotein-A1 (0.5 g L^{-1}). (B) Titration of a PS-Lut dispersion (10 g L^{-1}) with clusterin (0.45 g L^{-1}). (C) Dialyzed PS-NP dispersion (4.7 g L^{-1}) titrated with CTMA-Cl (1 g L^{-1}).

Table 4.3.3 Fit parameters obtained from independent binding model fits of ITC data displayed in Figure 4.3.7 and Figure 4.3.8.

	K_a / 10^4 L mol^{-1}	n	ΔH / kJ mol^{-1}	ΔS / J K^{-1} mol^{-1}
Apo-A1 + CTMA-Cl	0.37 ± 0.11	110 ± 10	-2.2 ± 0.1	60.6 ± 2.7
CLU + CTMA-Cl	33	23	-8.1	78.5
PS-NP + CTMA-Cl	15 ± 2	11550 ± 820	-9.2 ± 0.1	67.9 ± 1.3
PS-Lut + Apo-A1	240	305	-1438	-4700
PS-Lut + CLU	3710	69	-1237	-4004

The data points obtained for PS-Lut NPs titrated with Apo-A1 / CLU and CLU titrated with CTMA-Cl showed no lower plateau, which makes it difficult to apply a sound fit. Therefore, the fit parameters (especially *ΔH*) give only limited information and no reasonable errors can be given.

4.3.2 Conclusions

We have shown that the apolipoproteins Apo-A1 and CLU have different sensitivity to denaturation by the surfactant CTMA-Cl. As a consequence, their structure and thereby their binding behavior to NPs changes. In a complex protein mixture like plasma, surfactant denaturation most likely has a significant effect on protein adsorption to NPs and on the composition of the protein corona. The affinity of the surfactant to a protein can determine depletion or enrichment of the respective protein in the corona. Competition and cooperation with the entirety of proteins in the plasma have further influence on the corona composition. An altered protein corona means a different biological identity of the nanocarriers, which could result in drastic changes for the *in vivo* behavior.

The critical parameter is surfactant concentration: as long as saturation of the NP surface is not reached, no or only a small effect on the protein denaturation is to be expected. Once full coverage of the NPs with surfactant is exceeded and considerable amounts of free surfactant are in solution, special attention should be paid to protein denaturation by the surfactant.

As a conclusion, surfactants used for stabilization of NP dispersions can affect the protein corona and alter the stealth effect. It is possible that surfactant denaturation interferes with other measures taken to realize a stealth effect, such as PEGylation of the surface. Therefore, control of the surfactant level is required for a defined protein corona formation and the achievement or preservation of a stealth effect. In future studies, a quantification of the surfactant level should be carried out before protein corona experiments where possible. As not for all surfactants a suitable assay for quantification is available, additional purification to remove as much surfactant as possible can still be applied.

4.4 Effect of heat inactivation on adsorption properties of apolipoproteins

To this point, several aspects of a stealth protein corona have been regarded and different influence factors on protein adsorption have been investigated. Surfactant denaturation turned out to have a measurable effect on the adsorption behavior of certain proteins.

The impact of heat inactivation to proteins can potentially be similar to surfactant denaturation. Heat inactivation is a common procedure in cell culture that inactivates the complement system in serum and can induce aggregation of immunoglobulin G.[103-104] This procedure is applied as some cell types are sensitive to the presence of complement proteins, which may be an issue for certain experiments.[111] The heat inactivation may lead to consequences in the biological response of nanocarriers, such as change in uptake by different cell types. So far, the implication of heat inactivation on the protein corona has not been checked, so it is not clear if heat inactivated proteins still adsorb to nanocarriers and if their behavior can be preserved. It will thus be investigated how heat inactivation changes the folding state of the apolipoproteins Apo-A1 and CLU and whether adsorption of heat inactivated proteins to NPs does still take place or not. In further experiments, it shall be clarified if a stealth effect can still be maintained after heat inactivation.

The data presented in this chapter was obtained within a project together with [redacted] and [redacted] (MPI-P), in which the effect of heat inactivation on the development of the protein corona was analyzed. Herein, only data from experiments carried out by myself are shown. Results of further experiments by coworkers are mentioned in the end of this chapter, the corresponding data is not shown.

4.4.1 Results and Discussion

Experiments were conducted to investigate how protein adsorption on nanoparticles is affected by heat inactivation. Especially the apolipoproteins Apo-A1 and CLU, which were found to be of particular importance for the stealth effect of nanocarriers, are subject of detailed analysis.

Two different procedures were chosen for heat inactivation of the proteins: thermal treatment at 56 °C for 30 min and at 90 °C for 6 h. The treatment at 56 °C is a standard procedure commonly used for heat inactivation. Additionally, the treatment at 90 °C was chosen because it is assumed that the protein is denatured completely, while at 56 °C not all proteins might be affected.

Differential scanning fluorimetry (DSF) experiments were conducted to monitor and compare the unfolding of the differently treated proteins. In Figure 4.4.1, the fluorescence recorded at 330 nm while running a temperature ramp from 25 °C to 90 °C and the corresponding first derivative is plotted

for Apo-A1 and CLU. For both proteins a native sample, a sample treated at 56 °C for 30 min and a sample treated at 90 °C for 6 h were measured.

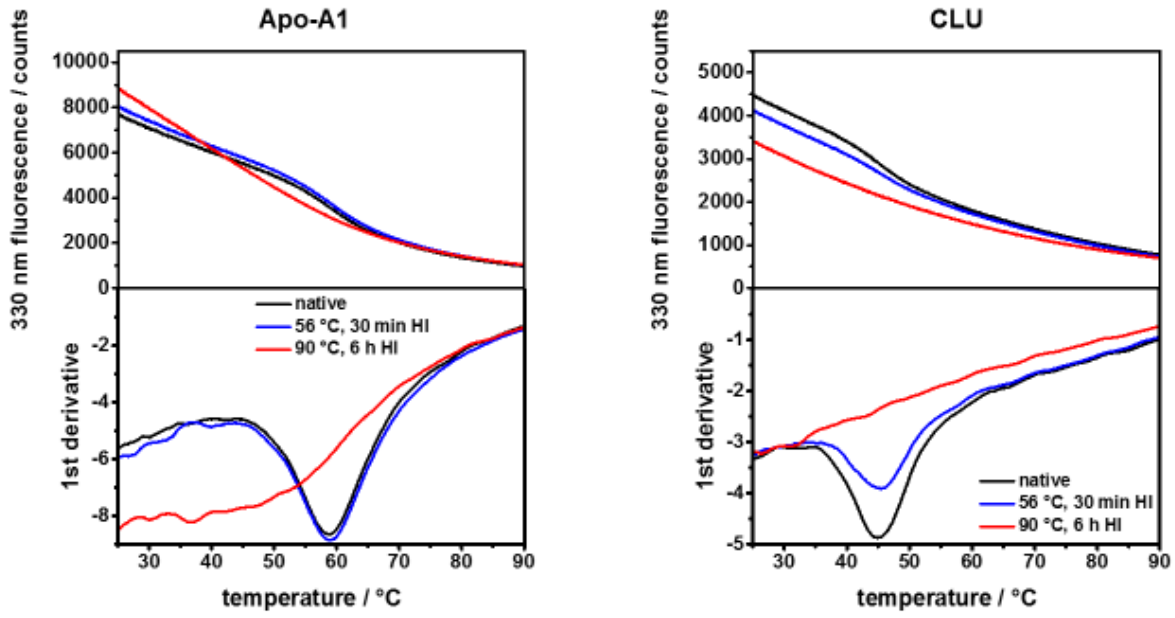

Figure 4.4.1 DSF unfolding experiment of native, 56 °C and 90 °C heat inactivated Apo-A1 and CLU. Upper graphs: fluorescence measured at 330 nm during controlled heating of the samples from 25 °C to 90 °C. Lower graphs: first derivative thereof.

Native Apo-A1 shows an inflection point in the fluorescence curve at around 58 °C, which can be identified more conveniently in the first derivative as a local minimum. The same is observed for the sample of Apo-A1, which was heat inactivated at 56 °C. As the inactivation temperature is little below the point of denaturation of Apo-A1, most of the protein still seems to be intact in its native folding state. The sample heat inactivated at 90 °C does not exhibit any transition, which means that it has been denatured completely by the heat inactivation prior to the measurement.

For CLU, an inflection point in the fluorescence occurs at around 45 °C for the native protein. The sample, which was heat inactivated at 56 °C, still shows this transition, but it does not reach the intensity of the signal for the native sample. This can be interpreted as a partial denaturation of the CLU. For CLU heat inactivated at 90 °C, no transition is observed anymore. In this case, the heat inactivation leads to a complete denaturation of the protein in the same way it is observed for Apo-A1.

In Figure 4.4.2, fluorescence curves for refolding experiments of the samples described above are displayed. These measurements were conducted following the unfolding measurements. The samples were cooled down to 25 °C again with a controlled cooling rate.

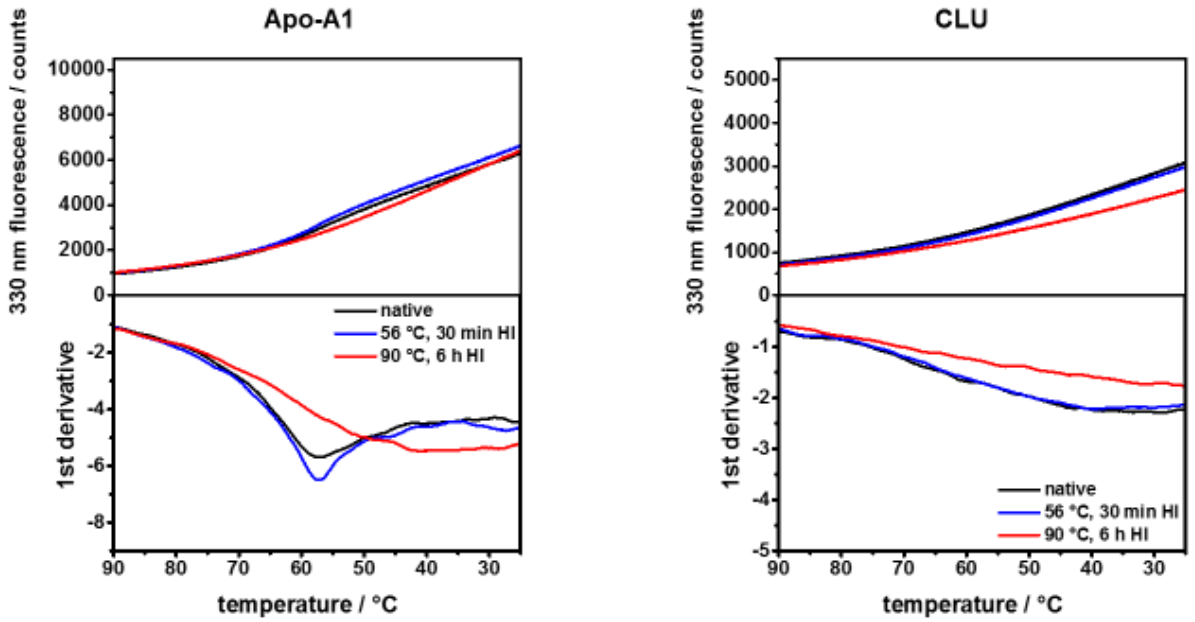

Figure 4.4.2 DSF refolding experiment of native, 56 °C and 90 °C heat inactivated Apo-A1 and CLU. Upper graphs: fluorescence measured at 330 nm during controlled heating of the samples from 25 °C to 90 °C. Lower graphs: first derivative thereof.

For Apo-A1, a (partial) refolding is observed for the native and the 56 °C heat inactivated sample, as a transition around 58 °C occurs. The 90 °C heat inactivated sample does not show any indication of refolding. Denaturation at this comparably high temperature for 6 h therefore is regarded as irreversible. For CLU, no refolding is observed for any of the three samples. Therefore, unfolding of CLU at whichever conditions is considered as irreversible.

To summarize the results from DSF, it can be stated that CLU is more sensitive to heat inactivation than Apo-A1, as it is already denatured at lower temperatures. Moreover, once CLU has been denatured, this process is irreversible, while for Apo-A1 this is only the case for the denaturation at 90 °C for 6 h.

The structural changes induced by denaturation of a protein might also alter its adsorption behavior to nanoparticles. To investigate this circumstance, ITC experiments with Lutensol-stabilized, unfunctionalized polystyrene nanoparticles (PS-Lut) were conducted. The same NPs were also used in experiments described in chapter 4.3, detailed specifications of PS-Lut can therefore be found in Figure

4.3.1. Figure 4.4.4 shows the data obtained for titrations with native and 90 °C heat inactivated CLU and Apo-A1. Both graphs were corrected for the heat of dilution and the corresponding heat rates are shown in Figure 4.4.3.

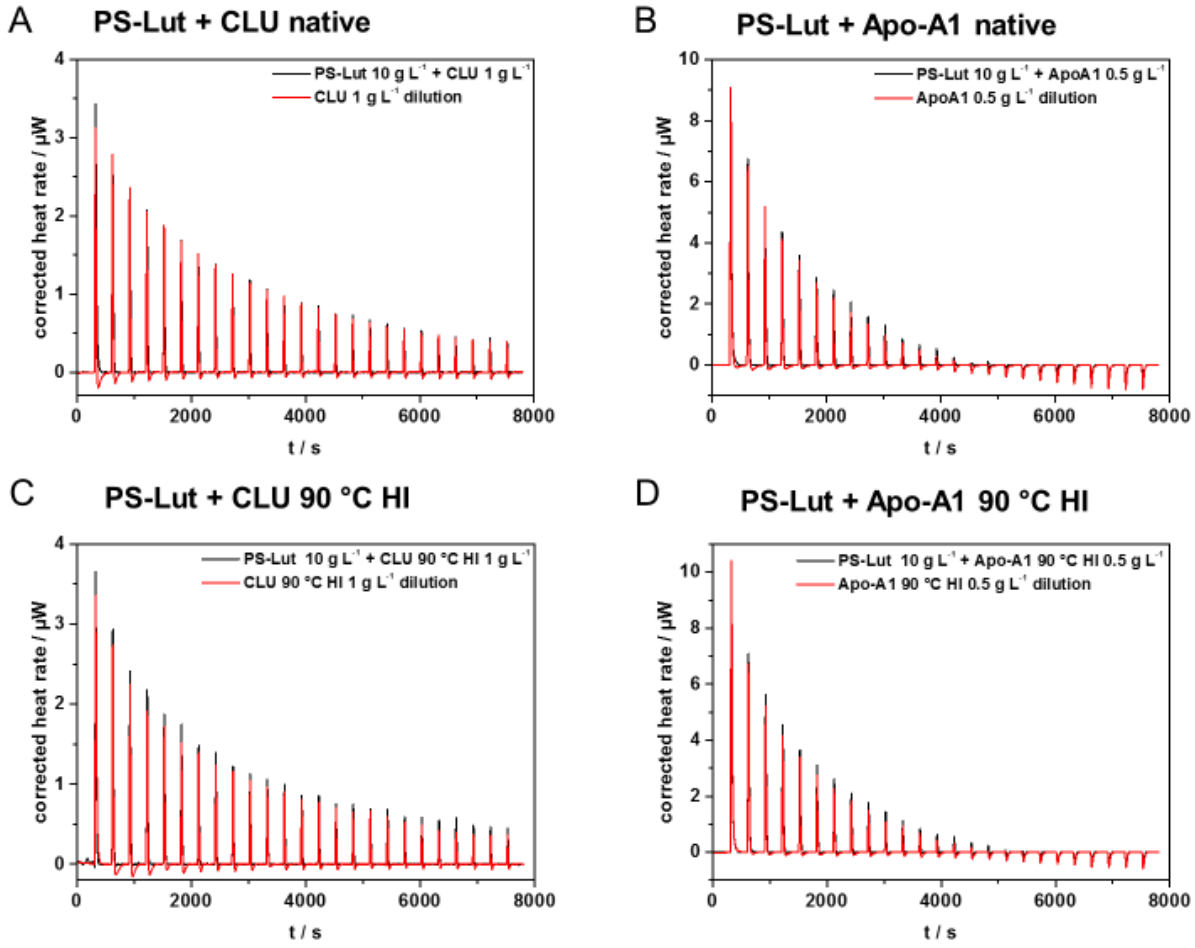

Figure 4.4.3 ITC heat rates of experiments with PS-Lut and native / heat inactivated CLU and Apo-A1.

The data points were fitted with independent binding model fits (where applicable) and the binding parameters displayed in Table 4.4.1 were obtained. For heat inactivated CLU, only a single measurement could be conducted due to low availability of this protein. Hence, no error can be given here.

For Apo-A1, the measurements of native and 90 °C heat inactivated protein only differ in the onset of the curves. The data of the 90 °C heat inactivated sample could not be fitted reasonably, and also the fits for three replicates of the native sample show some deviation.

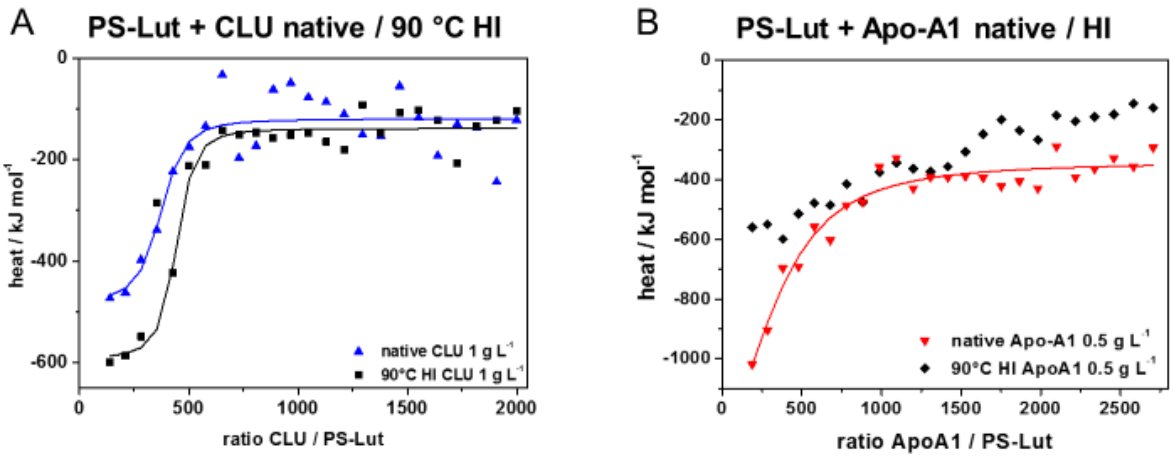

Figure 4.4.4 ITC measurements of PS-Lut with Apo-A1 and CLU, both native and 90 °C heat inactivated (HI).

Deviations between different replicates for both native CLU and Apo-A1 cause the high standard deviation of the fit parameters displayed in Table 4.4.1.

Table 4.4.1 Adsorption parameters obtained from ITC experiments of PS-Lut with CLU and Apo-A1.

	K_a / 10^8 M^{-1}	ΔH / kJ mol^{-1}	ΔS / J mol^{-1} K^{-1}	n
CLU native	0.3 ± 0.2	3240 ± 4290	26900 ± 41600	3240 ± 4290
CLU 90 °C HI	1.3	-455	-1372	412
Apo-A1 native	0.01 ± 0.01	-163900 ± 229000	-550000 ± 768000	9900 ± 13800

The error is even larger than the value in most cases, so the significance should not be ranked very high. Among the different replicates there is almost surely an outlier, which unfortunately cannot be identified due to the low number of repetitions. Because of the low availability of especially CLU, no additional repetitions or measurements with higher protein concentrations were performed so far. However, this would probably be a suitable approach to obtain better results. Based on this data, the adsorption behavior of native and 90 °C heat inactivated CLU cannot be differentiated clearly.

Additional experiments have been conducted in the context of this project by coworkers, the corresponding data is not shown here. Briefly, analysis of the protein corona of PS-Lut nanoparticles by LC-MS (work of [redacted]) showed that the amount of CLU was significantly reduced compared

to Apo-A1 after heat inactivation. Very similar results were observed for the protein denaturation by surfactant in chapter 4.3 (Figure 4.3.2).

Uptake of PS-Lut nanoparticles incubated with heat inactivated plasma/serum in RAW264.7 cells was found to be significantly higher than after incubation with untreated plasma/serum (work of [redacted]). This can be attributed to the altered protein corona after heat inactivation. Bare NPs without a protein corona show the highest uptake. For incubation with only a single protein (Apo-A1 or CLU), the same uptake is observed for incubation with native, 56 °C and 90 °C heat inactivated protein, which is reduced compared to uncoated NPs. Without other plasma proteins competing for adsorption, also heat inactivated Apo-A1 or CLU do adsorb to NPs. Heat inactivated CLU has a rather low binding affinity, so with other proteins competing for adsorption as in plasma, it cannot adsorb to the NPs anymore. The structural change of the proteins due to heat inactivation did not seem to have a significant effect on uptake in RAW264.7 cells, as it was still as low as for the native proteins.

4.4.2 Conclusions

The impact of heat inactivation on the protein structure was found to be different for Apo-A1 and CLU. Structural changes, as they are induced by heat inactivation, are likely to affect the adsorption behavior of proteins. However, in ITC experiments no significant differences between the native state and heat inactivated protein could be measured for Apo-A1 and CLU due to deviations in the fits and a low number of repetitions because of low protein availability. Still, besides these two exemplarily chosen proteins, there are many other plasma proteins, which were not investigated here. The binding affinities of these plasma proteins are most likely subject to change upon heat inactivation. It is hard to predict how each particular protein is affected, so a completely new composition of the protein corona must be expected.

Additional experiments by coworkers showed that nanocarriers incubated with heat inactivated plasma show higher uptake, which must be due to a different protein pattern compared to untreated plasma. It can therefore be concluded that the biological response to nanocarriers is altered after heat inactivation. Whenever heat inactivation is applied to the protein source of protein corona studies, it must be taken into account that different results will be obtained compared to an untreated protein source.

4.5 Interaction of poly(ethylene glycol) with proteins and nanoparticles

To achieve a stealth effect of nanocarriers, it has been a standard approach for several years to graft PEG chains to the surface. This results in a significantly reduced protein adsorption and generates a protein pattern, which prevents unspecific cellular uptake. As a shell of PEG chains helps to control protein adsorption, it would be of interest to gain further understanding of the interaction between PEG and proteins. So finally, the role of poly(ethylene glycol) (PEG) will be examined in further detail.

Settani *et al.* showed in molecular dynamics simulations that the interaction with PEG depends on the protein surface.[105] Based on these findings, different results depending on the protein type would be expected.

To date, no ITC data is available for the interaction of free PEG with proteins. Therefore, the heat released during the interaction of PEG with different proteins and lipoproteins will be measured and compared to the interaction with PEGylated nanocarriers. The existence of an effect of PEG on the protein folding state is also unclear.

In this chapter, a deeper insight into the functionality of PEG as a stealth polymer shall be gained and its role in the reduction of protein adsorption shall be studied. Thus, the interaction between PEG and several single proteins was investigated in ITC measurements. As a complementary approach, the effect of PEG on Apo-A1 and CLU stability was determined in DSF experiments.

4.5.1 Free PEG and (lipo-)proteins

ITC experiments were conducted with several different proteins to probe for a possible interaction with free poly(ethylene glycol). Therefore, aqueous solutions of the proteins were each titrated with PEG of a molecular weight of approximately 2000 g mol^{-1} (PEG-2000), which was chosen because this type is typically used for surface functionalization.[13] If any interaction was to be expected, it would be most likely for apolipoproteins (especially Apo-A1 and CLU), as these proteins were found to be enriched in the corona of PEGylated nanocarriers.

In Figure 4.5.1 the ITC raw data (heat rates) is depicted for the different proteins, including heat of dilution of the respective protein.

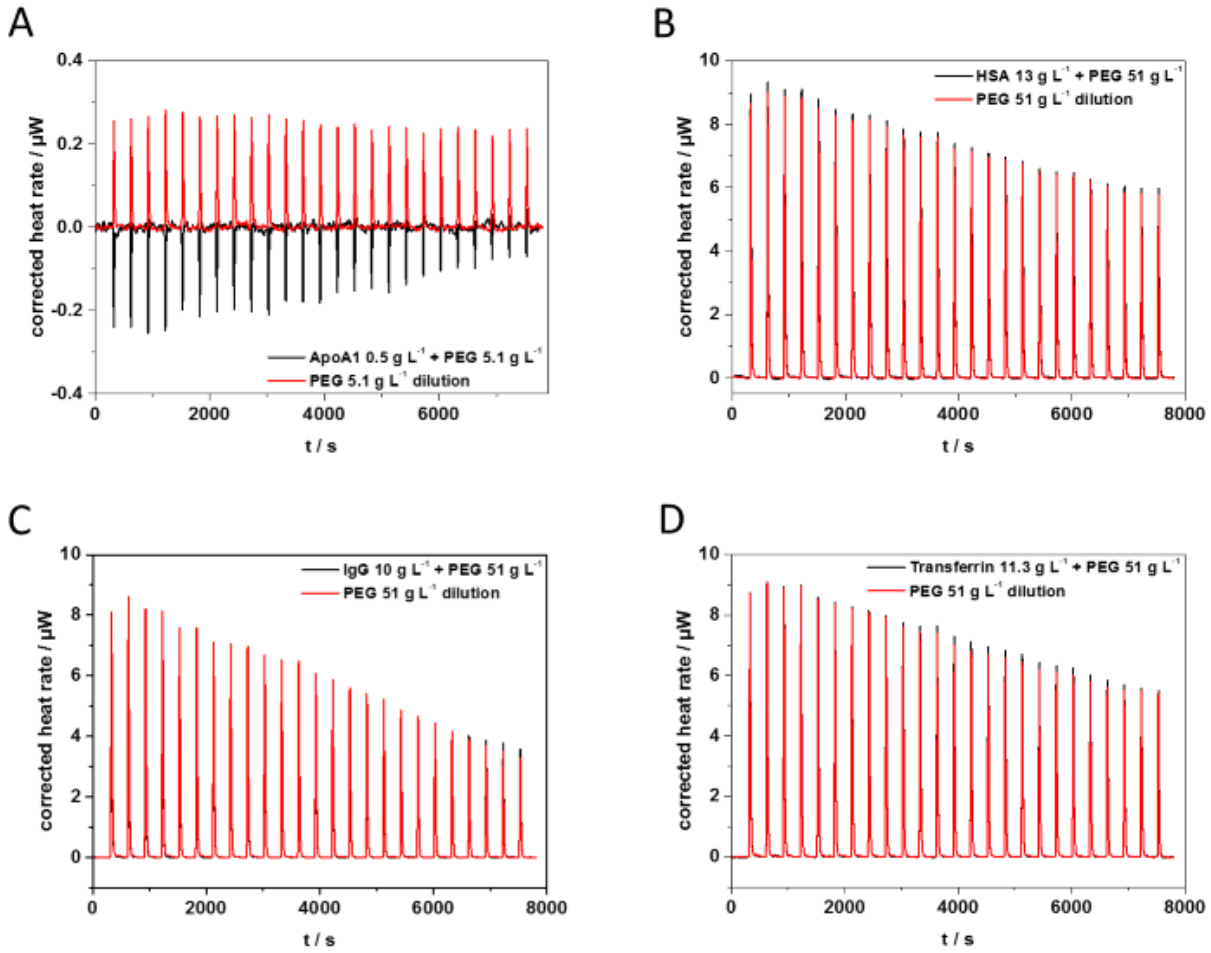

Figure 4.5.1 Corresponding heat rates of ITC measurements at 25 °C displayed in Figure 4.5.2 with heat of dilution.

Aqueous solutions of different proteins in the cell of the ITC device were titrated with an aqueous solution of PEG-2000. In Figure 4.5.2, the results of titrations of four proteins with PEG-2000 at 25 °C are shown. All graphs were corrected for the heat of dilution of PEG-2000 into water. The heat rates of the measurements and the dilution are shown in Figure 4.5.1.

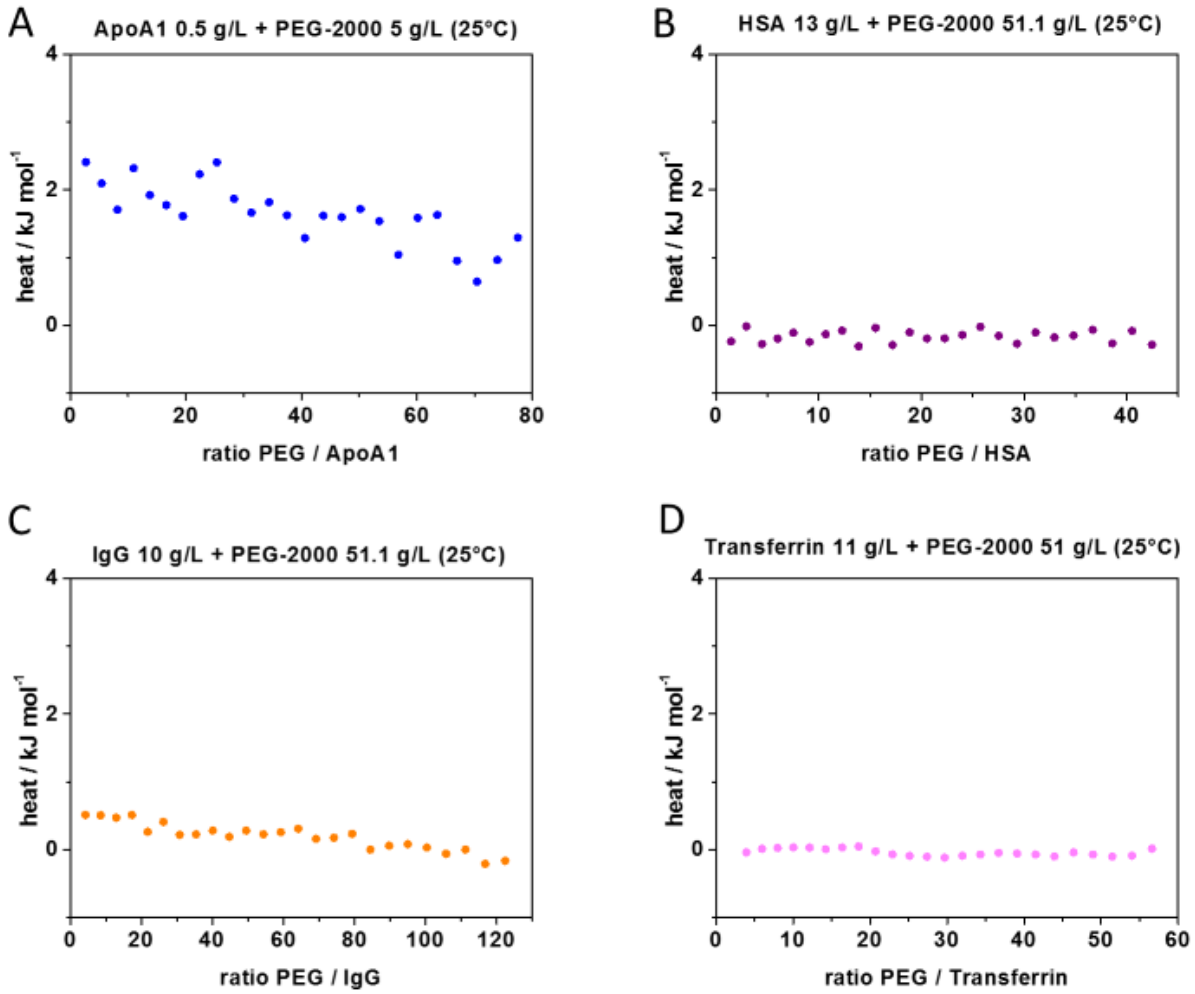

Figure 4.5.2 ITC experiment of aqueous solutions of different proteins each titrated with PEG-2000 at 25 °C.

The data points in all graphs of Figure 4.5.2 are close to zero or scatter slightly, but no clear heat evolvement is observable. Thus, for none of the proteins a defined interaction with PEG-2000 can be seen at this temperature. It could be the case that enthalpy contributions of simultaneously occurring processes compensate each other at this temperature, so the resulting heat is zero. According to the Gibbs-Helmholtz-equation, a change in temperature would solve this issue.

Therefore, further ITC experiments were conducted with PEG-2000 at a temperature of 15 °C. All graphs in Figure 4.5.4 were corrected for the heat of dilution of PEG-2000 into water, the heat rates of the measurements and the dilution experiment are shown in Figure 4.5.3.

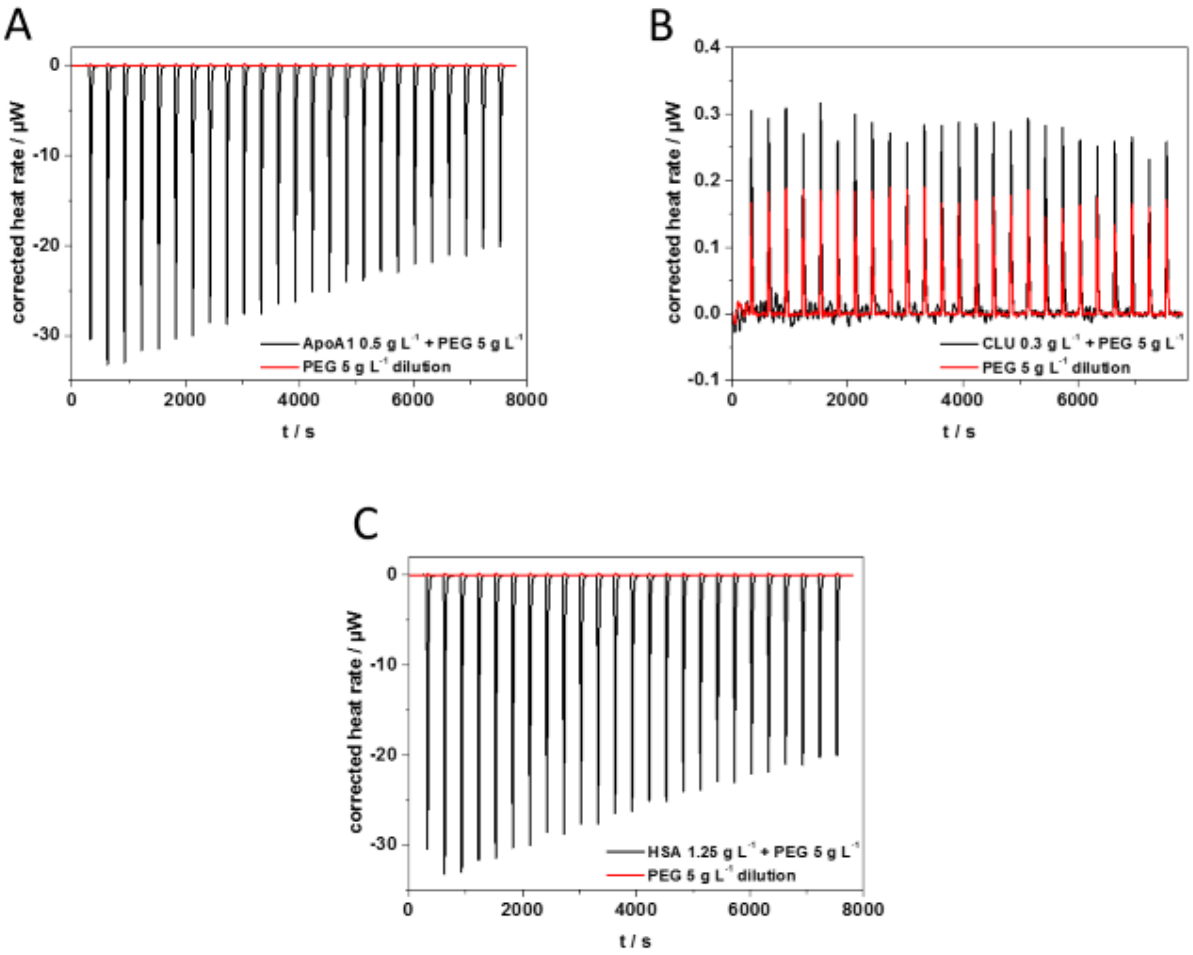

Figure 4.5.3 Corresponding heat rates of ITC measurements at 15 °C displayed in Figure 4.5.4 with heat of dilution.

For CLU and HSA (Figure 4.5.4-B and -C), the data points scatter around zero, so no interaction with PEG-2000 can be seen in this case. For Apo-A1 (Figure 4.5.4-A), an endothermal signal is observed. This indicates that there is some kind of interaction with PEG-2000 at 15 °C. Although no resulting heat was measurable at 25 °C as displayed in Figure 4.5.2-A, still an interaction can occur, with the enthalpy being compensated.

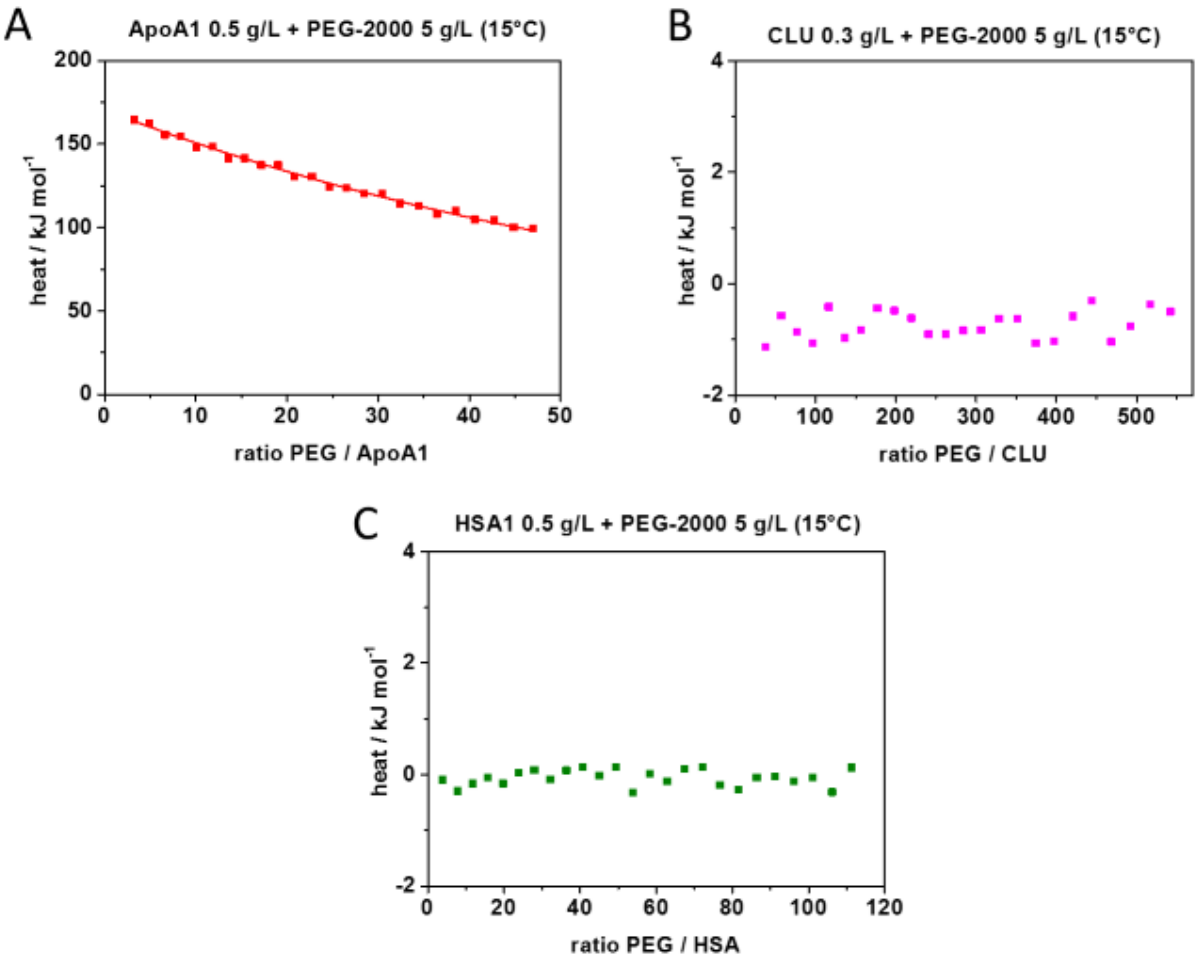

Figure 4.5.4 ITC experiments of aqueous protein solutions titrated with PEG-2000 at 15 °C. The data points obtained for Apo-A1 (panel A) were fitted with an independent binding model fit.

From an independent binding model fit, a binding affinity K_a of (182 ± 80) M^{-1} was obtained as mean value with standard deviation from triplicates. Regardless of the rather large error, the order of magnitude of the binding affinity K_a of 10^2 M^{-1} indicates a very weak interaction. The error mainly results from the non-sigmoidal shape of the curve, which does not show defined plateaus.

Except for the experiment with CLU, all measurements in Figure 4.5.2, Figure 4.5.4 and Figure 4.5.6 were performed as triplicates.

Apolipoproteins are of particular interest in this study, as they are crucial for the stealth effect of a nanocarrier. They do not occur freely in plasma, but accompanied by lipids in the form of lipoprotein complexes. Advancing from single proteins to these more complex biological clusters, the interaction of lipoproteins with PEG-2000 was investigated.

Molecular dynamics simulations showed that interaction of PEG with a protein depends on its surface composition. As reported by Settanni *et al.*, PEG particularly accumulates around non-polar residues.[105]

Figure 4.5.5 shows the heat rates of ITC experiments of commercial lipoproteins with PEG-2000. All measurements were corrected for the heat of dilution of PEG-2000 into water. The resulting graphs of heat versus molar ratio are displayed in Figure 4.5.6. For these experiments, the same commercial lipoproteins as in chapter 4.2 were used.

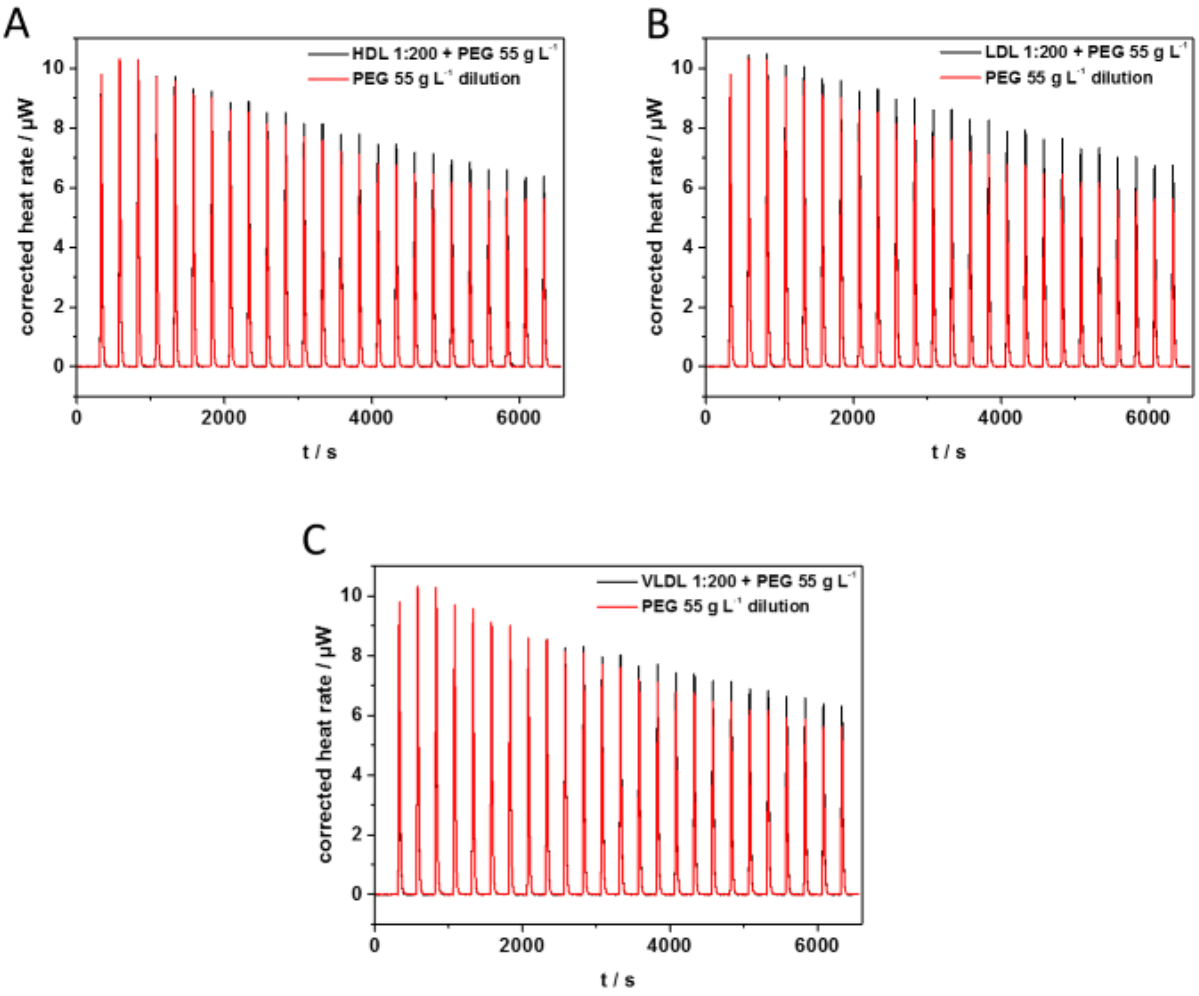

Figure 4.5.5 Corresponding heat rates of ITC measurements of lipoproteins with PEG at 25 °C displayed in Figure 4.5.6 with heat of dilution.

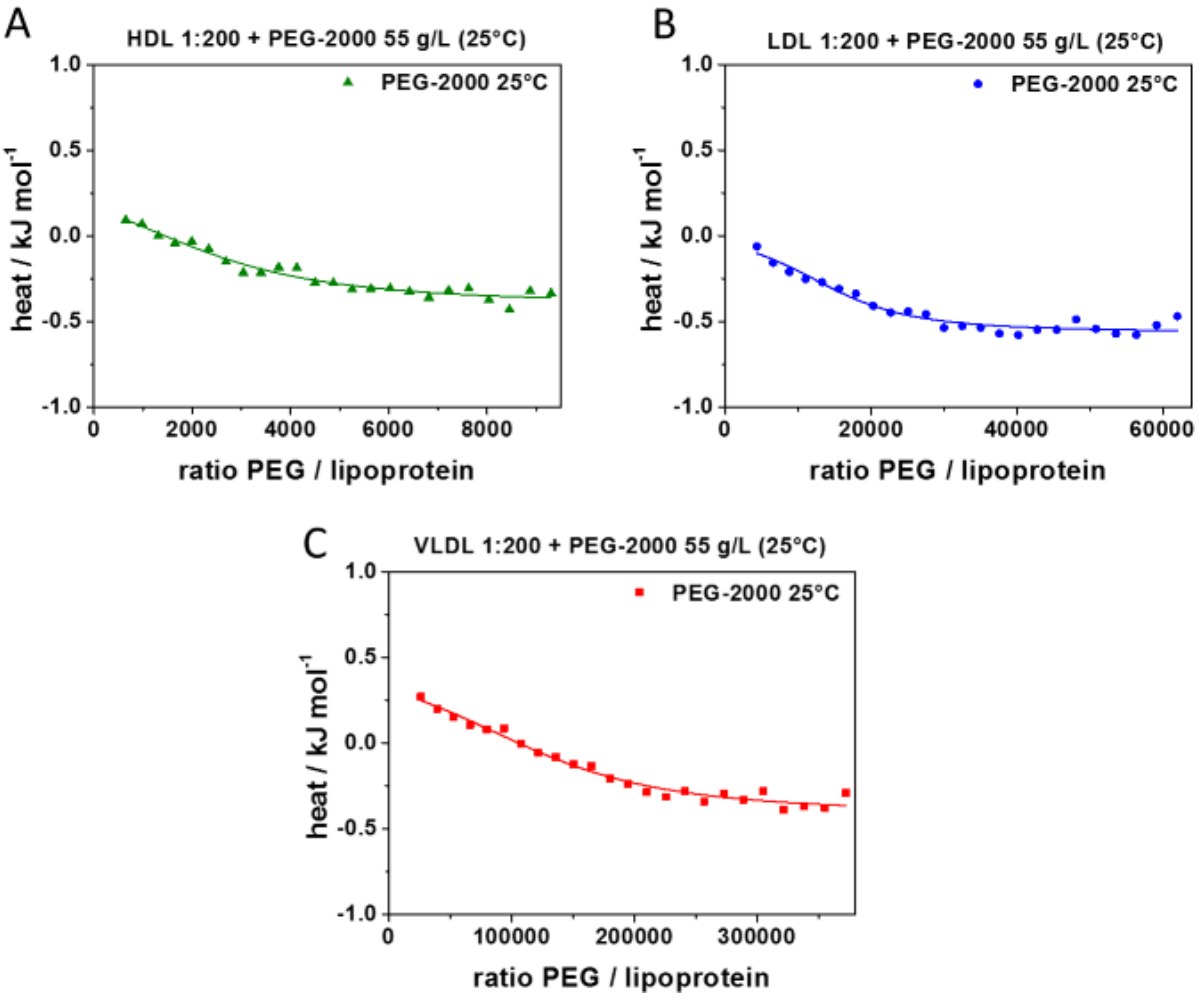

Figure 4.5.6 ITC experiments with aqueous solutions of commercial lipoproteins titrated with PEG-2000 at 25 °C. An independent binding model fit was applied to the data points, the fit parameters listed in Table 4.5.1 were obtained.

The data points of all different lipoproteins show a similar curve shape and are approximated with an independent binding model fit. The fit parameters (mean values and standard deviation from triplicates) are listed in Table 4.5.1.

Table 4.5.1 Fit parameters (ITC) for the interaction of commercial lipoproteins with PEG-2000.

	K_a / 10^3 M^{-1}	ΔH / kJ mol^{-1}	ΔS / J mol^{-1} K^{-1}	n (PEG per LP)	PEG per nm²
HDL comm.	1.2 ± 0.6	0.75 ± 0.07	60.7 ± 3.6	2680 ± 100	1.5
LDL comm.	2.4 ± 1.9	2.2 ± 2.4	66.1 ± 4.7	15500 ± 2600	2.8
VLDL comm.	1.3 ± 0.4	0.92 ± 0.11	62.3 ± 1.8	127000 ± 4000	5.7

In contrast to the observations for free Apo-A1 and CLU, which mainly do not exhibit an interaction, a weak interaction is observed between the lipoproteins and PEG-2000. Considering the values for the change in entropy ΔS, it can be stated that PEG shows an entropy-driven interaction with lipoproteins in ITC. The change in enthalpy ΔH in contrast is in the endothermal range, although rather low for all lipoproteins. The value for ΔH of LDL is physically not reasonable due to deviations in one measurement, but is still given here for the sake of completeness.

The stoichiometry n, which describes the number of PEG molecules interacting with one lipoprotein complex, correlates well with the increasing hydrodynamic diameter and therefore the available surface area of the lipoprotein complexes. For the largest of the three lipoproteins, VLDL, n is in the order of 10^5, while for HDL, the smallest lipoprotein, it is only in the order of 10^3.

From the values of n, the density of PEG chains on the surface of the lipoprotein complexes in the last column of Table 4.5.1 was calculated. As an approximation, the surface area of a nanoparticle was calculated with the radii from Figure 4.2.1 of each lipoprotein. The number of PEG chains per nm² increases from 1.5 for HDL to 5.7 for VLDL with the size of the lipoprotein. The phospholipids, which form a large part of the lipoprotein surface, are similar for each type and are most likely not the reason for these differences. However, each type of lipoprotein contains one or several specific apolipoproteins, which are integrated in the surface. For HDL, the PEG chains can probably form a dense monolayer while for LDL and VLDL with higher values, some form of multilayer seems more likely. To shed more light on the behavior of PEG on the lipoprotein surface, other analytical methods would need to be applied, as the molecular interaction is not clear at this point.

The binding affinity K_a is comparably low for all lipoproteins as values around 10^3 M^{-1} were obtained. For comparison, K_a for the adsorption of proteins to NPs is typically in the range of 10^5-10^6 M^{-1}.

Most ITC experiments discussed above indicate no or a rather low interaction between proteins and PEG. However, it is still not clear if an interaction occurs, which might be hard to detect with calorimetric methods. As a next step, it should be clarified if PEG has an influence on the folding state of proteins. Therefore, differential scanning fluorimetry (DSF) measurements were carried out with CLU and Apo-A1. These two apolipoproteins were chosen because they occur in the protein corona of stealth NPs in disproportionately high amounts and thus are of particular importance for the stealth effect, as described earlier.

Samples of pure protein and protein with four different concentrations of PEG-2000, covering several orders of magnitude, were subjected to a temperature ramp from 20 to 95 °C while the fluorescence was monitored. The ratio of two fluorescence channels (350 and 330 nm) and the respective first derivative are displayed in Figure 4.5.7.

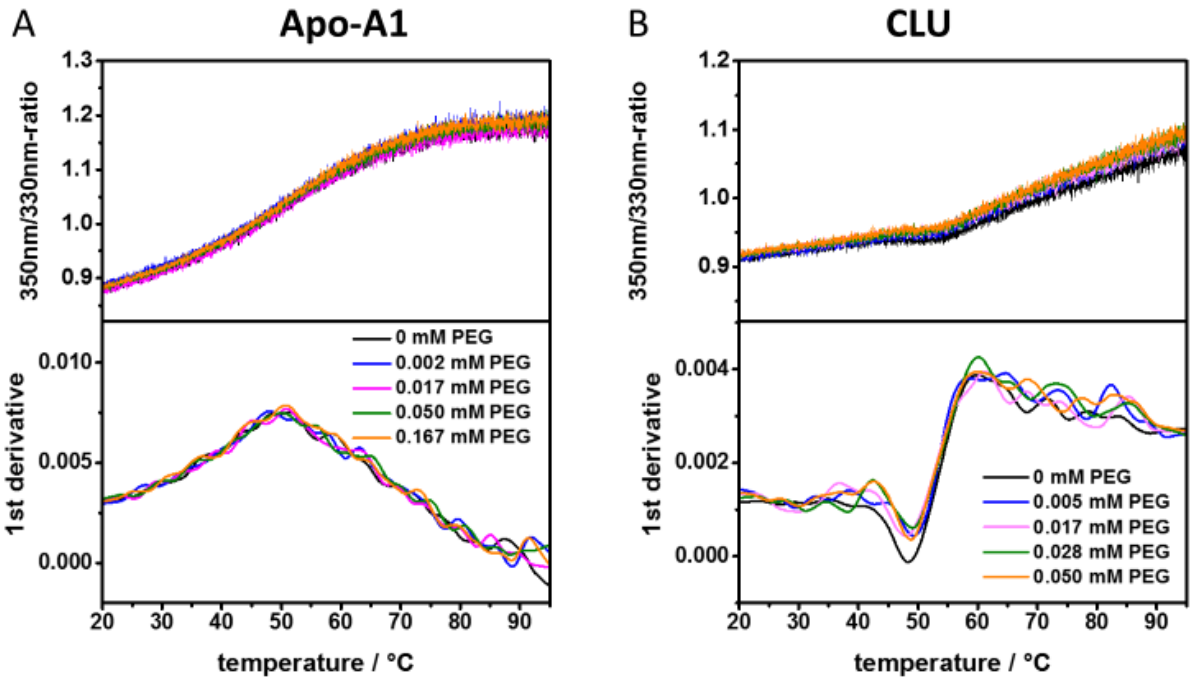

Figure 4.5.7 DSF experiments of Apo-A1 and CLU with different concentrations of PEG-2000.

For each of the two proteins, the fluorescence curves of the pure protein and the different concentrations of PEG are approximately superimposable. Also in the first derivative, no significant differences can be detected. It can therefore be stated that PEG does not affect the folding state of Apo-A1 and CLU, so it does not promote their denaturation or stability.

To summarize these first results briefly, no interaction between single proteins with PEG is observed. The only exception is Apo-A1, where a very weak interaction (K_a around 10^2 M^{-1}) is measured. From the enrichment of apolipoproteins reported for the corona of PEGylated stealth nanocarriers, one would expect an (attractive) interaction between these particular apolipoproteins and the PEG-NPs. Therefore, this interaction shall be analyzed as a next step.

4.5.2 PEGylated nanoparticles and proteins

Now the more application-related, but at the same time also more complex situation of proteins and PEGylated nanoparticles shall be analyzed for possible interactions. Depending on the density of PEG chains grafted to the NP surface, also the NP material itself can interact with proteins. Hydrophobic patches of the proteins may for example experience attraction by the nonpolar polystyrene surface. To probe this interaction, dispersions of PEGylated polystyrene nanoparticles (PS-PEG) were titrated with Apo-A1 and CLU in ITC at 25 °C, the results are displayed in Figure 4.5.9.

These experiments were performed with a different batch of PS-PEG nanoparticles than the ones from chapter 4.3. The synthesis was carried out in an analogous manner and similar specifications were obtained in the characterization, which are listed in Table 4.5.2.

Table 4.5.2 Specifications of the PS-PEG nanoparticles.

Material	Surfactant	# PEG chains per NP	M (PEG) / g mol^{-1}	R_h / nm	ζ / mV
PS	CTMA-Cl	3500	5000	58 ± 6	7.4 ± 1.0

The graphs in Figure 4.5.9 were corrected for the heat of dilution of the respective protein into water. The heat rates of the measurements and the dilution experiment are shown in Figure 4.5.8.

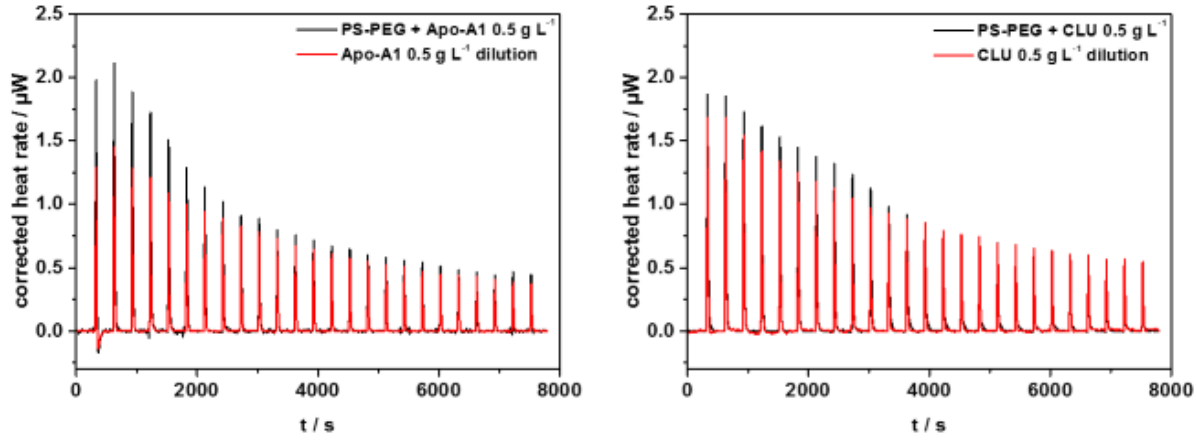

Figure 4.5.8 ITC heat rates PS-PEG with Apo-A1 and CLU shown in Figure 4.5.9.

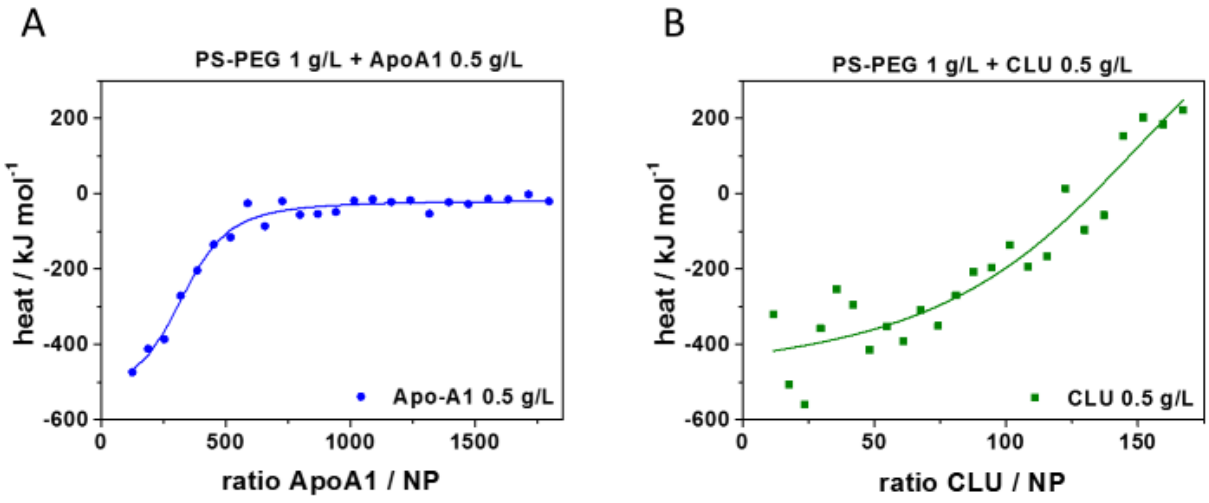

Figure 4.5.9 ITC experiments of PS-PEG-dispersions titrated with Apo-A1 and CLU at 25 °C.

The ITC adsorption curves of Apo-A1 and CLU to unfunctionalized NPs (PS-Lut) stabilized with the surfactant Lutensol (containing a PEG block) were already shown in Figure 4.3.8. In Table 4.5.3, the protein adsorption parameters of unfunctionalized PS-Lut are listed besides the results for PS-PEG for comparison. From the graphs in Figure 4.5.9 and the values for *ΔH*, it can be stated that a distinct exothermal interaction between the PS-PEG particles and both Apo-A1 and CLU occurs. Two major possibilities for this interaction are imaginable: it can either take place between the proteins and the PEG-shell or between proteins and the nanoparticle's polystyrene surface. The latter case can especially be possible for low densities of PEG chains on the NP surface. Further, also the conformation of the PEG-chains on the surface can play a role for protein adsorption. Depending on the surface

density of the chains, they can be in mushroom or brush conformation. These different conformations have been reported to have a significant effect on protein adsorption and phagocytosis.[106]

With the results about free PEG from chapter 4.5.1 in mind, which indicated no interaction between free PEG and the proteins, such a high enthalpy from an interaction with the PEG shell is unlikely.

In all four experiments, a highly negative change in entropy ΔS is observed.

Table 4.5.3 Fit parameters (ITC) for the interaction of PEGylated nanoparticles (PS-PEG) and unfunctionalized nanoparticles (PS-Lut) with Apo-A1 and CLU.

		K_a / 10^6 M^{-1}	ΔH / kJ mol^{-1}	ΔS / J mol^{-1} K^{-1}	n (PEG per protein)
PS-PEG +	Apo-A1	7.05 ± 2.94	-675 ± 222	-2135 ± 750	350 ± 98
	CLU	8.5	-1235	-4010	162
PS-Lut +	Apo-A1	2.4	-1438	-4700	305
	CLU	37.1	-1237	-4004	69

As no interaction with PEG is to expect from the results described above, there is probably an interaction with the NP surface. However, ITC only measures the resulting heat but cannot distinguish between different simultaneous processes. Hence, further complementary experiments would be necessary to allow a more definite conclusion.

The high exothermic change in enthalpy for the interaction of Apo-A1 and CLU with both NPs indicates a strong interaction on molecular level. Hydrophobic interactions would result in a positive change in entropy, so they can be excluded due to the highly negative values. Hydrogen bonds and van der Waals interactions are rather weak, so the large values of ΔH presumably result from electrostatic interactions. For more details on the different types of molecular interaction see chapter 2.2.2.

Charged moieties of a protein can interact with charges present on the NP surface. The electrostatic potential of the surface of Apo-A1 was shown by Ajees *et al*. It exhibits negatively as well as positively charged domains, although the overall net charge is negative at physiological pH.[107] Therefore, an electrostatic interaction with both types of NPs is possible although they are oppositely charged: ζ is -7 mV for PS-Lut (Figure 4.3.1) and +7 mV for the batch of PS-PEG used in this chapter (Table 4.5.2). As the crystal structure of CLU is not known, no mapping of its electrostatic potential is available, but it is assumed that the protein also contains differently charged moieties.

4.5.3 Conclusions

To summarize, DSF experiments clearly showed no effect of free PEG on the structure of Apo-A1 and CLU over a wide concentration range of PEG. It can therefore be seen as an 'inert' polymer, which is possibly also true for its interaction with other proteins.

From the theoretical calculations by Settani *et al.* different affinities of PEG depending on the protein type were expected. Experimentally, only for Apo-A1 a measurable interaction with free PEG was found in ITC measurements, all other proteins showed no heat. However, a weak interaction of free PEG with lipoproteins could be observed in ITC. This interaction can take place either with the apolipoproteins integrated in the shell of the lipoprotein complexes or with some of its other constituents, such as phospholipids. It can therefore be stated that PEG is not completely inert to all kinds of biomolecules, so still an interaction and therefore a biological response can occur.

Finally, it is concluded that although no interaction between free PEG and most proteins (except with Apo-A1 at 15 °C) could be measured, proteins do still interact with or rather adsorb to PEGylated nanocarriers. Especially for Apo-A1 and CLU, an adsorption was measurable in ITC (Figure 4.5.9). The binding affinities for this adsorption indicate a considerable interaction process.

One can imagine that the proteins migrate through the PEG shell and adsorb to the polystyrene surface of the NP. However, this adsorption cannot clearly be separated from possible interaction with the PEG chains, so this circumstance could be investigated further by suitable experiments. For example, ITC measurements could be conducted at different temperature or with higher concentrations of apolipoproteins to obtain a better signal-to-noise-ratio.

5 Experimental Part

5.1 Materials

All chemicals and proteins were used as received without further purification, unless stated otherwise.

Human blood was taken at the Department of Transfusion Medicine Mainz from ten healthy donors after physical examination and after obtaining informed consent in accordance with the Declaration of Helsinki. The study was approved by the local ethics committee "Landesärztekammer Rheinland-Pfalz" (837.439.12 (8540-F)). To prevent blood clotting sodium citrate was added. The blood was centrifuged to pellet red and white blood cells and the plasma supernatant was pooled. Aliquots were stored at -80 °C. A protein concentration of 66 mg mL^{-1} was determined with a Pierce 660 nm protein assay (Thermo Fisher Scientific, Waltham, USA) according to manufacturer's instructions with bovine serum albumin (BSA) as a standard. To remove any aggregated proteins the plasma aliquots were centrifuged for 1 h at 20000 g before use.

5.1.1 Proteins

Human Serum Albumin (HSA) was purchased from Sigma Aldrich (St. Louis, USA; Product No. A3782). From the same vendor, also Transferrin (Product No. T3309) and Immunoglobulin G (IgG, Product No. I4506) were purchased.

Commercial lipoproteins (HDL, LDL and VLDL) were purchased from Lee Biosolutions (Metro Ct, USA) and 100 fold diluted with saline after thawing in order to obtain lipoprotein solutions in physiological concentrations. Apolipoprotein-A1, apolipoprotein-B100 and apolipoprotein-E were obtained from MyBiosource (San Diego, USA). Another batch of apolipoprotein-A1 was purchased from Biopur (Reinach, Switzerland).

Lipoprotein fractions were obtained with an LDL/VLDL and HDL Purification Kit (Ultracentrifugation Free; Cell Biolabs, Inc.; Catalog Number STA-608) from human citrate plasma. 10 mL citrate plasma (stored at -80 °C) were thawed and centrifuged at 20000 g (4 °C; 30 min). The supernatant was collected and used for HDL and (V)LDL purification according to the kit. Purified fractions were stored at 4 °C.

Recombinant clusterin (CLU) was isolated from sCLU overexpressing HEK-293 cells by [redacted] (University of Mainz), as reported previously by Rohne *et al.*[53] Commercial CLU was acquired from BioVendor (Brno, Czech Republic). Apolipoprotein-A1 was purchased from MyBiosource (San Diego, USA) and Biopur (Reinach, Switzerland). Cetyltrimethylammonium chloride (CTMA-Cl) was purchased

as 25% solution from Sigma Aldrich (St. Louis, USA; Product No. 292737) and was diluted with Milli-Q water.

5.1.2 Miscellaneous

Table 5.1.1 Materials used in this thesis and their suppliers.

Substance	Conc.	Supplier
2,2'-azobis(2-methylbutyronitrile)		V59, Wako Chemicals, Neuss, Germany
Cetlytrimethylammonium chloride (CTMA-Cl)	25%	Sigma Aldrich, St. Louis, USA (Product No. 292737)
Coomassie Brilliant Blue G-250		SERVA Electrophoresis GmbH
Dulbecco´s modified eagle medium (DMEM)		Invitrogen, USA
Fetal bovine serum (FBS)	10%	Sigma Aldrich, St. Louis, USA
Hexadecane		Sigma Aldrich, St. Louis, USA
Ionic detergent compatibility reagent (Art.-No. 22663)		Thermo Fisher Scientific
Lutensol® AT50 (poly(ethylene glycol)-hexadecyl ether)		BASF AG
Milli-Q water		Merck Millipore
Penicillin/streptomycin		Invitrogen, USA
Poly(ethylene glycol) (PEG) 2000 g mol^{-1}		PSS Polymer Standards Service, Mainz, Germany
Poly(ethylene glycol) (PEG) 5000 g mol^{-1}		Fluka
SeeBlue Plus2 Pre-Stained Standard		Thermo Fisher Scientific, Waltham, USA
Sodium dodecyl sulfate (SDS)		Fluka (Product No. BCBN8007V)
Styrene		Merck, Darmstadt, Germany
Trypsin-ETDA	0.25%	Thermo Fischer, USA

5.2 Instrumentation and methods

5.2.1 Differential scanning fluorimetry (DSF)

A Prometheus NT.48 nanoDSF device from NanoTemper Technologies GmbH (Munich, Germany) was used with standard glass capillaries (NanoTemper Technologies GmbH). Capillaries were filled with 10 µL of the protein sample. The excitation power was set to 50% for all experiments and a temperature ramp from 20 to 95 °C was applied with a heat rate of 1 °C min^{-1}. For data analysis, either the fluorescence signal recorded at a single wavelength of 330 nm or the ratio of the 350 nm to the 330 nm channel was plotted against temperature. To enable clearer identification of folding state transitions, the first derivative of the fluorescence signal was depicted as well.

5.2.2 Dynamic light scattering

DLS experiments were carried out with a SP-81 goniometer and an ALV-5000 multiple tau full-digital correlator with 320 channels (resolution of 10^{-7} s ≤ t ≤ 10^{3} s) by ALV GmbH (Langen, Germany), unless stated otherwise. A type 1145P HeNe laser (632.8 nm, output power 25 mW) by JDS Uniphase (Milpitas, USA) was utilized as the light source.

The samples were measured in dust-free quartz light scattering cuvettes (Hellma, Müllheim), which were cleaned with acetone in a Thurmond-apparatus before use.[108]

5.2.3 Isothermal titration calorimetry

ITC experiments were performed with a NanoITC Low Volume from TA Instruments (Eschborn, Germany). The effective cell volume is 170 µL and a stirring rate of 350 rpm was chosen for the experiments. Only aqueous systems were measured, so the reference cell was filled with deionized water during all experiments. The obtained data was analyzed with an independent binding model [97] using the software NanoAnalyze, version 3.5.0 by TA Instruments.

5.2.4 Nanoparticle synthesis and characterization

The synthesis of model polystyrene nanoparticles (PS-NPs) was performed by [redacted] (MPI-P) according to the miniemulsion polymerization method as previously described.[21, 58] Briefly, 74 mg of sodium dodecyl sulfate (SDS) were dissolved in 24 mL deionized water. Simultaneously, 98 mg of the initiator 2,2'-azobis(2-methylbutyronitrile) (V59, Wako Chemicals, Neuss, Germany) and 323 µL of hexadecane (Sigma-Aldrich, St. Louis, USA) were dissolved in 6.6 mL of purified styrene (Merck,

Darmstadt, Germany). After separate preparation of the two phases, they were combined and stirred for 1 h at room temperature for pre-emulsification. Afterwards the mixture was homogenized by ultrasonication for 120 s at 90% intensity with a Branson W 450 digital sonifier (Branson Ultrasonics, Danbury, USA) equipped with a 1/2" tip whilst cooled with an ice-water bath. The polymerization was then carried out for 16 h at 72 °C. For purification, PS-NPs were dialyzed (MWCO 12000 g mol^{-1}) against deionized water for 24 h.

5.2.5 Nuclear magnetic resonance (NMR) spectroscopy

Nuclear magnetic resonance (NMR) analysis was performed by [redacted] (MPI-P). ^{13}C {H} and ^{31}P {H} NMR spectra were recorded on a Bruker AVANCE 300 MHz, 500 MHz or 700 MHz. ^{1}H NMR spectra were recorded on a Bruker AVANCE 250 MHz, 300 MHz, 500 MHz or 700 MHz. All spectra were measured in $CDCl_3$. The spectra were calibrated against the solvent signal and analyzed using MestReNova 8 from Mestrelab Research S.L.

5.2.6 Protein quantification

Protein quantification was performed using a Pierce 660 nm protein assay (Thermo Fisher Scientific, Waltham, USA) according to manufacturer's instructions with bovine serum albumin as a standard. Sample preparation was performed identically to gel electrophoresis. Ionic detergent compatibility reagent (Art.-No. 22663, Thermo Fisher Scientific) was added to ensure compatibility of the protein assay with SDS. Mean values of triplicates and standard deviations were calculated.

5.2.7 Ring tensiometry

The critical micellar concentration (CMC) of the surfactants has been determined by ring tensiometry with a ring tensiometer DCAT 21 from DataPhysics by [redacted] (MPI-P).

5.2.8 Sodium dodecyl sulfate polyacrylamide gel electrophoresis (SDS-PAGE)

After the last centrifugation step of the protein corona sample preparation prior to gel electrophoresis (sample preparation is described individually for the different chapters), the pellet was resuspended in 100 µL of a 62.5 M Tris*HCl solution containing 2% of SDS. After 5 min of incubation at 95 °C, the suspension was centrifuged for 1 h at 20000 g and 4 °C. 26 µL of the supernatant – which contained the desorbed proteins – were mixed with 4 µL of reducing agent and 10 µL of sample buffer. 40 µL of each sample were loaded onto a NuPAGE® Novex® 10% Bis-Tris Gel (Thermo Fisher Scientific,

Waltham, USA) and subjected to SDS-PAGE according to standard procedures. As a molecular marker SeeBlue Plus2 Pre-Stained Standard (Thermo Fisher Scientific) was run in parallel. After 1.5 h at 100 V, the electrophoresis was stopped. Staining was performed overnight using a ready-to-use Coomassie Brilliant Blue (SimplyBlue SafeStain) staining solution. The gels were destained with water overnight.

5.2.9 Transmission electron microscopy

TEM experiments were performed by [redacted] (MPI-P). The samples were diluted with water (1:100). 2 µL of each sample were placed on a lacey grid and washed three times. Then, the samples were embedded in a 1% trehalose solution, containing 4% uranyl acetate to increase contrast. Two replicates of each sample were produced. More details on the preparation method are reported at Kokkinopoulou *et al.*,2017 and Renz *et al.*, 2016.[100, 109] Tilt series from -65° to +65° were recorded at a magnification of 22000 x, using the SerialEM software.[110] The alignments and 3-D reconstructions were computed with eTomo (IMOD software package). The measurements were performed at the FEI Tecnai F20 transmission electron microscope operated at 200 kV. The electron micrographs were recorded on a 2k CCD camera (Gatan Ultrascan 1000). The Digital Micrograph software (Gatan) was used to collect the images.

5.2.10 Zeta potential measurements

Zeta potential measurements were performed using a Nano Z Zetasizer (Malvern Instruments GmbH; Herrenberg, Germany). 20 µL of each sample were diluted with 1 mL of a 1 M KCl solution and directly measured at 25 °C after two minutes of equilibration. Each measurement was repeated three times; mean values and standard deviations were calculated.

5.3 Coating nanoparticles with tunable poly(phosphoester) surfactants facilitates control over the protein corona

5.3.1 PPE-Surfactant synthesis and characterization

PPE-surfactant synthesis and characterization by NMR was carried out by [redacted] (MPI-P). Two surfactants (C_{18}-$PEEP_{21}$ and C_{18}-$PEEP_{78}$) were synthesized by ring-opening polymerization of 2-ethoxy-1,3,2-dioxaphospholane-2-oxide using 1-octadecanole as initiator and 1,5,7-triazabicyclo[4.4.0]dec-5-ene as catalyst. Two diblock copolymer surfactants were synthesized in an organocatalytic one-pot sequential ring-opening polymerization using 2-(benzyloxy)ethan-1-ol as

initiator according to a literature procedure.[111] The obtained polymers were characterized by ^{1}H-, ^{13}C- and ^{31}P-NMR spectroscopy as well as by size exclusion chromatography (SEC). A more detailed description of the synthesis is already published elsewhere.[9, 112]

5.3.2 Sample preparation for zeta potential

An aqueous nanoparticle suspension (0.0125 m² of surface area in a total volume of 75 µL) was mixed with 250 µL of freshly thawed plasma (total protein conc. 68 g L^{-1}, HSA conc. ~44 g L^{-1}) or a freshly prepared HSA solution (0.665 mM; 44 g L^{-1}) in an Eppendorf-tube. After 1 h of mild shaking in a sample shaker at 37 °C, the sample was centrifuged for 1 h at 20000 g and 4 °C. The supernatant was discarded and the pellet resuspended in 250 µL of phosphate-buffered saline (PBS). The suspension was centrifuged for 1 h at 20000 g and 4 °C. These washing steps were repeated for a total of three times. Before the last washing step, the suspension was transferred into a new Eppendorf-tube. After the last washing step, the pellet was resuspended in 250 µL of water and the resulting sample was used for zeta potential measurements.

5.3.3 Isothermal titration calorimetry (ITC)

ITC experiments were conducted at a temperature of 25 °C. To correct the data by the heat of dilution, the titrant was titrated into water and the resulting heats were subtracted from each titration of NPs with the corresponding titrant. Aqueous polystyrene-nanoparticle dispersions with a solid content adjusted to 6 g L^{-1} (equal to a molar concentration of $\sim 1.5 \cdot 10^{-5}$ mM) were titrated with different protein solutions. The NPs were used without additive and as a mixture with an aqueous solution of surfactant (10 g L^{-1}) to achieve stoichiometric coverage of the surface with a layer of surfactants. As protein solution (the titrant), either plasma diluted with a fourfold volume of Milli-Q water (resulting HSA conc. ~8.8 g L^{-1}) or a solution of HSA (8.8 g L^{-1}) in normal saline (9 g L^{-1} NaCl) was used. In a typical experiment 50 µL protein solution (diluted plasma or HSA) were titrated stepwise to 300 µL of a diluted aqueous NP suspension. For all experiments, 25 injections at 2 µL were performed. For titrations of surfactant to NP suspension, the association constant K_a, the binding enthalpy ΔH and the stoichiometry n could be deduced from the calculated fits. All values are an average of triplicates with the standard deviation.

5.3.4 Size exclusion chromatography (SEC)

Surfactant characterization by SEC was performed by Ute Heinz (MPI-P). SEC measurements of the polymers were performed in dimethylformamide (DMF, containing 0.25 g L^{-1} lithium bromide as

additive) with a flow rate of 1 mL min^{-1} at 50 °C using an Agilent 1100 Series integrated instrument with an autosampler, an Agilent G1310A pump and a PSS HEMA column ($10^6/10^5/10^4$ g mol^{-1}). The RI-detector G1362A RID was used for detection. Calibration was achieved using polystyrene provided by Polymer Standards Service. The software PSS-WinGPC UniChrom (PSS) was used for recording and evaluating the data.

5.3.5 Sample preparation for protein quantification and SDS-PAGE

Preparation of the samples, protein quantification and SDS-PAGE was carried out by [redacted] (MPI-P). An aqueous nanoparticle suspension (0.05 m² of surface area in a total volume of 300 µL) was mixed with 1 mL of freshly thawed plasma in an Eppendorf-tube. After 1 h of mild shaking in a sample shaker at 37 °C, the sample was centrifuged for 1 h at 20000 g and 4 °C. The supernatant was discarded and the pellet was resuspended in 1 mL of phosphate-buffered saline (PBS). The suspension was centrifuged for 1 h at 20000 g and 4 °C. These washing steps are repeated for a total of three times. Before the last washing step, the suspension was transferred into a new Eppendorf-tube and protein quantification was conducted as described above.

5.3.6 DLS sample preparation

To an aqueous NP-dispersion with a solid content of 1% a certain amount (equal to the stoichiometric factor *n* determined by ITC) of a 10 g L^{-1} solution of each surfactant was added. 1 mL of freshly thawed and centrifuged (20000 g, 30 min) citrate plasma were filtered through Millex GS filters with a pore size of 0.22 µm (Merck Millipore, Billerica, USA) and 1 µL of the NP-dispersion with surfactant was added.

5.3.7 Cell culture and flow cytometry

All cell culture and flow cytometry experiments of this chapter were performed by [redacted] (MPI-P). Murine macrophage-like cells (RAW 264.7) were cultured in Dulbecco´s modified eagle medium (DMEM, Invitrogen, USA) supplement with 10% fetal bovine serum (FBS, Sigma Aldrich, USA) and 1% penicillin/streptomycin (Invitrogen, USA) in a humidified incubator at 37 °C and 5% CO_2.

RAW 264.7 cells ($1.5 \cdot 10^5$ cells mL^{-1}) were seeded out in 24-well plates (1 mL per well) in DMEM with 10% FBS and cultured overnight. The following day cells were washed with PBS (1 mL) and kept in DMEM without FBS for two hours. L1 coated nanoparticles were incubated with human plasma (0.05 m² surface area per 1 mL of plasma) for 1 h, 37 °C. To remove unbound proteins, nanoparticles were centrifuged for 1 h, 4 °C and L1 + Plasma coated nanoparticles were isolated.

Bare, L1 and L1 + Plasma coated nanoparticles were added to cells (75 µg mL^{-1}) in DMEM without FBS and incubated for 2 h. For flow cytometry analysis, cells were washed with PBS (1 mL) three times. Cells were detached with Trypsin-ETDA (0.25%, Thermo Fischer, USA), centrifuged (5 min, 500 g) and re-suspended in PBS (1 mL). Flow cytometry measurements were performed on a CyFlow ML cytometer (Partec, Germany) with a 488 nm laser to excite the fluorescent labeled nanoparticles (BODIPY; 523/535) and a 527 nm pass filter for emission detection (FL1). Analysis was carried out with FCS Express V4 (DeNovo Software, USA). Therefore, cells were selected on a forward scatter/sideward scatter plot and the selected area was further analyzed in the FL1 channel. The median in the FL1 channel (MFI) was determined from a 1D histogram to analyze the amount of cells associated or taken up by cells.

5.4 Beyond the Protein Corona – Lipids Matter for Biological Response of Nanocarriers

5.4.1 Plasma fractionation into two different lipoprotein fractions

An LDL/VLDL and HDL Purification Kit (Ultracentrifugation Free) (Cell Biolabs, Inc.; Catalog Number STA-608) was used by [redacted] to obtain an HDL- and LDL/VLDL-fraction from human citrate plasma. 10 mL citrate plasma (stored at -80 °C) were thawed and centrifuged at 20000 g (4 °C; 30 min.). The supernatant was collected and used for HDL and (V)LDL purification according to the kit. Purified fractions were stored at 4 °C.

5.4.2 Protein corona preparation

Preparation of the protein corona was performed by [redacted] (MPI-P). The method of Schöttler *et al*. was used with subtle modifications.[13] The ratio of the volume of lipoprotein solution to total particle surface area was kept at 20 mL m^{-2} for all different lipoprotein sources. An amount of nanoparticle dispersion equivalent to 0.05 m^2 was incubated with 1 mL of either human plasma or a lipoprotein solution for 1 h at 37 °C with constant agitation. The particles were separated from the supernatant by centrifugation at 20000 g at 4 °C for 1 h. The particle pellet was resuspended in PBS and washed by three centrifugation steps (20000 g, 4 °C, 1 h). Nanoparticles with a total surface are of 0.05 m^2 were incubated in HDL or (V)LDL fractions obtained from 1 mL citrate plasma. The protein corona of a particle was isolated by desorbing it with 2% (w/v) SDS, 62.5 mM Tris-HCl solution (pH 7.4)

at 95 °C for 5 min. Subsequently, the SDS was removed from the sample using Detergent Removal Spin Column, 0.5 mL (Thermo Fisher Scientific).

Gel electrophoresis was carried out as described above, but a different staining was used. A silver staining solution (Invitrogen, Carlsbad, USA) was applied according to manufacturer's instructions. The gel was destained with water.

5.4.3 Cholesterol assay

A colorimetric cholesterol assay kit was purchased from BioVision (Milpitas, USA) and used according to the manufacturer's manual. To obtain a quantitative result, cholesterol is specifically oxidized by cholesterol oxidase, yielding hydrogen peroxide, which then reacts with a sensitive cholesterol probe to form a dye with an absorption maximum of λ = 570 nm. About 60 to 80% of cholesterol in human blood are esterified,[113] so a selective analysis method for free cholesterol (FC) and cholesteryl esters (CE) is needed. In the absence of cholesterol esterase, only the concentration of free cholesterol is detected, as cholesteryl esters cannot be oxidized by cholesterol oxidase to yield H_2O_2. However, in the presence of cholesterol esterase alongside cholesterol oxidase, cholesteryl esters are hydrolyzed to cholesterol before the oxidation reaction. In this case the concentration of total cholesterol (TC) is measured. Subtraction of the concentration for FC from the concentration of TC then yields the concentration of CE. Absorption was measured with a Tecan infinite M1000 plate reader.

5.4.4 Liquid chromatography-mass spectrometry (LC-MS) analysis

The digestion of corona proteins and subsequent LC-MS analysis were carried out by [redacted] (MPI-P) following the protocol described by Schöttler *et al*. with subtle modifications.[13] 25 µg of total protein was precipitated and digested by Trypsin with an enzyme-to-protein ratio of 1:50. For LC-MS analysis the digested samples were mixed with aqueous solution of formic acid (final concentration of 0.1%, v/v) and spiked with Hi3 E.coli Standard (final concentration of 20 fmol μL^{-1}) (Waters Corporation) for absolute quantification. Approximately 500 ng of digested proteins were injected into the LC-MS. LC-MS analysis of protein samples was carried out using a nanoACQUITY UPLC system coupled with a Synapt G2-S*i* mass spectrometer (Waters Corporation). Tryptic-digested peptides originated from 25 µg total protein were separated on the nanoACQUITY system equipped with a C18 analytical reversed-phase column (1.7 µm, 75 µm x 150 mm, Waters Corporation) and a C18 nanoACQUITY Trap Column (5 µm, 180 µm x 20 mm, Waters Corporation). The peptide separation was performed with a mobile phase A consisting of 0.1% (v/v) formic acid in water and a mobile phase B consisting of acetonitrile with 0.1% (v/v) formic acid at a flow rate of 0.3 µL min^{-1}, using a gradient of 2 - 40% mobile phase B for 70 min. As a reference compound 150 fmol μL^{-1} Glu-Fibrinopeptide was

infused at a flow rate of 0.5 µL min^{-1}. Data-independent acquisition (MS^E) experiments were performed on the Synapt G2-S*i* operated in resolution mode. Electrospray Ionization was performed in positive ion mode using a NanoLockSpray source. Data was acquired over a range of *m*/*z* 50-2000 Da with a scan time of 1 s, ramped trap collision energy from 20 to 40 V with a total acquisition time of 90 min. All samples were analyzed in two technical replicates and the PCA (Principal Component Analysis) was checked as a quality measure for the technical replicates. Data acquisition and processing was carried out using MassLynx 4.1 and Progenesis QI for proteomics v2.0 software was used to process data and identify peptides. Data were post acquisition lock mass corrected. Noise reduction thresholds for low energy, high energy and peptide intensity were fixed at 120, 25, and 750 counts, respectively. During database searches, the protein false discovery rate was set at 4%. The generated peptide masses were searched against a reviewed human protein sequence database downloaded from Uniprot. The following criteria were used for the search: one missed cleavage, maximum protein mass 600 kDa, fixed carbamidomethyl modification for cysteine and variable oxidation for methionine. For identification a peptide was required to have at least three assigned fragments and a protein was required to have at least two assigned peptides and five assigned fragments. Quantitative data were generated based on the TOP3/Hi3 approach. The intensities of unknown proteins and their peptides were compared to that of Hi3 protein. Since the concentration of the spiked Hi3 protein (fmol μL^{-1}) and injected volume (µL) were known the amount of unknown proteins (in fmol) could be calculated from that data. The protein corona was prepared as described above.

5.4.5 Cell culture and flow cytometry

Cell culture and flow cytometry experiments in this chapter were carried out by [redacted] (MPI-P).

Murine macrophage-like cells (RAW 264.7) were cultured in Dulbecco´s modified eagle medium (DMEM, Invitrogen, USA) supplement with 10% fetal bovine serum (FBS, Sigma Aldrich, USA), 1% Glutamine and 1% penicillin/streptomycin (Invitrogen, USA) in a humidified incubator at 37 °C and 5% CO_2.

RAW 264.7 cells ($1.5 \cdot 10^5$ cells mL^{-1}) were seeded in 24-well plates (1 mL per well) in DMEM with 10% FBS and cultured overnight. The following day cells were washed twice with PBS (1 mL) and kept in DMEM without FBS for two hours. Nanoparticles were incubated with human plasma or a lipoprotein solution (0.05 m^2 surface area per 1 mL of plasma/lipoprotein solution) for 1 h at 37 °C. To remove unbound proteins, nanoparticles were centrifuged for 1 h, 4 °C and plasma-coated nanoparticles were isolated.

Bare, plasma- and lipoprotein-coated nanoparticles were added to cells (75 µg mL^{-1}) in DMEM without FBS and incubated for 2 h. For flow cytometry analysis, cells were washed with PBS (1 mL) twice. Cells were detached with Trypsin-EDTA (0.25%, Thermo Fisher Scientific), centrifuged (5 min, 500 g) and re-suspended in PBS (1 mL). Flow cytometry measurements were performed on a CyFlow ML cytometer (Partec, Germany) with a 488 nm laser to excite the fluorescent labeled nanoparticles (BODIPY; 523/535) and a 527 nm pass filter for emission detection (FL1). Analysis was carried out with FCS Express V4 (DeNovo Software, USA). Cells were selected on a forward scatter/sideward scatter plot and the selected/gated area was further analyzed in the FL1 channel. The median in the FL1 channel (MFI) was determined from a 1D histogram. Each measurement had three technical replicates and the average fluorescence is mean ± SD.

5.4.6 Isothermal titration calorimetry (ITC)

Aqueous polystyrene-nanoparticle dispersions with a solid content adjusted to 3 g L^{-1} (equal to a molar concentration of $7 \cdot 10^{-6}$ mM) were titrated with different lipoprotein/apolipoprotein solutions. In a typical experiment, 50 µL (apo-)lipoprotein solution were titrated stepwise to 300 µL of a diluted aqueous NP suspension. For all experiments, 25 injections at 2 µL were performed.

For ITC experiments with HSA-coated polystyrene nanoparticles, 300 µL of an aqueous polystyrene-nanoparticle dispersion with a solid content adjusted to 4 g L^{-1} were incubated with 50 µL of a solution of 1 g L^{-1} HSA in saline in accordance to the stoichiometry of HSA per PS-NP determined in a previous publication.[9] Therefore, the solid content of polystyrene NPs of the resulting dispersion was adjusted to 3.4 g L^{-1} (equal to a molar concentration of $8.2 \cdot 10^{-6}$ mM). The resulting dispersion was incubated for 5 minutes before 50 µL lipoprotein solution were titrated stepwise to 300 µL of the PS-NPs-HSA dispersion.

To refer the fit parameters not only to the complete lipoprotein complexes but also to their single components, further calculations were conducted. As a first assumption, an average molar mass of 600 g mol^{-1} was considered for lipid-like molecules, such as cholesterol, cholesterol esters, triglycerides, phospholipids. The number of lipid-like molecules in a lipoprotein complex was then determined by dividing the total molar mass of the respective lipoprotein complex by this average molar mass. For the total molar mass of the lipoprotein complexes, values described by the supplier were used (Table 5.4.1).

Table 5.4.1 Total molar mass M_t of lipoprotein complexes.

Lipoprotein	M_t / g mol^{-1}
HDL	$3.6 \cdot 10^5$
LDL	$3.0 \cdot 10^6$
VLDL	$8.0 \cdot 10^7$

5.5 Different denaturation *via* surfactants changes composition of protein corona

5.5.1 Nanoparticle synthesis, characterization and purification

Synthesis of model polystyrene nanoparticles (PS-NPs) was performed by [redacted] (MPI-P) as described in the Methods section. For the batch of unfunctionalized, CTMA-Cl stabilized PS-NPs (compare Figure 4.3.8-C), microfluidization with a LM10 microfluidizer (Unitronics, Airport City, Israel) was applied instead of ultrasonication, as this method is more suitable for the synthesis of larger amounts. The polymerization was then carried out for 16 h at 72 °C. For standard purification, the PS-NPs were dialyzed (MWCO 12000 g mol^{-1}) against deionized water for 24 h.

Unfunctionalized polystyrene nanoparticles (PS-NPs) stabilized with CTMA-Cl were further dialyzed to minimize the coverage with CTMA-Cl while still maintaining a stable dispersion. Dialysis was carried out overnight (MWCO 50000 Da), obtaining a surface tension of (73 ± 1) mN m^{-1} afterwards. A dispersion of these purified PS-NPs was used for ITC titration with CTMA-Cl to investigate surfactant-nanoparticle-interactions (see Figure 4.3.8-C).

5.5.2 Synthesis of amino-functionalized PS-NPs (Precursor for PS-PEG)

Synthesis of amino-functionalized PS-NPs was carried out by [redacted] as previously reported.[13] A macroemulsion was prepared with a continuous phase containing CTMA-Cl solution (25% in water, 510 mg, $4.0 \cdot 10^{-4}$ mol) as surfactant and 2-aminoethyl methacrylate hydrochloride (AEMH) (121 mg, $7.3 \cdot 10^{-4}$ mol, 2% to styrene) in 23.5 g Milli-Q water and a dispersed phase containing distilled styrene (5.891 g, $5.7 \cdot 10^{-2}$ mol), hexadecane (254 mg, $1.1 \cdot 10^{-3}$ mol) as hydrophobe, Bodipy methacrylate (6 mg, $1.3 \cdot 10^{-5}$ mol) as fluorescent dye and 2,2'-azobis(2-methylbutyronitrile) (V59) (104 mg, $5.4 \cdot 10^{-4}$ mol) as oil soluble azo initiator. Both phases were homogenized by mechanical stirring and the continuous phase was added slowly to the stirring dispersed phase. The macroemulsion was stirred

for 1 h at 1000 rpm on a magnetic stirrer. Subsequently, the macroemulsion was ultrasonicated with a Branson Sonifier (1/2“ tip, 6.5 nm diameter) for 3 min at 450 W 90% amplitude under ice cooling to obtain a miniemulsion. The miniemulsion was directly transferred into a 50 mL flask and stirred in an oil bath at 72 °C. The polymerization was carried out for 12 h. The dispersion was purified by centrifugation (1 h, 14000 rpm; 1 h, 16000 rpm; 30 min; 18000 rpm), the supernatant always removed and the pellet redispersed in Milli-Q water.

5.5.3 Determination of the amount of -NH_2 groups per particle

The number of amino groups was calculated from the results of the titration experiments performed by [redacted] (MPI-P) on a particle charge detector PCD 02 (Mütek GmbH, Germany) in combination with a Titrino Automatic Titrator 702 SM (Metrohm AG, Switzerland). The amino groups were titrated against the negatively charged polyelectrolyte standard sodium poly(ethylene sulfonate) (PES-Na, 1 mM), to determine the isoelectric point. The titration was performed using 10 mL of the dispersion with a solid content of 1 g L^{-1} (0.1 wt%) in an aqueous solution with pH 2. The number of groups per particle was calculated from the consumed volume (an average of three titrations) of the polyelectrolyte solution as previously described.[13]

5.5.4 PEGylation of polystyrene nanoparticles

PEGylation of PS-NPs and the subsequent characterization were carried out by [redacted] (MPI-P). For poly(ethylene glycol) (PEG) modified NPs, 7 mL of amino-functionalized particle dispersion (1%, $1.5 \cdot 10^{14}$ particles, $9.0 \cdot 10^{-7}$ mol NH_2 groups) were basified with 56 µL pyridine (pH 8.5) and stirred for 20 min at room temperature at 500 rpm. Then 45 eq of PEG-NHS (203 mg, M_n = 5000 g mol^{-1}) dissolved in 1 mL sterile Milli-Q water were added in three portions within 30 min. The reaction was stirred for 24 h at room temperature and 500 rpm to ensure full conversion. The dispersion was purified by repeated centrifugation (3 x 1 h, 30000 g). Each time the supernatant was removed and the pellet redispersed in sterile Milli-Q water (2 x 3 mL, 1 x 2 mL). After determination of the solid content the dispersion was adjusted to 1% with sterile Milli-Q water.

5.5.5 Determination of degree of PEGylation

The number of PEG chains per particle was approximated *via* ^{1}H NMR spectroscopy (500 MHz, $CDCl_3$, 298 K). To do so, the integrals of the PS backbone (7.23 - 6.27 ppm) were compared with the integrals of the PEG (3.72 - 3.62 ppm) backbone as previously described.[13]

5.5.6 Sample preparation for DSF and ITC

For DSF experiments, a protein concentration of 0.167 g L^{-1} was used for Apo-A1, recombinant CLU and commercial CLU.

In ITC experiments, the protein concentration was 0.3 g L^{-1} for both Apo-A1 and recombinant CLU, while the concentration of CTMA-Cl was chosen as 10 g L^{-1} for the titration of Apo-A1 and 0.12 g L^{-1} for CLU. Only aqueous systems were measured, so the reference cell was filled with deionized water during all experiments. The measured heat rates were corrected for the heat of dilution of the surfactant (titration of surfactant into water, see Figure 4.3.6).

5.5.7 Nanoparticle coating with CTMA-Cl

The nanoparticle dispersion was centrifuged for 1 h, 20000 g (4 °C) and resuspended in a CTMA-Cl solution with varying concentration ranging from 0.1 mg mL^{-1} to 3 mg mL^{-1}.

5.5.8 Protein corona preparation

Preparation of the samples, protein quantification, SDS-PAGE and LC-MS was carried out by [redacted] (MPI-P). Nanoparticles (0.05 m^2) were incubated in human citrate plasma (1 mL) for 1 h at 37 °C and agitated at 300 rpm. Afterwards, nanoparticles were centrifuged at 20000 g at 4 °C for 1 h and the pellet was resuspended in PBS to remove unbound proteins. The washing step was repeated three times. Hard corona proteins were desorbed from the nanoparticles´ surface with 2% (w/v) SDS, 62.5 mM Tris-HCl solution (pH 7.4) at 95 °C for 5 min. The nanoparticle suspension was centrifuged (20000 g, 4 °C, 1 h) and the supernatant contained hard corona proteins. SDS was removed from the protein solution using Detergent Removal Spin Column, 0.5 mL (Thermo Fisher Scientific).

5.5.9 In solution digestion and liquid chromatography-mass spectrometry (LC-MS) analysis

LC-MS experiments were performed by [redacted] (MPI-P).

Tryptic digestion was performed as previously described.[13, 100] Peptide samples were further applied to a nanoACQUITY UPLC system coupled with a Synapt G2-S*i* mass spectrometer (Waters Corporation). A C18 analytical reversed-phase column (1.7 µm, 75 µm x 150 mm, Waters Corporation) and a C18 nanoACQUITY Trap Column (5 µm, 180 µm x 20 mm, Waters Corporation) were used for peptide separation. A two phase mobile systems consisting of mobile phase A 0.1% (v/v) formic acid in water and a mobile phase B consisting of acetonitrile with 0.1% (v/v) formic acid was chosen. Separation was

carried out using a gradient of 2 - 40% mobile phase B for 70 min and flow rate of 0.3 µL min^{-1}. The reference compound Glu-Fibrinopeptide (150 fmol $µL^{-1}$) was infused at a flow rate of 0.5 µL min^{-1}.

The Synapt G2-S*i* was operated in resolution mode performing data-independent acquisition (MS^E) experiments. Electrospray Ionization was performed in positive ion mode using a NanoLockSpray over a range of *m*/*z* 50-2000 Da.

To identify peptides MassLynx 4.1 and Progenesis QI for proteomics were used and data were post acquisition lock mass corrected. Several parameters were set for peptide identification: noise reduction thresholds for low energy, high energy and peptide intensity at 120, 25, and 750 counts. To identify proteins, peptides were searched against a reviewed human protein sequence database downloaded from Uniprot using the following criteria: maximum protein mass 600 kDa, fixed carbamidomethyl modification for cysteine, one missed cleavage and variable oxidation for methionine. A peptide was identified if at least three assigned fragments were found and for protein identification at least two assigned peptides and five assigned fragments were required. The TOP3/Hi3 approach was chosen for absolute quantification, hereby providing the amount of each protein in fmol.

5.5.10 Zeta potential sample preparation

Preparation of the protein corona was carried out as stated above until the fourth centrifugation step. After this last washing step, the pellet was resuspended in 250 µL of water and the resulting sample was used for zeta potential measurements.

5.5.11 Dynamic light scattering

A Nicomp zetasizer (PSS Nicomp, Port Richey, USA) was used to measure dynamic light scattering of NP samples at a fixed angle of 90°.

5.6 Effect of heat inactivation on adsorption properties of apolipoproteins

5.6.1 Sample preparation for DSF and ITC

For DSF experiments, the protein concentration was 0.5 g L^{-1} and the solutions were measured in standard capillaries.

ITC experiments were conducted at 25 °C. Dispersions of PS-Lut with a concentration of 10 g L^{-1} were titrated with CLU at a concentration of 1 g L^{-1} or Apo-A1 of 0.5 g L^{-1}. Besides the native proteins, also

heat inactivated proteins of the same concentrations were used, which were thermally treated at 90 °C for 6 h.

5.7 Interaction of poly(ethylene glycol) with proteins and nanoparticles

5.7.1 Differential scanning fluorimetry

Aqueous solutions of Apo-A1 and CLU at a concentration of 0.167 g L^{-1} with PEG-2000 of different concentrations were measured in standard capillaries.

5.7.2 Isothermal titration calorimetry (ITC)

In ITC experiments conducted at 15 °C, Apo-A1 with 0.5 g L^{-1}, CLU with 0.3 g L^{-1} and HSA with 1.25 g L^{-1} were titrated with PEG at a concentration of 5 g L^{-1}. Additional ITC measurements were conducted at 25 °C, in which Apo-A1 with 0.5 g L^{-1} was titrated with PEG at a concentration of 5.1 g L^{-1} and HSA with 13 g L^{-1}, Transferrin with 11.3 g L^{-1} as well as IgG with 10 g L^{-1} were titrated with PEG at a concentration of 51 g L^{-1}. Commercial lipoproteins diluted with Milli-Q water at a ratio of 1:200 were titrated with PEG at a concentration of 55 g L^{-1} at 25 °C.

In further ITC experiments with nanoparticles, a dispersion of PS-PEG at 1 g L^{-1} was titrated with CLU or Apo-A1 at 0.5 g L^{-1} at 25 °C.

6 Summary and Outlook

The protein corona, the crucial aspect of nanocarriers as drug delivery vehicles, has been studied extensively. The role of surfactants on the corona composition as well as their effect of denaturation of certain proteins has been illuminated. Especially the stealth proteins Apo-A1 and CLU were analyzed in detail by various methods. Also other biomolecules from blood plasma such as lipids were investigated regarding their adsorption behavior and significant adsorption was measurable. This also had an impact on the stealth effect.

The physical adsorption of biodegradable polymeric surfactants to the surface of nanocarriers has been applied successfully as an alternate approach towards stealth nanocarriers. The adsorption parameters of the surfactants can be tuned by systematic variation of their structure, which could be confirmed by ITC experiments. With this surfactant coating, a similar protein corona as for the covalent attachment of PEG-chains, the previous standard approach to stealth nanocarriers, could be found in SDS-PAGE. The stealth effect of surfactant coated NPs incubated with plasma was verified in cellular uptake experiments.

Our approach is not limited to polystyrene nanoparticles, but could easily be transferred to other nanocarrier systems, which is an advantage compared to PEGylation. In a next experiment, NPs made of a different material could be coated with our surfactants and be subjected to corona analysis as well as to assessment of the stealth effect. Surfactants could be improved even further towards a high binding affinity to the NPs to prevent possible desorption upon incubation with proteins. Besides, the necessity for modification of the surfactants to ensure compatibility with other NP materials could arise.

Apolipoproteins have been found in disproportionately high amounts in the corona of stealth nanocarriers. In plasma, they do not occur as free proteins but integrated in lipoprotein complexes.

Therefore, lipoprotein adsorption and the role of lipids for the corona of nanocarriers has been investigated in further experiments. Evidence for the disintegration of lipoprotein complexes upon adsorption has been found in TEM experiments. Therefore, the adsorption of single lipoprotein constituents such as phospholipids, apolipoproteins, cholesterol and other lipids takes place. Cholesterol could be detected in the corona with a specific assay.

The findings obtained in this study suggest to also consider lipid adsorption in the context of biological behavior of NPs and expand the view towards a ‘biomolecular corona’ instead of the protein corona.

Since almost every nanocarrier system requires some sort of surfactant to ensure colloidal stability, the effect of a commercially available surfactant on protein denaturation has been investigated. The influence of CTMA-Cl on the folding state of Apo-A1 and CLU, which are prominent apolipoproteins in

the stealth corona, has been screened in DSF measurements. CLU was found to be more sensitive to surfactant denaturation, as already for lower CTMA-Cl concentrations an effect could be observed. In addition, the interaction of this surfactant with the proteins as well as its adsorption to PS-NPs and the respective adsorption of the proteins have been measured with ITC and the binding affinities of the three interaction types were compared. For NP dispersions with additional CTMA-Cl, a change in the composition of the protein corona towards less CLU, more Apo-A1 and additional vitronectin compared to the standard NP dispersion could be detected in LC-MS and SDS-PAGE.

As a continuation of this work, the effect of different types of surfactants can be investigated in more detail. Regarding nonionic surfactants, first evidence for stabilization of certain proteins could be gained in DSF experiments (data not shown).

Similar to surfactant denaturation, heat inactivation, which is a standard procedure often used in cell culture, can also have an effect on protein adsorption to nanocarriers. It was found in DSF experiments that treatment at 56 °C for 30 min does not completely denature/unfold Apo-A1 and CLU. Only longer treatment at 90 °C leads to complete denaturation.

Differences in the binding affinity of native and heat inactivated proteins observed in ITC experiments were measurable, but vague. Also considering the findings from surfactant denaturation, a more distinct effect on the protein corona most likely only shows in a protein mixture like plasma, when other proteins are competing for adsorption, and not for experiments with isolated single proteins.

Finally, the interaction of poly(ethylene glycol) (PEG) with proteins has been investigated. PEG is frequently used as a stealth polymer, reducing the overall protein adsorption quantitatively and leading to an enrichment of certain apolipoproteins in the corona. No effect of free PEG on the folding state of the apolipoproteins Apo-A1 and CLU was observed in DSF measurements, so no alteration of the protein structure takes place. The interaction of a number of proteins with free PEG was screened in ITC measurements at different temperatures and no defined interaction was found, except for Apo-A1. An interaction with PEGylated NPs was measured for Apo-A1 and CLU. To specify the nature and mechanism of this interaction, further experiments with complementary methods are necessary. It should be clarified to which extent the interaction of the proteins with the underlying NP material plays a role.

A new approach to stealth nanocarriers in the form of PPE-surfactant coating has been introduced, which generates a protein pattern with confirmed stealth properties. Besides, new insights on the effect of surfactants on the protein corona have been gained, which can serve as a basis and support further studies on this subject. The impact of the surfactant CTMA-Cl on protein denaturation and on the composition of the protein corona has been studied. Different proteins are affected by surfactant denaturation in variable extent, so special attention must be paid to the surfactants present in the

nanocarrier dispersions. Furthermore, investigations on the interaction of lipoproteins with nanoparticles showed that lipids and other lipoprotein constituents do adsorb and thus affect the cellular uptake of nanoparticles. This represents another class of biomolecules besides proteins, which needs to be considered for the biological behavior of nanocarriers in future studies. Analysis and control of the protein corona on nanocarriers remains a complex task, possibilities for predictions of the behavior range between difficult and impossible. Even in the simplest case of an unfunctionalized NP, at least three types of interacting compounds (nanoparticle, surfactant, proteins) need to be considered.

7 Abbreviations

ΔG	Gibbs free energy
ΔH	enthalpy change
ΔS	entropy change
A	area
ACF	autocorrelation function
Apo-A1	apolipoprotein A1
Apo-B100	apolipoprotein B100
Apo-E	apolipoprotein E
c	concentration
CLU	clusterin
DLS	dynamic light scattering
DLVO	Derjaguin, Landau, Verwey, Overbeek
DSF	differential scanning fluorimetry
DMEM	Dulbecco's modified Eagle's medium
EDTA	ethylenediaminetetraacetic acid
FBS	fetal bovine serum
HDL	high density lipoprotein
HLB	hydrophilic-lipophilic-balance
HSA	human serum albumin
ITC	isothermal titration calorimetry
k	Boltzmann constant
K_a	binding affinity
kDa	kilo Dalton
LDL	low density lipoprotein
M_n	molecular weight, number average
M_w	molecular weight
$MWCO$	molecular weight cut off

n	stoichiometric ratio
NP	nanoparticle
PBS	phosphate buffered saline
PEG	poly(ethylene glycol)
PPE	poly-(phosphoester)
PS	polystyrene
q	scattering vector
R_h	hydrodynamic radius
SD	standard deviation
SDS	sodium dodecyl sulfate
SDS-PAGE	sodium dodecyl sulfate polyacrylamide gel electrophoresis
T	temperature
t	time
TEM	transmission electron microscopy
V	volume
VLDL	very low density lipoprotein

τ	relaxation time
λ	wavelength
θ	scattering angle
η	viscosity
ζ	zeta potential

8 Acknowledgements

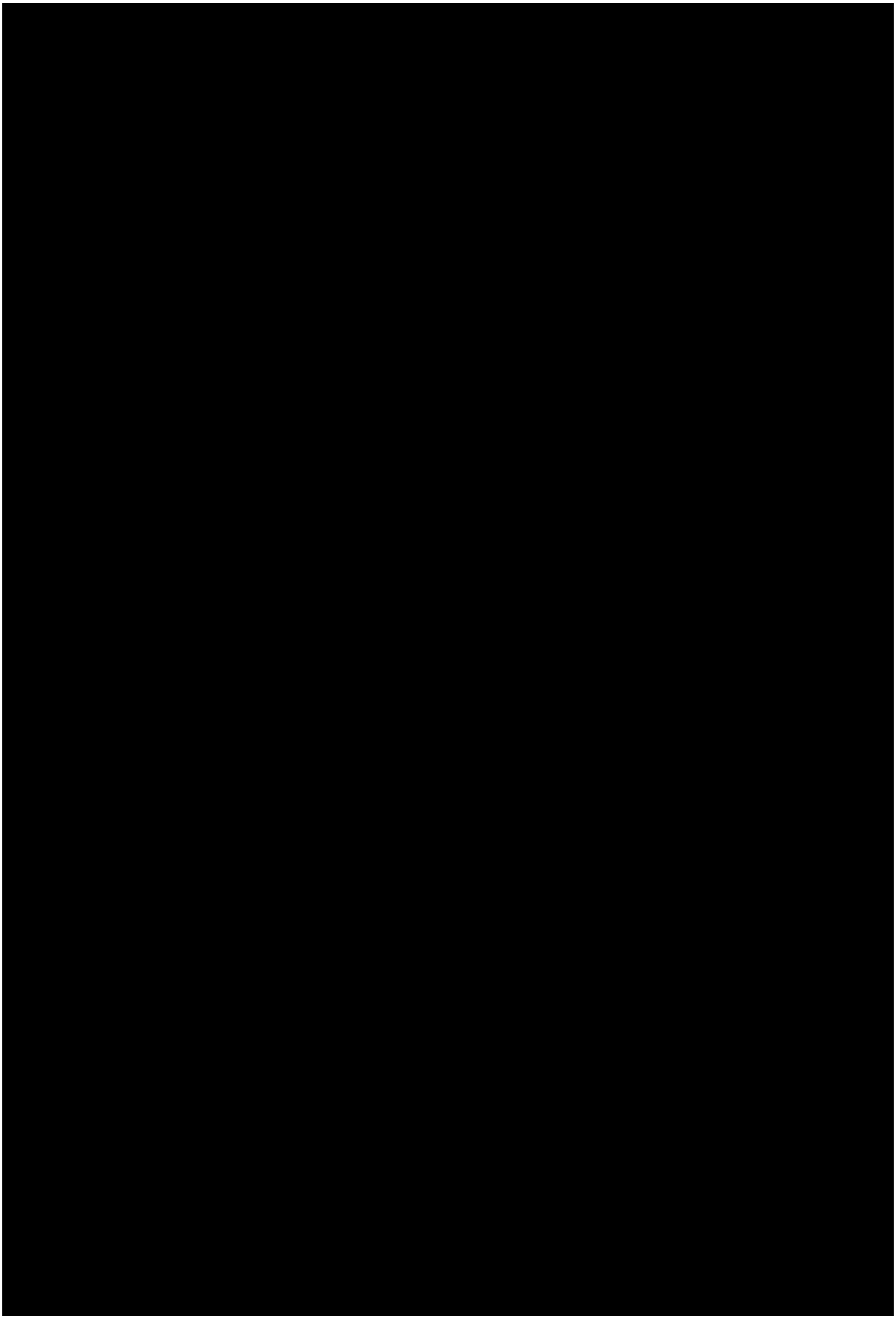

9 Appendix

9.1 Publications related to PhD thesis

[redacted]

Coating nanoparticles with tunable surfactants facilitates control over the protein corona
Biomaterials **2017**, 115, 1–8

Abstract:

Nanoparticles with long blood circulation time are a prerequisite for targeted drug delivery. To make the nanoparticles invisible for phagocytizing cells, functional moieties on the particle surface are believed to be necessary to attract specific so-called 'stealth' proteins forming a protein 'corona'. Currently, covalent attachment of those moieties represents the only way to achieve that attraction. However, that approach requires a high synthetic effort and is difficult to control. Therefore, we present the coating of model nanoparticles with biodegradable polymeric surfactants as an alternative method. The thermodynamic parameters of the coating process can be tuned by adjusting the surfactants' block lengths and hydrophilicity. Consequently, the unspecific protein adsorption and aggregation tendency of the particles can be controlled, and stealth proteins inhibiting cell uptake are enriched on their surface. This non-covalent approach could be applied to any particle type and thus facilitates tuning the protein corona and its biological impact.

[redacted]

Beyond the Protein Corona – Lipids Matter for Biological Response of Nanocarriers
Accepted as a full paper in Acta Biomaterialia.

Abstract:

The interaction of nanocarriers with blood plasma components influences the biological response and therefore needs to be controlled. Whereas protein adsorption to nanocarriers has been investigated to a large extent, the role of lipid interaction for drug delivery and its biological impact is not yet clear. However, lipids represent an important constituent of blood plasma and are usually bound in the form of lipoproteins. Since already for many nanocarriers systems an enrichment of apolipoproteins in their protein corona was reported, we examine the interaction of lipoproteins with nanocarriers. If interaction occurs in terms of lipoprotein

adsorption, two scenarios are possible: adsorption of intact lipoprotein complexes or disintegration of the complexes with adsorption of the single components. To investigate the interaction and clarify which scenario occurs, polymeric model nanoparticles and different lipoprotein types have been studied by isothermal titration calorimetry, transmission electron microscopy and other methods. Our data indicates that upon contact with polymeric nanoparticles, disintegration of lipoproteins and adsorption of lipids occurs. Further, the effect of lipoprotein adsorption on cell uptake has been examined and a major impact of the lipoproteins has been found.

[redacted]

Different denaturation via surfactants changes composition of protein corona

Submitted.

Abstract:

The use of nanocarriers as drug delivery vehicles brings them into contact with blood plasma proteins. Polymeric nanocarriers require some sort of surfactant to ensure colloidal stability. Formation of the protein corona is therefore not only determined by the intrinsic properties of the nanocarrier itself, but also by the accompanying surfactant. Although it is well known that surfactants have an impact on protein structure, only few studies were conducted on the specific effect of surfactants on the composition of protein corona of nanocarriers. Therefore, we analyzed the composition of the protein corona on nanoparticles with additional surfactant (cetyltrimethylammonium chloride, CTMA-Cl) after plasma incubation. Additional CTMA-Cl lead to an enrichment of apolipoprotein-A1 and vitronectin in the corona, while less clusterin could be found. Further, the structural stability of apolipoprotein-A1 and clusterin was monitored for a wide range of CTMA-Cl concentrations. Clusterin turned out to be more sensitive to CTMA-Cl, with denaturation occurring at lower concentrations.

A Photoresponsive Orthogonal Supramolecular Complex Based on Host–Guest Interactions
Chemistry - A European Journal **2017**, 23, 2628–2634

Abstract:

We synthesized a novel green-light-responsive tetra-*ortho*-isopropoxy-substituted azobenzene (ipAzo). *Cis*-ipAzo forms a strong host–guest complex with γ-cyclo dextrin (γ-CD) whereas *trans*-ipAzo binds weakly. This new photoresponsive host–guest interaction is reverse to the well-known azobenzene (Azo)/α-cyclodextrin (α-CD) complex, which is strong only between *trans*-Azo and α-CD. By combining the UV-light-responsive Azo/a-CD and greenlight-responsive ipAzo/γ-CD host–guest complexes, a photoresponsive orthogonal supramolecular system is developed

Small Surfactant Concentration Differences Influence Adsorption of Human Serum Albumin on Polystyrene Nanoparticles
Biomacromolecules **2016**, 17, 3845−3851

Abstract:

Surfactants, even in miniscule amounts, are often used for the synthesis and especially the stabilization of nanomaterials, which is essential for *in vivo* applications. In this study, we show that the interaction between nanoparticles and proteins strongly depends on the type of stabilizing surfactants and their (small) concentration changes. The reaction between human serum albumin and polystyrene nanoparticles stabilized by an ionic or nonionic surfactant − sodium dodecyl sulfate or Lutensol AT50®, respectively − was monitored using isothermal titration calorimetry. It was found that the amount of surfactant molecules on the surface significantly determines the protein binding affinity and adsorption stoichiometry, which is important for all nanomaterials coming into contact with biological components such as blood plasma proteins. Thus after synthesizing nanomaterials for *in vivo* applications as drug delivery agents, it is crucial to perform a detailed analysis of the obtained surface chemistry that accounts for the presence of minimal amounts of stabilizing agents.

[redacted]

Protein structure detrimentally affects biomolecular corona formation and cellular interactions
In preparation.

9.2 Conference Contributions

06/2017 **Gordon Research Seminar – Cancer Nanotechnology;** Vermont, USA
Oral presentation

06/2017 **Gordon Research Conference – Cancer Nanotechnology;** Vermont, USA
Poster presentation

09/2016 **Symposium SFB1066: Chemical Design – Biomedical Applications;** Mainz, Germany
Poster presentation

06/2016 **International Society for Biological Calorimetry, XIXth Conference;** Basel, Switzerland
Oral presentation

9.3 Curriculum Vitae

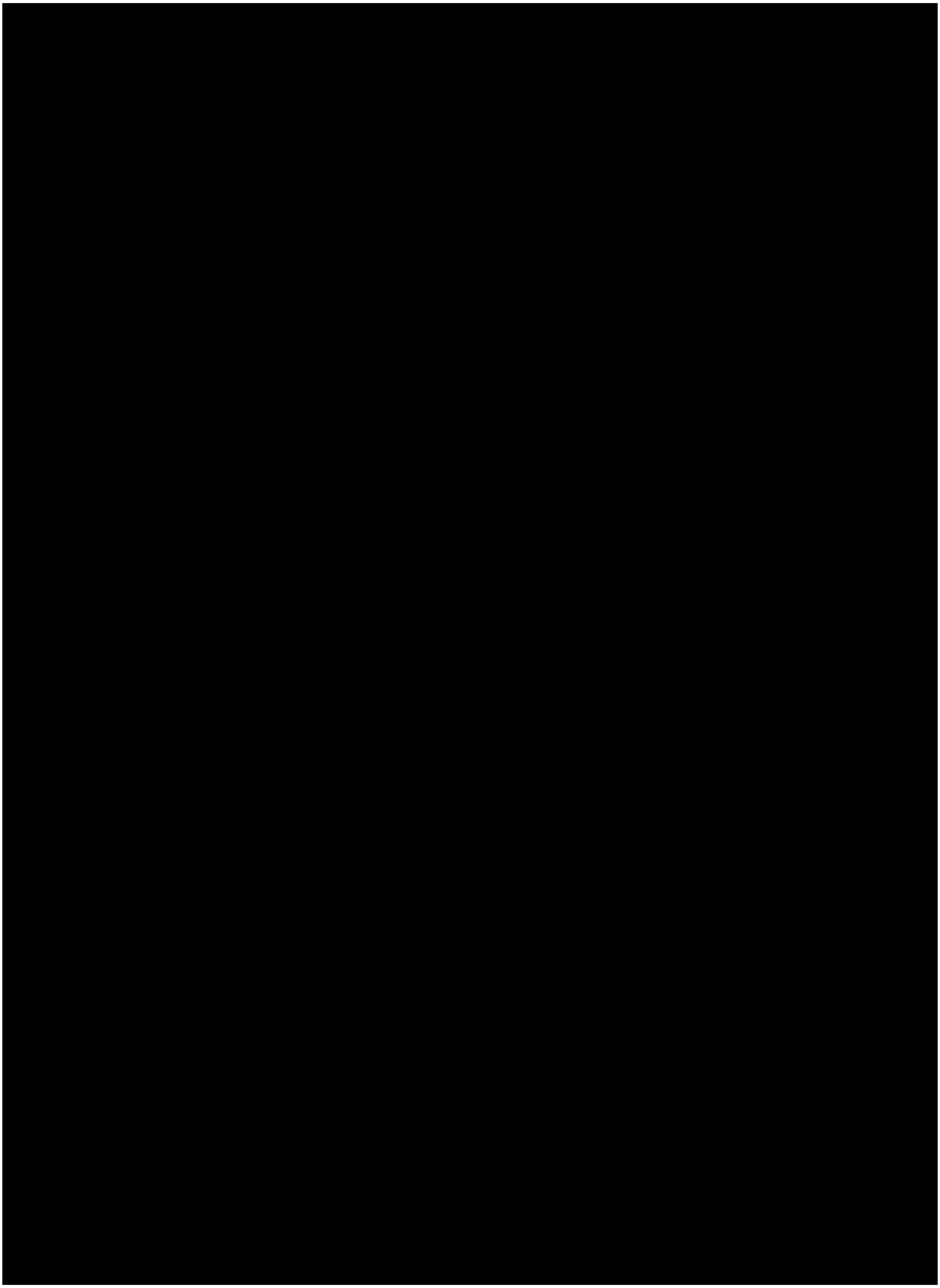

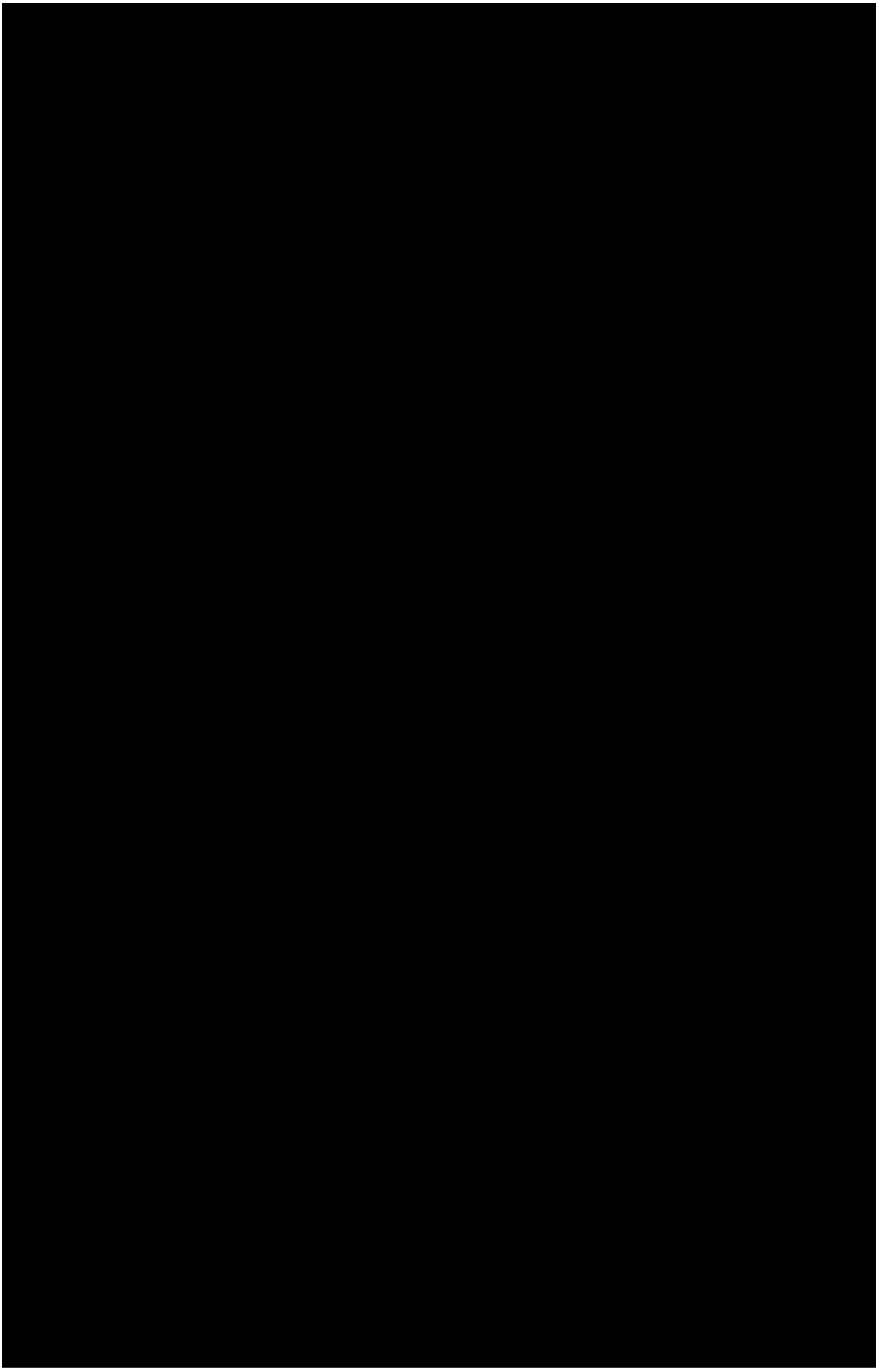

Bibliography

1. Milani, S.; Bombelli, F. B.; Pitek, A. S.; Dawson, K. A.; Radler, J., Reversible versus Irreversible Binding of Transferrin to Polystyrene Nanoparticles: Soft and Hard Corona. *Acs Nano* **2012,** *6* (3), 2532-2541.

2. Pearson, R. M.; Juettner, V. V.; Hong, S., Biomolecular corona on nanoparticles: a survey of recent literature and its implications in targeted drug delivery. *Front Chem* **2014,** *2*, 108.

3. Cedervall, T.; Lynch, I.; Lindman, S.; Berggard, T.; Thulin, E.; Nilsson, H.; Dawson, K. A.; Linse, S., Understanding the nanoparticle-protein corona using methods to quantify exchange rates and affinities of proteins for nanoparticles. *P Natl Acad Sci USA* **2007,** *104* (7), 2050-2055.

4. Owens, D. E.; Peppas, N. A., Opsonization, biodistribution, and pharmacokinetics of polymeric nanoparticles. *Int J Pharmaceut* **2006,** *307* (1), 93-102.

5. Kang, B.; Okwieka, P.; Schöttler, S.; Seifert, O.; Kontermann, R. E.; Pfizenmaier, K.; Musyanovych, A.; Meyer, R.; Diken, M.; Sahin, U.; Mailänder, V.; Wurm, F. R.; Landfester, K., Tailoring the stealth properties of biocompatible polysaccharide nanocontainers. *Biomaterials* **2015,** *49*, 125-34.

6. Lundqvist, M.; Stigler, J.; Elia, G.; Lynch, I.; Cedervall, T.; Dawson, K. A., Nanoparticle size and surface properties determine the protein corona with possible implications for biological impacts. *P Natl Acad Sci USA* **2008,** *105* (38), 14265-14270.

7. Lynch, I.; Salvati, A.; Dawson, K. A., PROTEIN-NANOPARTICLE INTERACTIONS What does the cell see? *Nature Nanotechnology* **2009,** *4* (9), 546-547.

8. Monopoli, M. P.; Aberg, C.; Salvati, A.; Dawson, K. A., Biomolecular coronas provide the biological identity of nanosized materials. *Nat Nanotechnol* **2012,** *7* (12), 779-86.

9. Müller, J.; Bauer, K. N.; Prozeller, D.; Simon, J.; Mailänder, V.; Wurm, F. R.; Winzen, S.; Landfester, K., Coating nanoparticles with tunable surfactants facilitates control over the protein corona. *Biomaterials* **2017,** *115*, 1-8.

10. Winzen, S.; Schöttler, S.; Baier, G.; Rosenauer, C.; Mailänder, V.; Landfester, K.; Mohr, K., Complementary analysis of the hard and soft protein corona: sample preparation critically effects corona composition. *Nanoscale* **2015,** *7* (7), 2992-3001.

11. Palchetti, S.; Colapicchioni, V.; Digiacomo, L.; Caracciolo, G.; Pozzi, D.; Capriotti, A. L.; La Barbera, G.; Lagana, A., The protein corona of circulating PEGylated liposomes. *Biochim Biophys Acta* **2016,** *1858* (2), 189-96.

12. Caracciolo, G.; Palchetti, S.; Colapicchioni, V.; Digiacomo, L.; Pozzi, D.; Capriotti, A. L.; La Barbera, G.; Lagana, A., Stealth effect of biomolecular corona on nanoparticle uptake by immune cells. *Langmuir* **2015,** *31* (39), 10764-73.

13. Schöttler, S.; Becker, G.; Winzen, S.; Steinbach, T.; Mohr, K.; Landfester, K.; Mailänder, V.; Wurm, F. R., Protein adsorption is required for stealth effect of poly(ethylene glycol)- and poly(phosphoester)-coated nanocarriers. *Nature Nanotechnology* **2016,** *11* (4), 372-377.

14. Capriotti, A. L.; Caracciolo, G.; Cavaliere, C.; Colapicchioni, V.; Piovesana, S.; Pozzi, D.; Lagana, A., Analytical Methods for Characterizing the Nanoparticle-Protein Corona. *Chromatographia* **2014,** *77* (11-12), 755-769.

15. Mirshafiee, V.; Kim, R.; Park, S.; Mahmoudi, M.; Kraft, M. L., Impact of protein pre-coating on the protein corona composition and nanoparticle cellular uptake. *Biomaterials* **2016,** *75*, 295-304.

16. Veronese, F. M.; Pasut, G., PEGylation, successful approach to drug delivery. *Drug Discov Today* **2005,** *10* (21), 1451-1458.

17. Alconcel, S. N. S.; Baas, A. S.; Maynard, H. D., FDA-approved poly(ethylene glycol)-protein conjugate drugs. *Polym Chem-Uk* **2011,** *2* (7), 1442-1448.

18. Bazile, D.; Prudhomme, C.; Bassoullet, M. T.; Marlard, M.; Spenlehauer, G.; Veillard, M., Stealth Me.Peg-Pla Nanoparticles Avoid Uptake by the Mononuclear Phagocytes System. *J Pharm Sci* **1995,** *84* (4), 493-498.

19. Ritz, S.; Schöttler, S.; Kotman, N.; Baier, G.; Musyanovych, A.; Kuharev, J.; Landfester, K.; Schild, H.; Jahn, O.; Tenzer, S.; Mailänder, V., Protein Corona of Nanoparticles: Distinct Proteins Regulate the Cellular Uptake. *Biomacromolecules* **2015,** *16* (4), 1311-1321.

20. Gref, R.; Luck, M.; Quellec, P.; Marchand, M.; Dellacherie, E.; Harnisch, S.; Blunk, T.; Muller, R. H., 'Stealth' corona-core nanoparticles surface modified by polyethylene glycol (PEG): influences of the corona (PEG chain length and surface density) and of the core composition on phagocytic uptake and plasma protein adsorption. *Colloid Surface B* **2000,** *18* (3-4), 301-313.

21. Landfester, K.; Bechthold, N.; Tiarks, F.; Antonietti, M., Miniemulsion polymerization with cationic and nonionic surfactants: A very efficient use of surfactants for heterophase polymerization. *Macromolecules* **1999,** *32* (8), 2679-2683.

22. Jiang, L. Q.; Gao, L.; Sun, J., Production of aqueous colloidal dispersions of carbon nanotubes. *J Colloid Interf Sci* **2003,** *260* (1), 89-94.

23. Hecht, L. L.; Schoth, A.; Munoz-Espi, R.; Javadi, A.; Kohler, K.; Miller, R.; Landfester, K.; Schuchmann, H. P., Determination of the Ideal Surfactant Concentration in Miniemulsion Polymerization. *Macromol Chem Phys* **2013,** *214* (7), 812-823.

24. Baier, G.; Costa, C.; Zeller, A.; Baumann, D.; Sayer, C.; Araujo, P. H. H.; Mailänder, V.; Musyanovych, A.; Landfester, K., BSA Adsorption on Differently Charged Polystyrene Nanoparticles using Isothermal Titration Calorimetry and the Influence on Cellular Uptake. *Macromolecular Bioscience* **2011,** *11* (5), 628-638.

25. Wang, M.; Briggs, M. R., HDL: the metabolism, function, and therapeutic importance. *Chem Rev* **2004,** *104* (1), 119-37.

26. Gofman, J. W., Serum lipoproteins and the evaluation of atherosclerosis. *Ann N Y Acad Sci* **1956,** *64* (4), 590-5.

27. Lynch, I.; Dawson, K. A., Protein-nanoparticle interactions. *Nano Today* **2008,** *3* (1–2), 40-47.

28. Monopoli, M. P.; Aberg, C.; Salvati, A.; Dawson, K. A., Biomolecular coronas provide the biological identity of nanosized materials. *Nat Nano* **2012,** *7* (12), 779-786.

29. Lundqvist, M.; Stigler, J.; Cedervall, T.; Berggård, T.; Flanagan, M. B.; Lynch, I.; Elia, G.; Dawson, K., The Evolution of the Protein Corona around Nanoparticles: A Test Study. *ACS nano* **2011,** *5* (9), 7503-7509.

30. Tenzer, S.; Docter, D.; Kuharev, J.; Musyanovych, A.; Fetz, V.; Hecht, R.; Schlenk, F.; Fischer, D.; Kiouptsi, K.; Reinhardt, C.; Landfester, K.; Schild, H.; Maskos, M.; Knauer, S. K.; Stauber, R. H., Rapid formation of plasma protein corona critically affects nanoparticle pathophysiology. *Nat Nanotechnol* **2013,** *8* (10), 772-81.

31. Hellstrand, E.; Lynch, I.; Andersson, A.; Drakenberg, T.; Dahlback, B.; Dawson, K. A.; Linse, S.; Cedervall, T., Complete high-density lipoproteins in nanoparticle corona. *FEBS J* **2009,** *276* (12), 3372-81.

32. Lara, S.; Alnasser, F.; Polo, E.; Garry, D.; Lo Giudice, M. C.; Hristov, D. R.; Rocks, L.; Salvati, A.; Yan, Y.; Dawson, K. A., Identification of Receptor Binding to the Biomolecular Corona of Nanoparticles. *Acs Nano* **2017**.

33. Nam, N. N.; Han, S. Y., Formation of High-Density Lipoprotein (HDL) Coronas on Silica Nanoparticles Occurs by Adsorption of Intact HDL Particulates. *B Korean Chem Soc* **2016,** *37* (1), 3-4.

34. Raesch, S. S.; Tenzer, S.; Storck, W.; Rurainski, A.; Selzer, D.; Ruge, C. A.; Perez-Gil, J.; Schaefer, U. F.; Lehr, C. M., Proteomic and Lipidomic Analysis of Nanoparticle Corona upon Contact with Lung Surfactant Reveals Differences in Protein, but Not Lipid Composition. *Acs Nano* **2015,** *9* (12), 11872-85.

35. Berg, J. M.; Tymoczko, J. L.; Stryer, L., *Biochemistry*. 6 ed.; Elsevier: Munich, 2007.

36. Winzen, S.; Schwabacher, J. C.; Müller, J.; Landfester, K.; Mohr, K., Small Surfactant Concentration Differences Influence Adsorption of Human Serum Albumin on Polystyrene Nanoparticles. *Biomacromolecules* **2016,** *17* (11), 3845-3851.

37. Musyanovych, A.; Dausend, J.; Dass, M.; Walther, P.; Mailänder, V.; Landfester, K., Criteria impacting the cellular uptake of nanoparticles: A study emphasizing polymer type and surfactant effects. *Acta Biomater* **2011,** *7* (12), 4160-4168.

38. Jirgensons, B., Factors Determining the Reconstructive Denaturation of Proteins in Sodium Dodecyl Sulfate Solutions. Further Circular Dichroism Studies on Structural Reorganization of Seven Proteins. *Journal of Protein Chemistry* **1981,** *1* (1), 71-84.

39. Miyazawa, K.; Ogawa, M.; Mitsui, T., The Physicochemical Properties and Protein Denaturation Potential of Surfactant Mixtures. *Int J Cosmetic Sci* **1984,** *6* (1), 33-46.

40. Oakes, J., Protein-Surfactant Interactions - Nuclear Magnetic-Resonance and Binding Isotherm Studies of Interactions between Bovine Serum-Albumin and Sodium Dodecyl-Sulfate. *J Chem Soc Farad T 1* **1974,** *70*, 2200-2209.

41. Steinhardt, J.; Scott, J. R.; Birdi, K. S., Differences in the solubilizing effectiveness of the sodium dodecyl sulfate complexes of various proteins. *Biochemistry* **1977,** *16* (4), 718-25.

42. Laemmli, U. K., Cleavage of structural proteins during the assembly of the head of bacteriophage T4. *Nature* **1970,** *227* (5259), 680-5.

43. Jones, L. S.; Bam, N. B.; Randolph, T. W., Surfactant-stabilized protein formulations: A review of protein-surfactants interactions and novel analytical methodologies. *Acs Sym Ser* **1997,** *675*, 206-222.

44. Goddard, E. D. A., K. P., *Interactions of Surfactants with Polymers and Proteins*. CRC Press: Boca Raton, 1992.

45. Kelley, D.; McClements, D. J., Interactions of bovine serum albumin with ionic surfactants in aqueous solutions. *Food Hydrocolloid* **2003,** *17* (1), 73-85.

46. Nielsen, A. D.; Borch, K.; Westh, P., Thermochemistry of the specific binding of C12 surfactants to bovine serum albumin. *Biochim Biophys Acta* **2000,** *1479* (1-2), 321-31.

47. Chi, E. Y.; Krishnan, S.; Randolph, T. W.; Carpenter, J. F., Physical stability of proteins in aqueous solution: Mechanism and driving forces in nonnative protein aggregation. *Pharm Res-Dordr* **2003,** *20* (9), 1325-1336.

48. Anderson, N. L.; Anderson, N. G., The human plasma proteome - History, character, and diagnostic prospects. *Mol Cell Proteomics* **2002,** *1* (11), 845-867.

49. Berman, H. M.; Westbrook, J.; Feng, Z.; Gilliland, G.; Bhat, T. N.; Weissig, H.; Shindyalov, I. N.; Bourne, P. E., The Protein Data Bank. *Nucleic Acids Res* **2000,** *28* (1), 235-242.

50. Haab, B. B.; Geierstanger, B. H.; Michailidis, G.; Vitzthum, F.; Forrester, S.; Okon, R.; Saviranta, P.; Brinker, A.; Sorette, M.; Perlee, L.; Suresh, S.; Drwal, G.; Adkins, J. N.; Omenn, G. S., Immunoassay and antibody microarray analysis of the HUPO Plasma Proteome Project reference specimens: Systematic variation between sample types and calibration of mass spectrometry data. *Proteomics* **2005,** *5* (13), 3278-3291.

51. Tu, C.; Rudnick, P. A.; Martinez, M. Y.; Cheek, K. L.; Stein, S. E.; Slebos, R. J.; Liebler, D. C., Depletion of abundant plasma proteins and limitations of plasma proteomics. *J Proteome Res* **2010,** *9* (10), 4982-91.

52. Wyatt, A. R.; Yerbury, J. J.; Wilson, M. R., Structural Characterization of Clusterin-Chaperone Client Protein Complexes. *Journal of Biological Chemistry* **2009,** *284* (33), 21920-21927.

53. Rohne, P.; Prochnow, H.; Wolf, S.; Renner, B.; Koch-Brandt, C., The Chaperone Activity of Clusterin is Dependent on Glycosylation and Redox Environment. *Cell Physiol Biochem* **2014,** *34* (5), 1626-1639.

54. Jones, S. E.; Jomary, C., Clusterin. *Int J Biochem Cell Biol* **2002,** *34* (5), 427-31.

55. Phillips, J. C.; Wriggers, W.; Li, Z.; Jonas, A.; Schulten, K., Predicting the structure of apolipoprotein A-I in reconstituted high-density lipoprotein disks. *Biophys J* **1997,** *73* (5), 2337-46.

56. Segrest, J. P.; Jones, M. K.; De Loof, H.; Dashti, N., Structure of apolipoprotein B-100 in low density lipoproteins. *Journal of Lipid Research* **2001,** *42* (9), 1346-1367.

57. Zhu, C.; Pradhan, P.; Huo, D.; Xue, J.; Shen, S.; Roy, K.; Xia, Y., Reconstitution of Low-Density Lipoproteins with Fatty Acids for the Targeted Delivery of Drugs into Cancer Cells. *Angew Chem Int Ed Engl* **2017**.

58. Landfester, K.; Bechthold, N.; Tiarks, F.; Antonietti, M., Formulation and stability mechanisms of polymerizable miniemulsions. *Macromolecules* **1999,** *32* (16), 5222-5228.

59. Baier, G.; Baumann, D.; Siebert, J. M.; Musyanovych, A.; Mailänder, V.; Landfester, K., Suppressing Unspecific Cell Uptake for Targeted Delivery Using Hydroxyethyl Starch Nanocapsules. *Biomacromolecules* **2012,** *13* (9), 2704-2715.

60. Steinman, R. M.; Hawiger, D.; Nussenzweig, M. C., Tolerogenic dendritic cells. *Annu Rev Immunol* **2003,** *21*, 685-711.

61. Shen, L. M.; Higuchi, T.; Tubbe, I.; Voltz, N.; Krummen, M.; Pektor, S.; Montermann, E.; Rausch, K.; Schmidt, M.; Schild, H.; Grabbe, S.; Bros, M., A Trifunctional Dextran-Based Nanovaccine Targets and Activates Murine Dendritic Cells, and Induces Potent Cellular and Humoral Immune Responses In Vivo. *Plos One* **2013,** *8* (12).

62. Kang, B.; Okwieka, P.; Schöttler, S.; Winzen, S.; Langhanki, J.; Mohr, K.; Opatz, T.; Mailänder, V.; Landfester, K.; Wurm, F. R., Carbohydrate-Based Nanocarriers Exhibiting Specific Cell Targeting with Minimum Influence from the Protein Corona. *Angew Chem Int Ed Engl* **2015,** *54* (25), 7436-40.

63. Freichels, H.; Wagner, M.; Okwieka, P.; Meyer, R. G.; Mailänder, V.; Landfester, K.; Musyanovych, A., (Oligo)mannose functionalized hydroxyethyl starch nanocapsules: en route to drug delivery systems with targeting properties. *J Mater Chem B* **2013,** *1* (34), 4338-4348.

64. Salvati, A.; Pitek, A. S.; Monopoli, M. P.; Prapainop, K.; Bombelli, F. B.; Hristov, D. R.; Kelly, P. M.; Aberg, C.; Mahon, E.; Dawson, K. A., Transferrin-functionalized nanoparticles lose their targeting capabilities when a biomolecule corona adsorbs on the surface. *Nature Nanotechnology* **2013,** *8* (2), 137-143.

65. Vroman, L.; Adams, A. L., Findings with Recording Ellipsometer Suggesting Rapid Exchange of Specific Plasma Proteins at Liquid/Solid Interfaces. *Surf Sci* **1969,** *16*, 438-&.

66. Jung, S. Y.; Lim, S. M.; Albertorio, F.; Kim, G.; Gurau, M. C.; Yang, R. D.; Holden, M. A.; Cremer, P. S., The Vroman effect: A molecular level description of fibrinogen displacement. *J Am Chem Soc* **2003,** *125* (42), 12782-12786.

67. Winzen, S. Influence of different factors on the interaction between polymeric nanomaterials and blood plasma proteins. Dissertation, Johannes Gutenberg-Universität Mainz, Mainz, 2015.

68. Leroux, J. C.; Allemann, E.; DeJaeghere, F.; Doelker, E.; Gurny, R., Biodegradable nanoparticles - From sustained release formulations to improved site specific drug delivery. *J Control Release* **1996,** *39* (2-3), 339-350.

69. Gref, R.; Domb, A.; Quellec, P.; Blunk, T.; Muller, R. H.; Verbavatz, J. M.; Langer, R., The Controlled Intravenous Delivery of Drugs Using Peg-Coated Sterically Stabilized Nanospheres. *Adv Drug Deliver Rev* **1995,** *16* (2-3), 215-233.

70. Israelachvili, J., The different faces of poly(ethylene glycol). *P Natl Acad Sci USA* **1997,** *94* (16), 8378-8379.

71. Van Alstine, J. M. V., F. M.; Yomo, T.; Yoshinaga, K.; Zalipsky, S. , *Poly(Ethylene Glycol) Chemistry: Biotechnical and Biomedical Applications*. Springer Science + Business Media New York: 1992.

72. Vennemann, N.; Lechner, M. D.; Oberthur, R. C., Thermodynamics and Conformation of Polyoxyethylene in Aqueous-Solution under High-Pressure .1. Small-Angle Neutron-Scattering and Densitometric Measurements at Room-Temperature. *Polymer* **1987,** *28* (10), 1738-1748.

73. Marruecos, D. F.; Kastantin, M.; Schwartz, D. K.; Kaar, J. L., Dense Poly(ethylene glycol) Brushes Reduce Adsorption and Stabilize the Unfolded Conformation of Fibronectin. *Biomacromolecules* **2016,** *17* (3), 1017-1025.

74. Molino, N. M.; Bilotkach, K.; Fraser, D. A.; Ren, D. M.; Wang, S. W., Complement Activation and Cell Uptake Responses Toward Polymer-Functionalized Protein Nanocapsules. *Biomacromolecules* **2012,** *13* (4), 974-981.

75. Griffin, W. C., Calculation of HLB values of non-ionic surfactants. *Am Perfumer Essent Oil Rev* **1955,** *65* (5), 26-29.

76. Otzen, D. E.; Sehgal, P.; Westh, P., alpha-Lactalbumin is unfolded by all classes of surfactants but by different mechanisms. *J Colloid Interf Sci* **2009,** *329* (2), 273-283.

77. Bam, N. B.; Cleland, J. L.; Yang, J.; Manning, M. C.; Carpenter, J. F.; Kelley, R. F.; Randolph, J. W., Tween protects recombinant human growth hormone against agitation-induced damage via hydrophobic interactions. *J Pharm Sci* **1998,** *87* (12), 1554-1559.

78. Otzen, D., Protein-surfactant interactions: A tale of many states. *Bba-Proteins Proteom* **2011,** *1814* (5), 562-591.

79. Waninge, R.; Paulsson, M.; Nylander, T.; Ninham, B.; Sellers, P., Binding of sodium dodecyl sulphate and dodecyl trimethyl ammonium chloride to beta-lactoglobulin: A calorimetric study. *Int Dairy J* **1998,** *8* (2), 141-148.

80. Schärtl, W., *Light scattering from polymer solutions and nanoparticle dispersions*. Springer: Berlin, 2007.

81. Urban, C.; Schurtenberger, P., Characterization of turbid colloidal suspensions using light scattering techniques combined with cross-correlation methods. *J Colloid Interf Sci* **1998,** *207* (1), 150-158.

82. Berne, B. J. P., R., *Dynamic Light Scattering: With Applications to Chemistry, Biology, and Physics*. Dover: Mineola, NY, 2000.

83. Rausch, K.; Reuter, A.; Fischer, K.; Schmidt, M., Evaluation of Nanoparticle Aggregation in Human Blood Serum. *Biomacromolecules* **2010,** *11* (11), 2836-2839.

84. Lewis, E.; Murphy, K., Isothermal Titration Calorimetry. In *Protein-Ligand Interactions*, Ulrich Nienhaus, G., Ed. Humana Press: 2005; Vol. 305, pp 1-15.

85. Freire, E.; Mayorga, O. L.; Straume, M., Isothermal titration calorimetry. *Analytical Chemistry* **1990,** *62* (18), 950A-959A.

86. Strutz, W., Exploring Protein Stability by NanoDSF. *Biophysical Journal* **2016,** *110* (3), 393a-393a.

87. Zeta potential measurement principle (Laser Doppler Electrophoresis). http://laser.spbu.ru/en/research-eng/dzeta-eng.html (accessed 07-11-2017).

88. Bhushan, V., *First aid for the USMLE step 1 2007*. McGraw-Hill Medical: New York, 2007; p xvii, 534 p.

89. Winzen, S.; Schöttler, S.; Baier, G.; Rosenauer, C.; Mailänder, V.; Landfester, K.; Mohr, K., Complementary analysis of the hard and soft protein corona: sample preparation critically effects corona composition. *Nanoscale* **2015,** *7* (7), 2992-3001.

90. Liu, W.; Rose, J.; Plantevin, S.; Auffan, M.; Bottero, J. Y.; Vidaud, C., Protein corona formation for nanomaterials and proteins of a similar size: hard or soft corona? *Nanoscale* **2013,** *5* (4), 1658-1668.

91. Gonzalez-Quintela, A.; Alende, R.; Gude, F.; Campos, J.; Rey, J.; Meijide, L. M.; Fernandez-Merino, C.; Vidal, C., Serum levels of immunoglobulins (IgG, IgA, IgM) in a general adult population and their relationship with alcohol consumption, smoking and common metabolic abnormalities. *Clin Exp Immunol* **2008,** *151* (1), 42-50.

92. Helander, A., Absolute or relative measurement of carbohydrate-deficient transferrin in serum? Experiences with three immunological assays. *Clin Chem* **1999,** *45* (1), 131-135.

93. Provencher, S. W., Inverse Problems in Polymer Characterization - Direct Analysis of Polydispersity with Photon Correlation Spectroscopy. *Makromol Chem* **1979,** *180* (1), 201-209.

94. Provencher, S. W., Contin - a General-Purpose Constrained Regularization Program for Inverting Noisy Linear Algebraic and Integral-Equations. *Comput Phys Commun* **1982,** *27* (3), 229-242.

95. Koppel, D. E., Analysis of Macromolecular Polydispersity in Intensity Correlation Spectroscopy - Method of Cumulants. *J Chem Phys* **1972,** *57* (11), 4814-&.

96. Steinbach, T.; Wurm, F. R., Poly(phosphoester)s: A New Platform for Degradable Polymers. *Angew Chem Int Edit* **2015,** *54* (21), 6098-6108.

97. Freire, E.; Mayorga, O. L.; Straume, M., Isothermal Titration Calorimetry. *Anal Chem* **1990,** *62* (18), A950-A959.

98. Norde, W., Adsorption of proteins from solution at the solid-liquid interface. *Adv Colloid Interface Sci* **1986,** *25* (4), 267-340.

99. Privalov, P. L.; Khechinashvili, N. N., A thermodynamic approach to the problem of stabilization of globular protein structure: a calorimetric study. *J Mol Biol* **1974,** *86* (3), 665-84.

100. Kokkinopoulou, M.; Simon, J.; Landfester, K.; Mailänder, V.; Lieberwirth, I., Visualization of the protein corona: towards a biomolecular understanding of nanoparticle-cell-interactions. *Nanoscale* **2017,** *9* (25), 8858-8870.

101. Schneider, C. A.; Rasband, W. S.; Eliceiri, K. W., NIH Image to ImageJ: 25 years of image analysis. *Nat Methods* **2012,** *9* (7), 671-5.

102. Niesen, F. H.; Berglund, H.; Vedadi, M., The use of differential scanning fluorimetry to detect ligand interactions that promote protein stability. *Nat Protoc* **2007,** *2* (9), 2212-2221.

103. Lesniak, A.; Campbell, A.; Monopoli, M. P.; Lynch, I.; Salvati, A.; Dawson, K. A., Serum heat inactivation affects protein corona composition and nanoparticle uptake. *Biomaterials* **2010,** *31* (36), 9511-8.

104. Soltis, R. D.; Hasz, D.; Morris, M. J.; Wilson, I. D., The effect of heat inactivation of serum on aggregation of immunoglobulins. *Immunology* **1979,** *36* (1), 37-45.

105. Settanni, G.; Zhou, J.; Suo, T.; Schöttler, S.; Landfester, K.; Schmid, F.; Mailänder, V., Protein corona composition of poly(ethylene glycol)- and poly(phosphoester)-coated nanoparticles correlates strongly with the amino acid composition of the protein surface. *Nanoscale* **2017,** *9* (6), 2138-2144.

106. Vonarbourg, A.; Passirani, C.; Saulnier, P.; Benoit, J. P., Parameters influencing the stealthiness of colloidal drug delivery systems. *Biomaterials* **2006,** *27* (24), 4356-4373.

107. Ajees, A. A.; Anantharamaiah, G. M.; Mishra, V. K.; Hussain, M. M.; Murthy, H. M. K., Crystal structure of human apolipoprotein A-I: Insights into its protective effect against cardiovascular diseases. *P Natl Acad Sci USA* **2006,** *103* (7), 2126-2131.

108. Thurmond, C. D., Control of Dust in Solutions for Turbidimetry. *J Polym Sci* **1952,** *8* (6), 607-609.

109. Renz, P.; Kokkinopoulou, M.; Landfester, K.; Lieberwirth, I., Imaging of Polymeric Nanoparticles: Hard Challenge for Soft Objects. *Macromol Chem Phys* **2016,** *217* (17), 1879-1885.

110. Kremer, J. R.; Mastronarde, D. N.; McIntosh, J. R., Computer visualization of three-dimensional image data using IMOD. *J Struct Biol* **1996,** *116* (1), 71-6.

111. Zhang, S. Y.; Zou, J.; Zhang, F. W.; Elsabahy, M.; Felder, S. E.; Zhu, J. H.; Pochan, D. J.; Wooley, K. L., Rapid and Versatile Construction of Diverse and Functional Nanostructures Derived from a Polyphosphoester-Based Biomimetic Block Copolymer System. *J Am Chem Soc* **2012,** *134* (44), 18467-18474.

112. Bauer, K. N. In-Chain Poly(phosphonate)s: Synthesis, Degradation and Biomedical Applications. Johannes Gutenberg-Universität, Mainz, 2017.

113. Saier, E. L.; Nordstrand, E.; Juves, M. W.; Hartsock, R. J., The ratio of free to esterified cholesterol in serum. A new discriminant in correlating lipid metabolism with disease state. *Am J Clin Pathol* **1979,** *71* (1), 83-7.